1967

A calorimetric study of the effects of surface energy in a type II superconductor

Robert Rex Rice

A CALORIMETRIC STUDY OF THE EFFECTS OF SURFACE ENERGY IN A TYPE II SUPERCONDUCTOR

by

ROBERT REX RICE

A DISSERTATION

Presented to the Faculty of the Graduate School of the

UNIVERSITY OF MISSOURI AT ROLLA

In Partial Fulfillment of the Requirements for the Degree

DOCTOR OF PHILOSOPHY

1967

Leon C. Hopkins
Advisor

Charles E. MacFarland

Henry A. Brown

Charles E. Gentle

Charles A. Ehrlich

A CALORIMETRIC STUDY OF THE EFFECTS OF SURFACE ENERGY IN A TYPE II SUPERCONDUCTOR

ABSTRACT

A calorimetric study of the effects of the interphase surface free energy has been conducted on ellipsoidal samples of first and second kind superconductors. The measurements were performed using a specially designed magnetization calorimeter by two different techniques. The measurements were made on lead, tin, lead-4at%thallium, and tin-6at% indium. The results confirm the existence and expected sign of the surface energy in a well annealed lead-4at%thallium sample, and indicate that the interphase surface energy in lead and tin is too small to be directly detected by this method. The measured latent heats of transition of lead and tin agree well with the latent heats deduced from the critical field curves. The tin-6at%indium sample was too hysteretic to yield meaningful data. The results of measurements performed on lead-4at%thallium were compared to predictions based on laminar and vortex models of the mixed state.

Robert Rex Rice

ACKNOWLEDGEMENTS

The author wishes to express his gratitude to Dr. Don C. Hopkins, Assistant Professor of Physics, for suggesting the problem and providing advice and assistance throughout the project. He would also like to thank Dr. Robert Gerson, Professor of Physics, and Dr. Robert Bell, Assistant Professor of Physics, for many helpful discussions and suggestions. The author gratefully acknowledges the assistance of Mr. James M. Carter in performing the experiment and reducing the data. The author is also grateful to Professor Emeritus A. V. Kilpatrick for precision machining of the samples, and to Dr. H. P. Leighly for metallurgical consultation.

The author is indebted to the United States Army Research Office, Durham, North Carolina, for financial support in the form of a research fellowship.

The assistance and encouragement of the author's wife, Mary, in the preparation of this manuscript is gratefully acknowledged.

TABLE OF CONTENTS

LIST OF TABLES

LIST OF FIGURES

LIST OF PLATES

I. INTRODUCTION

A. GENERAL INTRODUCTION

H. London pointed out in 1935 that a superconducting body exhibiting total flux exclusion can not be in a state of lowest free energy unless there is a surface free energy associated with the boundary between the normal and superconducting phases [1]. Landau proposed a laminar model of the intermediate state which incorporated the surface free energy [2]. In 1950 Pippard proposed his non-local theory, in which he suggests that the superconducting order parameter can not change in a distance shorter than the coherence length, ξ [3]. In this approach the surface energy will be positive if the coherence length is greater than the penetration depth, λ, while it will be negative if the coherence length is less than the penetration depth.

Ginzburg and Landau proposed a phenomenological approach to superconductivity in 1950 which characterizes a material by two parameters, λ and ξ, which must be experimentally determined [4]. In this treatment the surface energy is positive or negative depending on whether K, the ratio of λ, to ξ, is greater than or less than $1/\sqrt{2}$. A material having $K < 1/\sqrt{2}$ is designated type I, while a material having $K > 1/\sqrt{2}$ is designated type II. The intermediate state is observed in type I materials having non-zero demagnetizing

coefficients, while the mixed state is observed in type II materials. A. A. Abrikosov solved the Ginzburg-Landau equations for materials having $\kappa > 1/\sqrt{2}$ in 1957, and his solution indicates that the mixed state consists of quantized magnetic flux lines, or supercurrent vortices, arranged in a regular, two-dimensional lattice normal to the direction of the field. (5) It has been shown that only a lattice of flux lines possessing six-fold symmetry is dynamically stable with respect to small displacements from equilibrium (6),(7).

A. L. Fetter has calculated the energy of a lattice of quantized flux lines as a function of applied magnetic field (8). From his expressions it is possible to obtain thermodynamic functions such as entropy for the mixed state. B. B. Goodman earlier proposed a simple laminar model for the mixed state which includes a surface energy parameter (9). The thermodynamic properties of this model are particularly simple to deduce, and will be discussed in this work.

This work is a calorimetric study of the mixed and intermediate states. It should be possible to detect the effects of an interphase surface free energy by monitoring the heat which must be supplied to an adiabatically mounted sample in order to maintain isothermal conditions while the sample is slowly driven through the superconducting-to-

normal transition by an externally applied field. Moreover, it should be possible to calculate this heat on the basis of the two mixed state models mentioned, viz., the laminar model of Goodman and the vortex model of Fetter, and to compare the results with the experimental results obtained in this work. During the course of this work, F. A. Otter has reported the results of a similar study, and his results can also be compared with the results of this experiment [10].

B. THERMODYNAMICS OF THE TRANSITION

The properties of a bulk superconductor, or a long cylindrical sample having a negligible demagnetizing factor, can be expressed by: [11]

$$\bar{E} = 0 \qquad \bar{B} = 0 \qquad \text{if} \quad H_a < H_c \tag{1a}$$

$$\bar{J} = \sigma \bar{E} \qquad \bar{B} = \bar{H}_a \qquad \text{if} \quad H_a > H_c \tag{1b}$$

TYPE I

where E is the electric field in the interior of a superconductor.

B is the magnetic induction in the interior.

J is the current density in the interior.

σ is the normal state conductivity of a material.

H_a is the applied magnetic field.

H_c is the field at which superconductivity is destroyed.

The first pair of equations (1a) express the facts that a superconductor carries dc current without loss and that magnetic flux is excluded from the interior when the

material is superconducting. The second equation implies that when the applied field exceeds a certain value, H_c, called the critical field, superconductivity is destroyed and the metal behaves as a normal metal. The exclusion of flux from the interior is called the "Meissner effect" and is a requirement for thermodynamic reversibility [12]. The thermodynamic analysis that follows is a Clausius-Clapyron arguement first proposed by Gorter and Casimir in 1934 [13].

The critical field is strongly temperature dependent, and the temperature dependence is given to within a few percent by:

$$H_c = H_o \left(1 - T^2 / T_c^2 \right) \qquad (2)$$

where H_o is the critical field at absolute zero.

T is the absolute temperature.

T_c is the transition temperature in zero field (critical temperature.)

The curve obtained by plotting $H_c(T)$ is called the critical field curve and represents the locus of points for which the normal and superconducting phases are in equilibrium. For situations in which the applied field is generated by an external current distribution, the appropriate thermodynamic potential is the magnetic Gibbs function defined by:

$$G = U - \nu M H_a - TS \qquad (3)$$

where G is the Gibbs free energy.

U is the internal energy.

V is the volume of the sample.

M is the magnetization of the sample.

S is the entropy.

The differential form is given by:

$$dG = dU - VM dH_a - V H_a dM - T dS - S dT \qquad (4)$$

The first law of thermodynamics for this situation can be written:

$$dQ = T dS = dU - V H_a dM \qquad (5)$$

This expression of the first law of thermodynamics can be used to simplify the differential of the Gibbs function:

$$dG = -VM dH_a - S dT \qquad (6)$$

It has been assumed that the processes involved in the transition have produced no irreversible energy changes. Were this not the case, equation (5) could not have been used to simplify equation (4), since TdS is equal to dQ only for reversible processes.

Two useful results may be obtained from equation (6). Considering G to be a function of H_a and T, dG can be written:

$$dG = (\partial G/\partial H_a)_T dH_a + (\partial G/\partial T)_{H_a} dT \qquad (7)$$

Identification of the coefficients of the differentials in equation (6) with the corresponding partial derivatives in (7)

leads to:

$$(\partial G/\partial T)_{H_a} = -S \qquad (\partial G/\partial H_a)_T = -VM \tag{8}$$

The first relation is important as it stands, since it enables one to compute the entropy of a superconductor as a function of temperature if the temperature dependence of the Gibbs function is known. The second relation can be integrated with respect to applied field, H_a, to get:

$$G_s(H_a) - G_n(0) = -V\int_0^{H_a} M(H_a)\,dH_a \tag{9}$$

where the s and n subscripts refer to the superconducting and normal phases respectively, in the remainder of this work. Along the critical field curve, the two phases are in equilibrium; therefore, the Gibbs function of the two phases must be equal:

$$G_s(H_c) = G_n(H_c) \tag{10}$$

However, the Gibbs function for the normal state depends very little on the applied field. The Gibbs function of the normal state in applied field H_c is therefore equal to the Gibbs function of the normal state in zero field:

$$G_n(H_c) = G_n(0) \tag{11}$$

The difference in Gibbs free energy between the normal and the superconducting states in zero field is obtained by substituting (11) and (10) into (9) to get:

$$G_n(0) - G_s(0) = -V\int_0^{H_c} M(H_a)\,dH_a \tag{12}$$

This result can be simplified by inserting the expression for M in terms of H_a and carrying out the integration. The relation between B, M, and H_a is given by [14]:

$$B = H_a + 4\pi M \tag{13}$$

If B vanishes in the interior of a superconductor body, the body is behaving as a perfect diamagnet, and the magnetization is given in terms of H_a by:

$$M = -H_a / 4\pi \tag{14}$$

When this expression for M is inserted in (12) and the integration performed, the resulting expression for the Gibbs free energy difference between the normal and superconducting states in zero field is:

$$G_n(0) - G_s(0) = V H_c^2 / 8\pi \tag{15}$$

Below T_c, the superconducting state is the stable state in zero field. The situation in type II materials is a bit different, but the transition is reversible in principle and can be treated in the same way [15],[16].

The properties of a bulk type II superconductor can be expressed by:

$$\bar{E} = 0 \qquad \bar{B} = 0 \qquad \text{if} \quad H_a < H_{c1} \qquad \text{TYPE II} \tag{16}$$

$$\bar{E} = 0 \qquad \bar{B} = \bar{B}(H_a) \qquad \text{if} \quad H_{c1} < H_a < H_{c2}$$

$$\bar{J} = \sigma \bar{E} \qquad \bar{B} = \bar{H}_a \qquad \text{if} \quad H_a > H_{c2}$$

where H_{c1} is called the lower critical field.

H_{c2} is called the upper critical field.

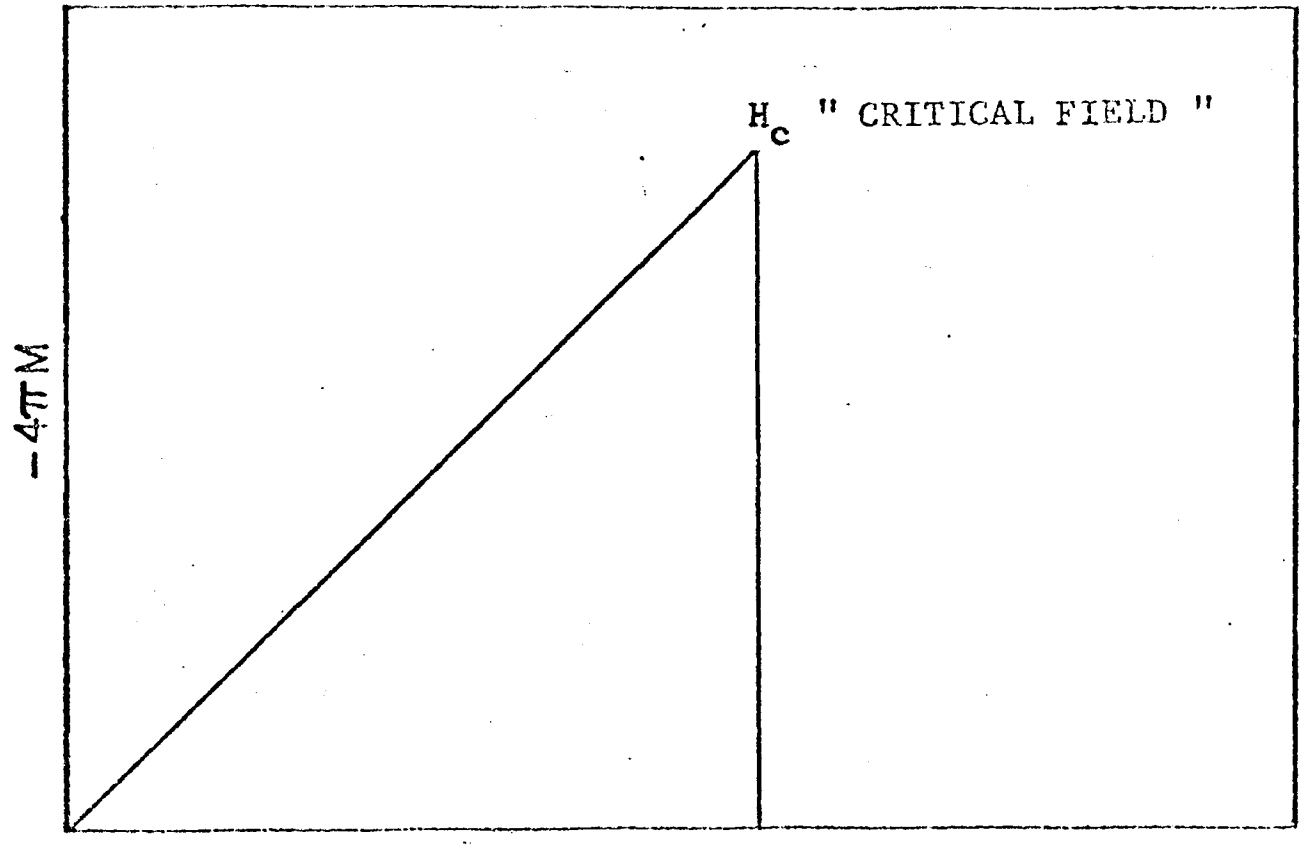

MAGNETIZATION OF A TYPE I SUPERCONDUCTOR

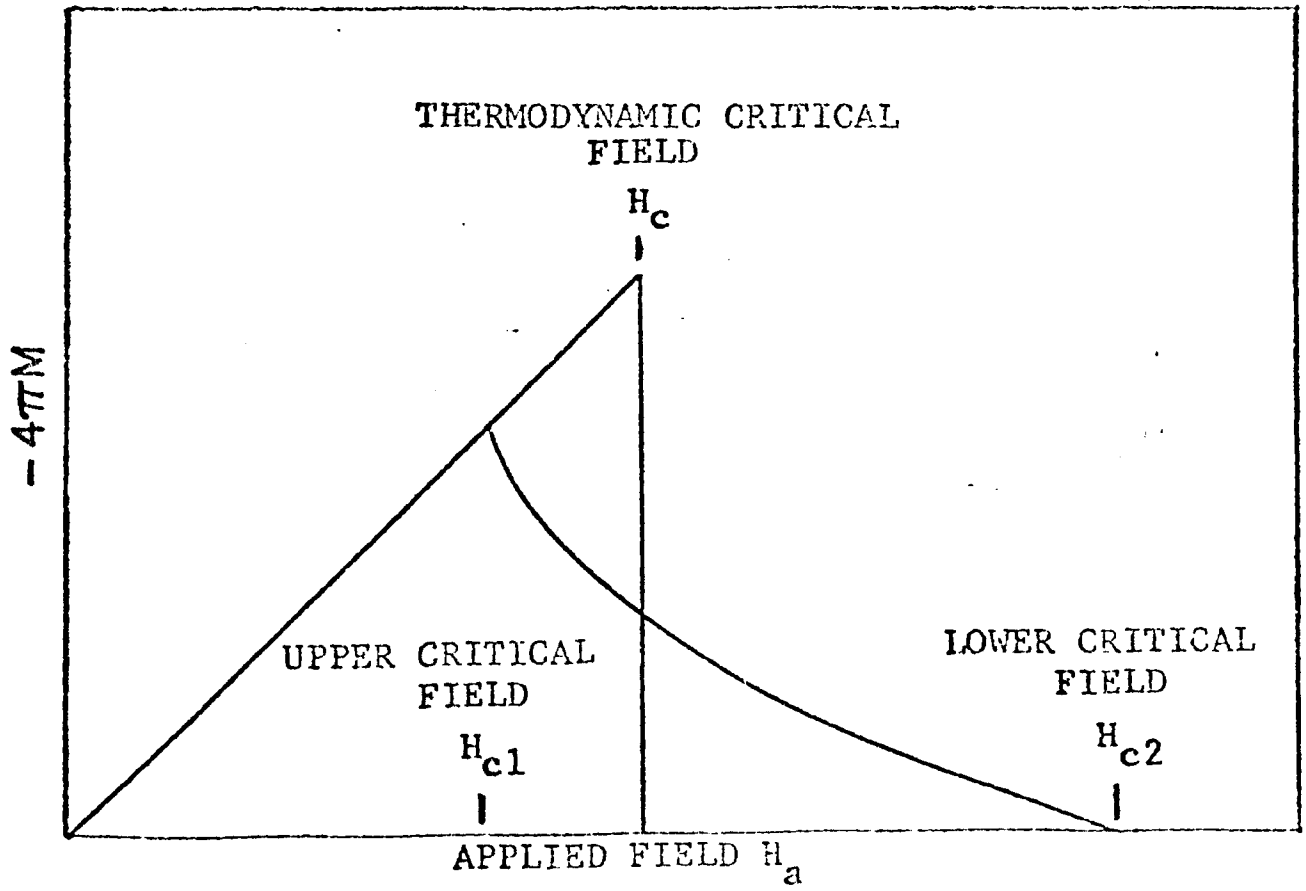

MAGNETIZATION OF A TYPE II SUPERCONDUCTOR

FIGURE 1. Magnetization of type I and II superconductors

The first figure shows magnetization curves for type I and type II superconductors. An arguement identical to that presented for a type I superconductor can be followed for a type II material giving an expression for the Gibbs free energy difference in zero field identical in form to equation (12). The only modification required is that the upper limit of integration in equation (12) be replaced by H_{c2}:

$$G_n(0) - G_s(0) = -V\int_0^{H_{c2}} M(H_a)\,dH_a \qquad (17)$$

In fact, the thermodynamic critical field, H_c, is defined for a type II superconductor by combining equations (17) and (15) to get:

$$\frac{H_c^2}{8\pi} = -\int_0^{H_{c2}} M(H_a)\,dH_a \qquad (18)$$

Having obtained the free energy difference between the normal and superconducting states in zero field, the entropy difference can be computed using equation (8). Differentiating equation (15) with respect to temperature and then changing signs gives:

$$S_n(0) - S_s(0) = -\left(\frac{VH_c}{4\pi}\right)\left(\frac{dH_c}{dT}\right) \qquad (19)$$

The derivative (dH_c/dT) is always negative, so the entropy of the normal state is always higher than the entropy of the superconducting state. The latent heat, L, of the transition is obtained by definition from the product of the entropy change and the temperature:

$$L = T(S_n - S_s) = -\left(\frac{TVH_c}{4\pi}\right)\left(\frac{dH_c}{dT}\right) \qquad (20)$$

If so desired, the heat capacity may be obtained by further differentiating equation (19) and multiplying the result by the temperature. In this way the heat capacity is found to be different for the two states.

The way in which the transition occurs is of some interest. As the external field is increased, the entropy of a superconducting body does not increase, and no latent heat is absorbed. When the applied field reaches the critical field, magnetic flux begins to penetrate a body and destroy superconductivity. If the field is held exactly at H_c, the relative proportions of the normal and superconducting phases present do not change with time, since the phases are in equilibrium. If energy is slowly supplied to the sample, the normal regions will grow at the expense of the superconducting regions until the transition is driven to completion, and the latent heat is absorbed. This process is analogous to the melting of ice at constant temperature and pressure.

If the transition occurs over a range of applied fields, as with a type II material or an ellipsoidal sample of type I material, the situation is slightly different. The transition is driven to completion by slowly increasing the applied field. An adiabatically mounted sample cools as the field is increased, because the latent heat of transition is taken from the internal energy of the lattice. To maintain isothermal conditions, energy must be supplied from an external

source.

Transitions to the normal state in a constant applied field or at a constant temperature are related by the fourth Maxwell thermodynamic relation [17]:

$$(\partial M/\partial T)_{H_a} = (\partial S/\partial H_a)_T \qquad (21)$$

If the temperature dependence of the magnetization at a given applied field is known, the entropy can be computed as a function of applied field for an isothermal transition at that temperature.

C. PHENOMENOLOGICAL THEORIES OF SUPERCONDUCTIVITY

F. and H. London proposed that two additional equations be added to Maxwell's equations to describe electromagnetic behavior in superconducting materials [18]. The London equations are:

$$\bar{E} = \frac{4\pi\lambda_L^2}{c^2}\dot{\bar{J}} \qquad \frac{4\pi\lambda_L^2}{c^2}\bar{\nabla}\times\bar{J} + \bar{H} = 0 \qquad (22)$$

where H is the magnetic field at a point.

J is the current density at a point.

E is the electric field at a point.

λ_L is the London penetration depth.

The London penetration depth is given by:

$$\lambda_L = \frac{mc^2}{4\pi ne^2} \qquad (23)$$

where m is the mass of an electron.

n is the number density of conduction electrons.

e is the charge of an electron.

The London approach is strictly local, i.e., the current at a point is determined by the field at that point. If a wave function, Ψ , is written for the superconducting electrons, it can be proven that the London equations result if Ψ is unaffected by the application of a magnetic field [12]. Pippard proposed that the order parameter* is not rigid, but changes slowly over a characteristic length known as the coherence length ξ [19]. In 1953, Pippard proposed that the electromagnetic response of a superconductor in an applied field is given by [19]:

$$\bar{J}(\bar{r}) = -\frac{3ne^2}{4\pi\xi_0 m}\int \frac{\bar{J}(\bar{r}\cdot\bar{A})\exp(-r/\xi)}{r^4}\, d^3r \qquad (24)$$

where J(r) is the current density at position r.

r is the position vector of the point under consideration.

A is the vector potential of the applied field.

ξ is the coherence length of the actual material.

ξ_0 is the coherence length of the pure, unstrained material.

The quantity ξ depends on the electronic mean free path, l, according to:

$$\frac{1}{\xi} = \frac{1}{\xi_0} + \frac{1}{l} \qquad (25)$$

Equation (24) states that the current density at a point r depends on the magnetic field at all points within a distance

*The order parameter is a quantity from which the superconducting charge carrier density can be determined.

§ of that point. The coherence length may be thought of as the distance to which order extends in the bulk material. Figure (2), page 20, depicts the phase boundary between a normal and superconducting region. The local field in the normal region is H_a and drops to zero in the superconductor. The order parameter is zero in the normal region and increases to its fully ordered value in the superconductor. The magnetic boundary, M, is defined so that if the local field were H_c up to M and zero thereafter, the magnetic energy of the boundary would be the same as the value obtained by integrating $BH_a/8\pi$ over the superconductor. The configuration boundary, C, is defined so that were the order parameter to maintain its fully ordered value up to C and than vanish, the free energy of the superconductor would be the same as the actual amount. The Gibbs free energy in the superconducting state is lower by an amount $VH_c^2/8\pi$, so the system energy has been raised by an amount C-M times $H_c^2/8\pi$. The surface energy parameter, Δ, is given by:

$$\Delta \approx \xi - \lambda \tag{26}$$

The criterion for stability of the Meissner state up to H_c is:

$$\lambda < \xi \tag{27}$$

The sign of the interphase surface free energy may be negative if λ is greater than ξ, in which case the Meissner state is not stable up to H_c, and the material in question exhibits

type II behavior.

The Ginzburg-Landau equations are a pair of coupled, non-linear, partial differential equations which describe the penetration of a magnetic field into a superconductor and the spatial variation of the order parameter that results. The Ginzburg-Landau equations were derived originally on the basis of physical intuition, but Gor'kov has shown that the G-L equations can be derived from the microscopic BCS theory under appropriate conditions [20]. In the G-L theory, the order parameter, Ψ , is normalized such that:

$$|\Psi|^2 = n_s \tag{28}$$

where n_s is the density of superconducting charge carriers. The order parameter is an effective wave function for the superconducting charge carriers, or more correctly for the centers of mass of the Cooper pairs. Near the transition temperature, T_c, the Gibbs free energy of a superconductor can be expanded in powers of $|\Psi|^2$. Thus near T_c the free energy in the absence of applied magnetic fields is given by:

$$G_s(o) = G_n(o) + \alpha|\Psi|^2 + \beta|\Psi|^4 \tag{29}$$

When the Gibbs function is minimized with respect to $|\Psi|^2$, two results are obtained:

$$|\Psi_o|^2 = -\frac{\alpha}{\beta} \qquad G_s(o) - G_n(o) = -\frac{\alpha^2}{2\beta} \tag{30}$$

where $|\Psi_o|^2$ is the zero field equilibrium value of n_s. The temperature variation of $|\Psi_o|^2$ and H_c can be determined

if the temperature dependence of α and β is known. In the presence of an external applied field, the Gibbs free energy is increased by a volume term $H_a^2/8\pi$ and a tern associated with a gradient of ψ. The Gibbs free energy of a superconductor must be invariant under a gauge transformation. The additional term must be chosen so that the Gibbs function will not depend on the gauge chosen for the vector potential, A. Such a term would be:

$$\frac{1}{2m}\left(-i\hbar\bar{\nabla}\psi - \frac{2e}{c}\bar{A}\psi\right)^2 \tag{31}$$

The expansion for the free energy in an applied field near T_c is given by:

$$G_s(H_a) = G_s(o) + \frac{H_a^2}{8\pi} + \frac{1}{2m}\left(-i\hbar\bar{\nabla}\psi - \frac{2e}{c}\bar{A}\psi\right)^2 \tag{32}$$

The Gibbs function must now be minimized with respect to $\psi(r)$ and A(r). The Gibbs function for a superconducting body is given by:

$$\mathcal{G} = \int_{body} G\, d^3r \tag{33}$$

Taking a variation of G with respect to A(r) and $\psi(r)$ and integrating by parts leads to: (21)

$$\delta\mathcal{G} = \int d^3r \left\{ \delta\psi^* \left[\alpha\psi + \beta|\psi|^2 + \frac{1}{2m}\left(-i\hbar\bar{\nabla} - \frac{2e}{c}\bar{A}\psi\right)^2\psi\right] + c.c.\right\} \tag{34}$$

$$+ \int d^3r\, \delta\bar{A}\cdot\left\{\frac{1}{4\pi}\bar{\nabla}\times\bar{B} - \frac{e}{mc}\left[\psi^*\left(-i\hbar\bar{\nabla} - \frac{2e}{c}\right)\psi + c.c.\right]\right\}$$

The equilibrium state is obtained by setting $\delta\mathcal{G}$ equal to zero. Since δA and $\delta\psi$ are independent variations, one immediately obtains:

$$\alpha\psi + \beta|\psi|^2\psi + \frac{1}{2m}\left(-i\hbar\nabla - \frac{2e}{c}\right)^2\psi = 0 \tag{35}$$

if the temperature dependence of α and β is known. In the presence of an external applied field, the Gibbs free energy is increased by a volume term $H_a^2/8\pi$ and a tern associated with a gradient of ψ. The Gibbs free energy of a superconductor must be invariant under a gauge transformation. The additional term must be chosen so that the Gibbs function will not depend on the gauge chosen for the vector potential, A. Such a term would be:

$$\frac{1}{2m}\left(-i\hbar\bar{\nabla}\psi - \frac{2e}{c}\bar{A}\psi\right)^2 \tag{31}$$

The expansion for the free energy in an applied field near T_c is given by:

$$G_s(H_a) = G_s(0) + \frac{H_a^2}{8\pi} + \frac{1}{2m}\left(-i\hbar\bar{\nabla}\psi - \frac{2e}{c}\bar{A}\psi\right)^2 \tag{32}$$

The Gibbs function must now be minimized with respect to $\psi(r)$ and A(r). The Gibbs function for a superconducting body is given by:

$$\mathcal{G} = \int_{\text{body}} G\, d^3r \tag{33}$$

Taking a variation of G with respect to A(r) and $\psi(r)$ and integrating by parts leads to: (21)

$$\delta\mathcal{G} = \int d^3r \left\{ \delta\psi^* \left[\alpha\psi + \beta|\psi|^2 + \frac{1}{2m}\left(-i\hbar\bar{\nabla} - \frac{2e}{c}\bar{A}\psi\right)^2\psi\right] + c.c.\right\} \tag{34}$$

$$+ \int d^3r\, \delta\bar{A}\cdot\left\{\frac{1}{4\pi}\bar{\nabla}\times\bar{B} - \frac{e}{mc}\left[\psi^*\left(-i\hbar\bar{\nabla} - \frac{2e}{c}\right)\psi + c.c.\right]\right\}$$

The equilibrium state is obtained by setting $\delta\mathcal{G}$ equal to zero. Since δA and $\delta\psi$ are independent variations, one immediately obtains:

$$\alpha\psi + \beta|\psi|^2\psi + \frac{1}{2m}\left(-i\hbar\nabla - \frac{2e}{c}\right)^2\psi = 0 \tag{35}$$

Using Ampere's law to replace $\bar{\nabla}\times\bar{B}$ by $\frac{4\pi}{c}\bar{J}$, one also obtains:

$$\bar{J} = -\frac{e\hbar}{im}(\psi^*\bar{\nabla}\psi - \psi\bar{\nabla}\psi^*) - \frac{4e^2}{mc}\psi^*\psi\bar{A} \qquad (36)$$

Equations (35) and (36) are the Ginzburg-Landau equations. In the Ginzburg-Landau theory, any material is characterized by the coherence length and the penetration depth. These material parameters are temperature dependent, and near T_c the temperature dependence is given by:

$$\lambda(T) = \frac{1}{\sqrt{2}}\lambda_L(0)\left(\frac{T_c}{T_c - T}\right)^{\frac{1}{2}} \qquad (37)$$

$$\xi(T) = \frac{1}{\sqrt{2}}\xi(0)\left(\frac{T_c}{T_c - T}\right)^{\frac{1}{2}}$$

where $\lambda_L(0)$ is the London penetration depth at absolute zero.

$\xi(0)$ is the coherence length at absolute zero.

The ratio of λ to ξ is temperature independent near T_c and is called the Ginzburg-Landau parameter, K:

$$K = \frac{\lambda(T)}{\xi(T)} \qquad (38)$$

While it was remarked earlier that the surface Gibbs free energy could be negative if $\lambda > \xi$, and the material would exhibit type II behavior, the exact separation occurs when K has a value of $1/\sqrt{2}$. It can be shown that the surface Gibbs free energy vanishes for K equal to $1/\sqrt{2}$ [21].

If magnetic flux links a superconducting region, such as occurs in a multiply connected superconductor cooled in an external field or in the vortex cores that penetrate a type II material above H_{c1}, the order parameter must be single valued

with respect to circulation about the hole or core. This leads to a quantization of the flux linking the hole or core. The quantum of magnetic flux is given by:

$$\phi_o = \frac{hc}{2e} \tag{39}$$

The critical field near T_c is given by:

$$H_c(T) = \frac{\phi_o}{2\pi\sqrt{2}\,\lambda(T)\,\xi(T)} \tag{40}$$

Equations (40) and (38) permit evaluation of K from a measurement of $H_c(T)$ and (T). There are other, more practical ways to determine K, but discussion will be deferred.

D. THE INTERMEDIATE STATE

Due to equivalent surface currents produced by the magnetization of a body, the field within the body is different from the field that would exist in free space at the same location. This difference is called the demagnetizing field, and for an arbitrary shape, may be quite complicated. The demagnetizing field within an ellipsoid of revolution in a uniform external field is uniform, and depends only on the susceptibility, orientation, and eccentricity of the ellipsoid. In general, there is a tensor relation between the external field and the internal field [22]:

$$H_{a\,i} = H_{e\,i} - 4\pi \sum_{j} n_{ij} M_j(H) \tag{41}$$

where $H_{a\,i}$ is the ith component of the field, H_a.

$H_{e\,i}$ is the ith component of the external field, H_e.

$M_j(H)$ is the jth component of the magnetization, M

n_{ij} is the i, j th element of the demagnetization tensor n.

For the case of an ellipsoid oriented parallel to the external field, the demagnetizing field is parallel to the external field, and the tensor equation (41) simplifies to:

$$H_a = H_e - 4\pi N M(H_a) \tag{42}$$

where H_e is the external applied field.

H_a is the internal field.

N is the demagnetizing coefficient in the axial direction.

The magnetization of an ellipsoid in an external field has been thoroughly discussed elsewhere, and the values of N have been tabulated for different eccentricities [23]. Considering a superconducting ellipsoid in field H_e, equation (14) may be used to simplify equation (42) for fields less than H_{c1}:

$$H_a = \frac{H_e}{1-N} \tag{43}$$

The internal field is therefore greater than the external applied field in a superconducting ellipsoid. Consider an ellipsoidal type I superconductor in the applied field range:

$$(1-N)H_c < H_a < H_c \tag{44}$$

At an external applied field $(1-N)H_c$, the internal field is equal to the bulk critical field, and the purely superconducting state is no longer energetically favored. No single large portion of the sample can become normal, since it would be in a field less than the bulk critical field. Landau proposed a

laminar structure of normal and superconducting regions for an ellipsoidal superconductor in this applied field range, and numerous workers have subsequently observed a laminar structure for the intermediate state directly [24]. The laminar structures actually observed have corrugated boundaries and are convoluted to some extent. A curious fact is that the exact structure of the intermediate state is fundamentally different, depending upon whether it is entered from the normal or superconducting state [25][26].

No present model adequately accounts for all the details of the intermediate state. However, if one assumes that the internal field H_a is equal to H_c in the intermediate state, and that the induction B is equal to H_c in the normal regions, the magnetization curve of an ellipsoidal superconductor can be obtained easily. These assumptions are quite plausible, and measured magnetization curves agree well with prediction. Assuming a plane, laminar structure parallel to the field as shown in figure (3), the fraction of the material in the superconducting state is given by:

$$x = \frac{d_s}{d_s + d_n} \tag{45}$$

where x is the superconducting fraction.

d_s is the width of the superconducting laminae.

d_n is the width of the normal laminae.

The exact values of d_s and d_n will depend on the magnitude of

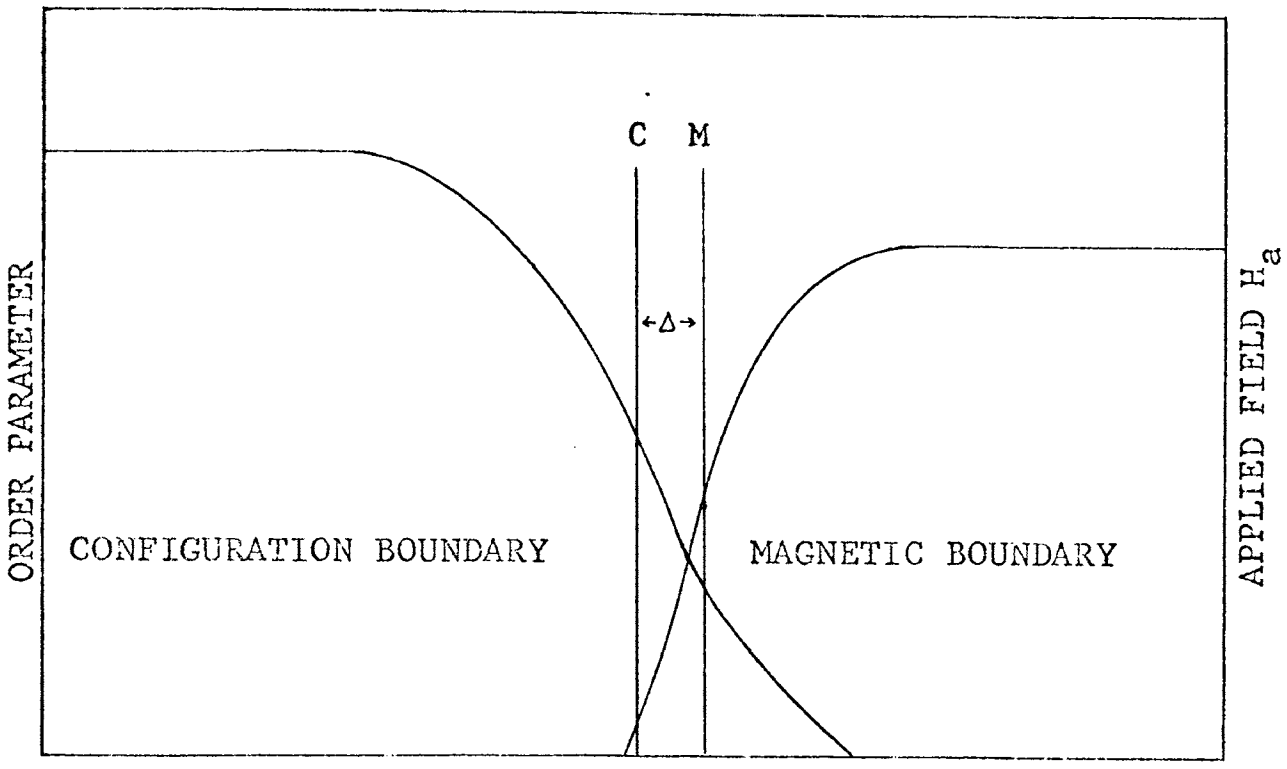

FIGURE 2. Interphase Boundary

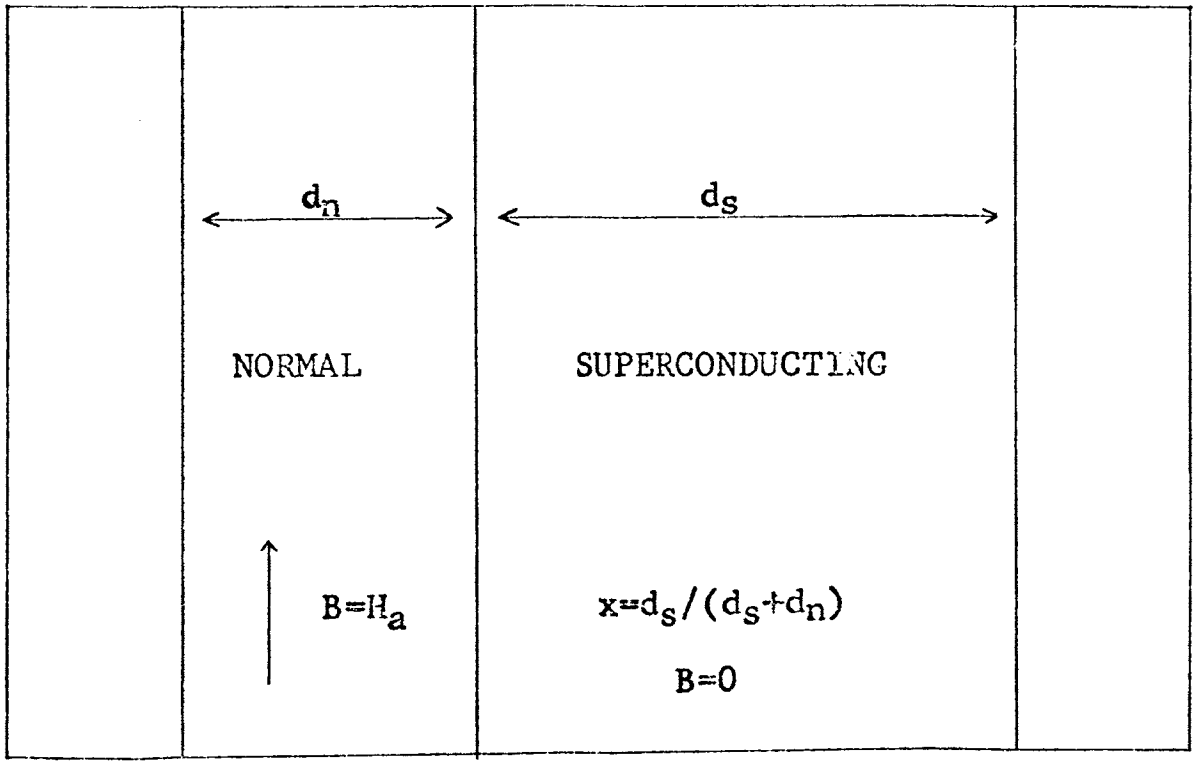

FIGURE 3. Intermediate State Model

the interphase surface energy Δ . The average induction B is given by:

$$\overline{B} = (1-x) H_c \tag{46}$$

Substituting this expression for B, and H_c for H_a, into equation (13) leads to:

$$-4\pi M = x H_c \tag{47}$$

To obtain an expression for x in terms of H_e, equation (47) is substituted into equation (42), along with H_c for H_a, to get:

$$x = \frac{H_c - H_e}{N H_c} \tag{48}$$

The magnetization of an ellipsoidal type I superconductor as a function of external applied field can be summed up as:

$$\begin{aligned} -4\pi M &= \frac{H_e}{1-N} && \text{if} \quad H_e < (1-N) H_c \\ -4\pi M &= \frac{1}{N}(H_e - H_c) && \text{if} \quad H_e > (1-N) H_c \end{aligned} \tag{49}$$

The observed curves do not exactly follow (49), but figure (10), page 63, shows how closely a typical type I superconductor obeys the prediction. The powder patterns of the field distribution in the gap between two superconducting tin hemispheres indicates that the induction may not really be uniform on a macroscopic scale [26]. This could account for deviations from the ideal magnetization curve. The superconductor divides itself to seek the state of lowest free energy, and when the external field field distribution, the interphase boundary energy, and the free energy contribution at the

surface of the ellipsoid are taken into account, it seems plausible that a slightly non-uniform internal field distribution may lead to the state of lowest free energy.

The increment of heat absorbed by a superconductor in the intermediate state is given by:

$$\Delta Q = \frac{\Delta Q}{\Delta x}\Delta x + \frac{\Delta Q}{\Delta T}\Delta T + \frac{\Delta Q}{\Delta A}\Delta A \qquad (51)$$

where ΔQ is the incremental heat absorbed per unit volume.

ΔA is the incremental boundary area change per unit volume.

ΔT is the incremental temperature change.

Δx is the amount by which the superconducting fraction changes.

The ratio of ΔQ to Δx is the negative of the latent heat, since increasing x results in the rejection of heat. The ratio of ΔQ to ΔT is the heat capacity in constant field. The ratio of ΔQ to ΔA is the surface energy parameter. The extrinsic variables subject to control are external field and temperature, while A must be regarded as determined by field, temperature, and composition. In an isothermal transition, Q, the heat required to maintain isothermal conditions, is obtained by integrating (51) with respect to H_e:

$$Q = \frac{L}{NH_c}\left[H_e - (1-N)H_c\right] + \Delta \int_{(1-N)H_c}^{H_c} \frac{\partial A}{\partial H_e}\, dH_e \qquad (52)$$

The ratio of Q to L and of B to H_a are given as functions of H_e using equations (52) and (46):

$$\frac{Q}{L}(H_e) = \frac{1}{NH_c}\left[(N-1)H_c + H_e\right] + \frac{\Delta A(H_e)}{L}$$
$$\frac{B}{H_a}(H_e) = \frac{1}{NH_c}\left[(N-1)H_c + H_e\right] \qquad (53)$$

The ratio of Q/L to B/H_a is given by:

$$(Q/L)/(B/H_a) = 1 + \frac{\Delta}{L}\left[\frac{NH_c}{(N-1)H_c - H_e}\right] A(H_e) \qquad (54)$$

Figure (4) shows the expected behavior of Q/L versus B/H_a for a positive surface energy. The second term in (54) must vanish at the endpoints of the transition.

E. MIXED STATE

The mixed state exists in the absence of the geometric considerations which lead to the intermediate state. The interphase boundary energy is negative for $\kappa > 1/\sqrt{2}$ and the state of lowest free energy is attained when a material has divided itself into normal and superconducting regions on the finest scale possible. Ultimately, the quantization of flux limits this process of subdivision.

1. GOODMAN'S MODEL

Goodman treats the mixes state as alternate laminae of normal and superconducting material [21][9] . The situation is similar to that depicted in figure (3), page 20, and the same nomenclature will be used here. The normal laminae are extremely thin ($d_n \sim 2\xi$), and the field in the normal regions is H_a. The penetration of the field into the superconducting laminae is significant, and the London equations (22) are assumed to hold. The solution to London's equations has been

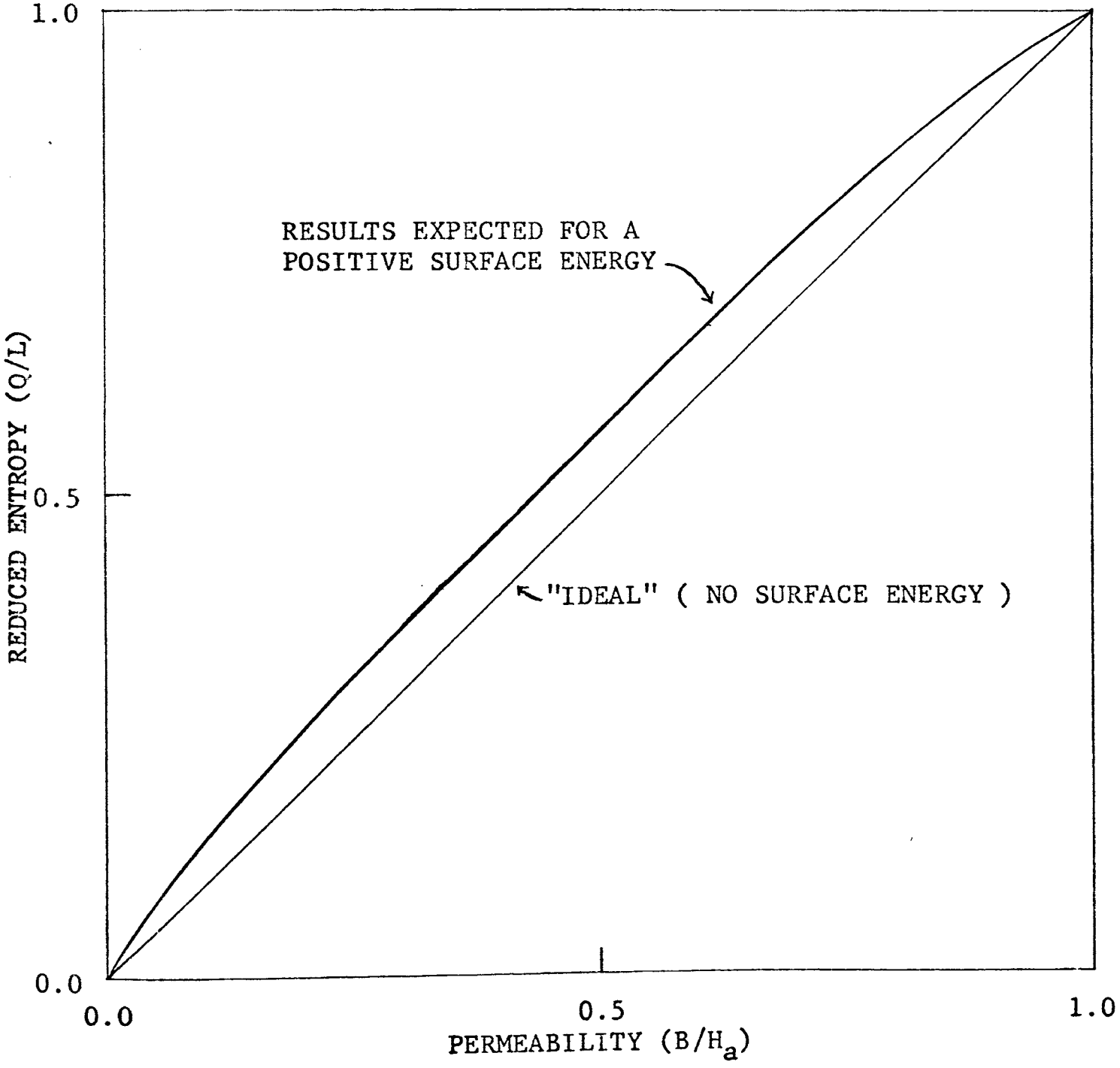

FIGURE 4. Q/L Versus B/H for positive Δ

worked out elsewhere for the case of an infinite plane slab in a uniform parallel applied field [26]. The magnetization of a slab of thickness d_s is given by:

$$-4\pi M_s = H_a \left(1 - \frac{\tanh p}{p}\right) \tag{55}$$

where p is the ratio of d_s to 2λ .

The magnetization of a material divided into normal and superconducting laminae is then given by:

$$-4\pi M = H_a \left(1 - \frac{\tanh p}{p}\right) \tag{56}$$

The free energy of the material can be constructed by adding a term due to penetration of the field into the superconducting laminae and a term due to the interphase surface free energy to equation (9) to get:

$$G(H_a) - G_s(0) = \frac{VH_c^2}{8\pi}\left\{1 - x\left[1 - \frac{q}{p} - h^2\left(1 - \frac{\tanh p}{p}\right)\right]\right\} \tag{57}$$

where h is the reduced field H_a/H_c.

q is the ratio of $\Delta-\lambda$ to λ .

The parameter q is closely related to 1/K of the G-L theory.

Minimizing the free energy with respect to p and h leads to two transition fields.

$$h' = q^{\frac{1}{2}} \qquad h'' + (1-h''^2)\tanh^{-1} h'' = q \tag{58}$$

Below h' (analogous to H_{c1}), the superconducting state is stable, and one finds x=1 and p= ∞ . Above h" (analogous to H_{c2}), the normal state is stable with x= 0 and p= 0 . For fields between h'and h", the laminar structure is stable, with p and x being determined from:

$$x = 1 \qquad q/h^2 = \tanh p - p \operatorname{sech}^2 p \tag{59}$$

The first condition implies that the normal laminae are of negligible thickness throughout the transition, and that the magnetization changes by virtue of changes in d_s. The second condition determines the equilibrium value of d_s for a given value of h. The free energy and equilibrium magnetization can be calculated knowing $d_s(h)$. Using (59) and (57), the free energy change upon applying field H_a is given by:

$$G(H_a) - G_s(0) = \frac{V H_a^2}{8\pi} \tanh^2 p \tag{60}$$

The entropy change is obtained using relation (8) as:

$$S(H_a) - S_s(0) = -\frac{V H_a^2}{4\pi} \tanh p \operatorname{sech}^2 p \frac{dp}{dT} \tag{61}$$

An expression for dp/dT is obtained by differentiating (59) with respect to T to get:

$$\frac{dp}{dT} = \frac{q H_c}{p \operatorname{sech}^2 p \tanh p H_a^2} \frac{dH_c}{dT} \tag{62}$$

Substituting (62) into (61) and multiplying by T leads to:

$$Q = -\frac{V T H_c}{4\pi} \frac{dH_c}{dT} \frac{q}{p} \tag{63}$$

Using equation (20) for L, the ratio of Q to L is obtained from (63) as:

$$\frac{Q}{L} = \frac{q}{p} \tag{64}$$

The induction B is obtained from (13) and (56) with x equal to unity:

$$B = H_a \left(\frac{\tanh p}{p}\right) \tag{65}$$

The ratio of Q/L to B/H_a is therefore given by:

$$(Q/L)/(B/H_a) = \frac{q}{\tanh p} \tag{66}$$

The value of tanh p is approximately equal to p for small values of p, and unity for large values of p. For the beginning of the transition, p is very large, so the initial slope of the B/H versus Q/L curve should be q. Figure (5) shows the behavior expected for q=.35 and h''=2, which corresponds to Pb-5%Tl at 1.82°. A discussion of the preceeding derivation is also found in the research proposal which lead to the funding of this work [27].

2. VORTEX MODEL

The structure of the vortex phase was first deduced by Abrikosov in 1957. The magnetic field penetrates a type II superconductor in the form of quantized supercurrent vortices. Each vortex interacts with other vortices repulsively, leading to the formation of a periodic, two-dimensional arrangement of the vortices in the plane normal to the direction of the field. Each vortex consists of a core surrounded by circulating supercurrents which shield the bulk material from the magnetic field in the core. The core has a radius approximately equal to the coherence length, and the material at the axis of the core is normal. The screening currents which circulate about the core follow the contours of the order parameter, and have appreciable magnitude up to about a penetration depth from the axis of the core. The order parameter must be single valued with respect to circulation about a core, so the total

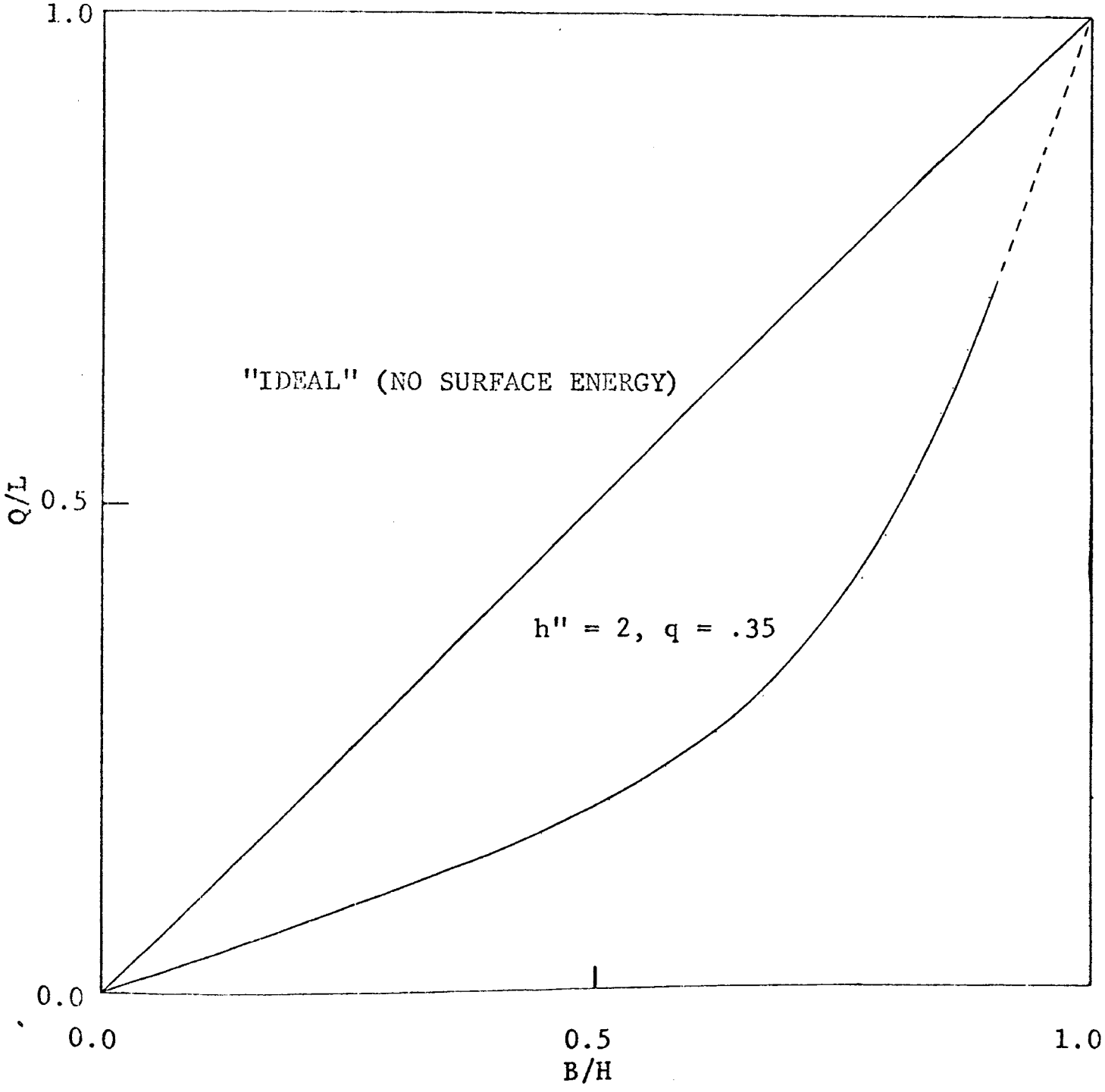

FIGURE 5. Behavior predicted by Goodman's model

flux linking the core must be equal to ϕ_o, the flux quantum. A vortex may be pinned by structural defects or inhomogeneities, so that irreversible work must be done to magnetize a body containing such imperfections.

The solution to the G-L equations which predicts the properties and structure of the vortex state has been obtained and reported elsewhere, and only the pertinent results will be mentioned here [5][21]. The induction in the bulk material must be given by:

$$B = n\phi_o \tag{67}$$

where n is the number of vortices per unit area.

ϕ_o is the flux quantum, 2.07×10^{-7} gauss/cm^2.

The upper transition field is related to the thermodynamic critical field by:

$$H_{c2} = \sqrt{2}\, \kappa H_c \tag{68}$$

This relation also serves to determine K when H_c and H_{c2} are obtained from the equilibrium magnetization curve. The lower transition field is given for large values of K by:

$$H_{c1} = \frac{\phi_o}{4\pi\lambda^2} (\ln \kappa + 0.081) \tag{69}$$

The transition to the normal state is of the second order, and the magnetization varies linearly with applied field near H_{c2}. The magnetization near H_{c2} is given by:

$$-4\pi M = \frac{H_{c2} - H_a}{1.16(2\kappa^2 - 1)} \tag{70}$$

The slope of the magnetization curve at H_{c2} can be used to

determine K by the preceeding relation. The value of K can not be determined from (69), since H_{c1} is extremely sensitive to structural flaws. The interaction potential between two vortex lines ar r_1, and r_2 is given by:

$$V_{12} = \frac{\phi_0}{8\pi^2\lambda^2} K_0\left(\frac{|r_1 - r_2|}{\lambda}\right) \tag{71}$$

where K_0 is the Bessel function that vanishes exponentially for large values of its arguement.

This is precisely the interaction which leads to the formation of a lattice of lines. The range of this potential is approximately equal to the penetration depth. As was pointed out earlier, only a lattice posessing six fold symmetry is dynamically stable, and such a structure has actually been observed in neutron diffraction experiments [28]. The triangular lattice in a strong field and the structure of a flux line is shown in figure (6).

The calculation of the thermodynamic properties of a lattice of vortices falls into three distinct field regimes:

$$H_a \geq H_{c1} \qquad H_{c1} \ll H_a \ll H_{c2} \qquad H_a \leq H_{c2} \tag{72}$$

The simplest case to analyze is the latter, for which the magnetization is given by equation (70). Substituting (70) into (9) leads to:

$$G(H_a) - G(H_{c2}) = -\frac{(H_{c2} - H_a)^2}{8\pi}\left\{1.16(2\kappa^2 - 1)\right\}^{-1} \tag{73}$$

The entropy difference is obtained by substituting (73) into (8) to get:

$$S(H_a) - S(H_{c2}) = -\frac{(H_{c2} - H_a)}{4\pi}\left\{1.16(2\kappa^2 - 1)\right\}^{-1}\left(\frac{dH_{c2}}{dT}\right) - \frac{(H_{c2} - H_a)^2}{2\pi}\left\{1.16(2\kappa^2 - 1)\right\}^{-1} K\frac{dK}{dT} \tag{74}$$

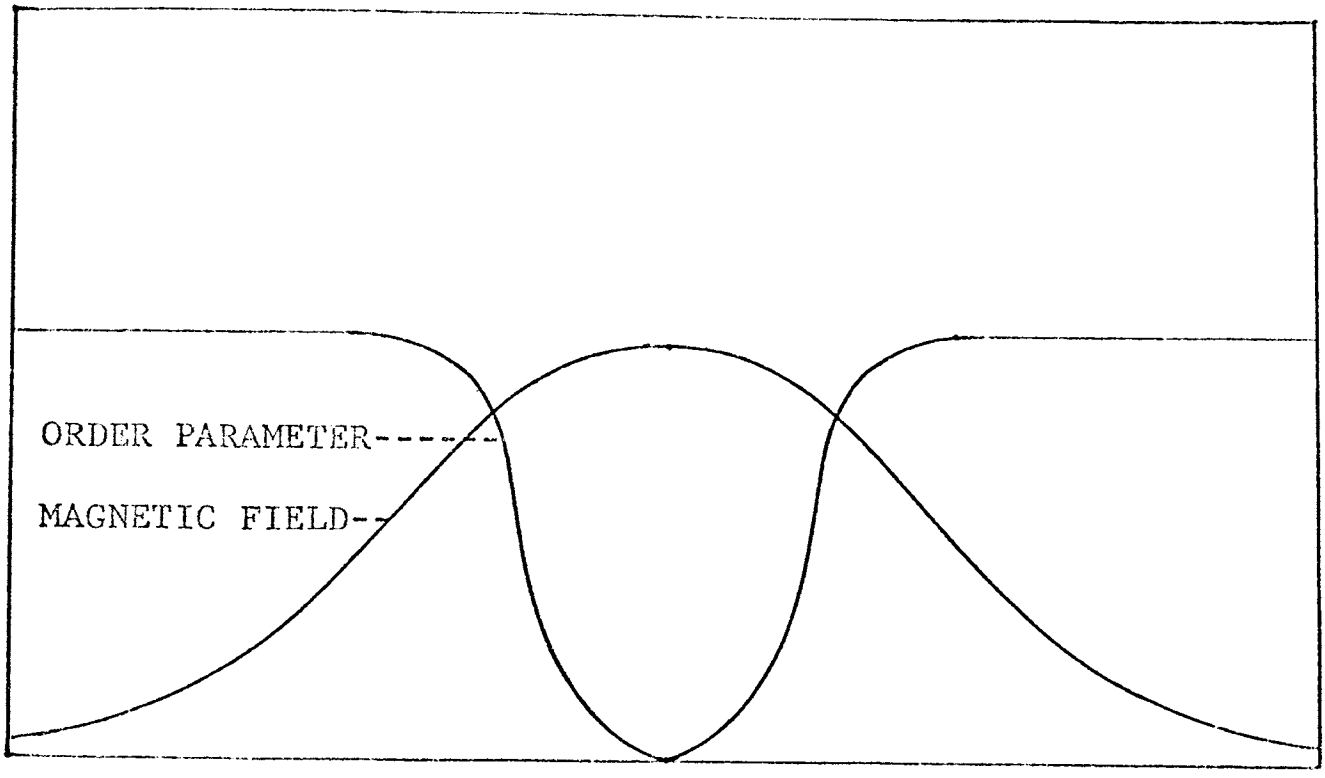

STRUCTURE OF A VORTEX CORE

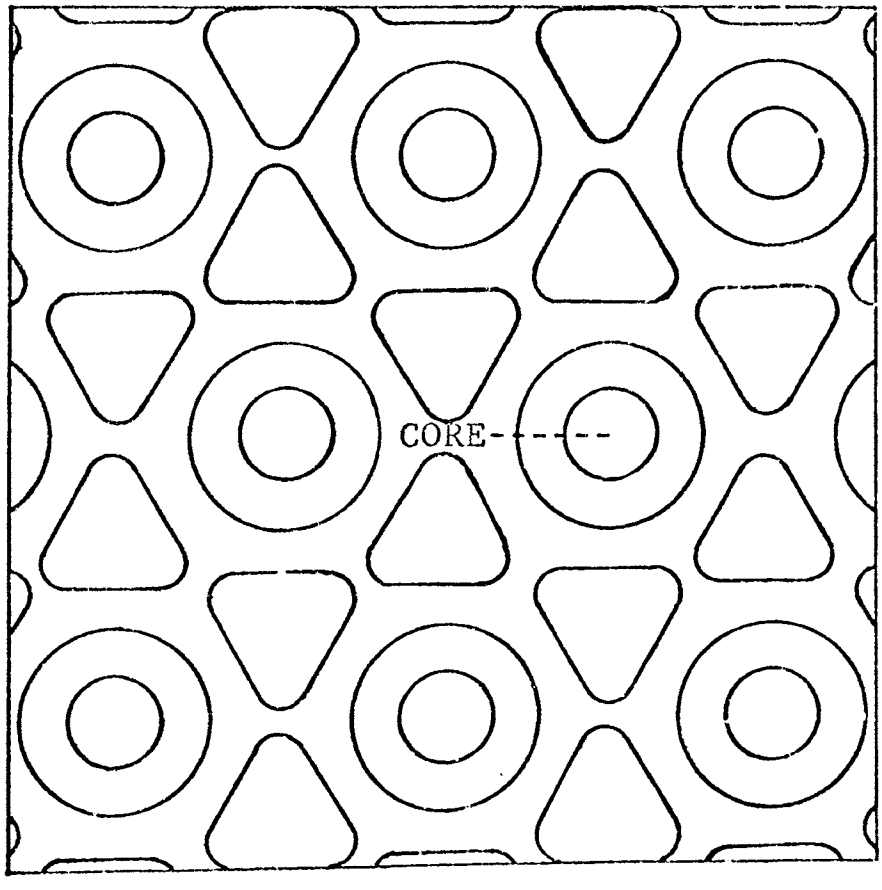

VORTEX PHASE NEAR H_{c2}

FIGURE 6. Vortex core and vortex phase in high field

The entropy difference depends linearly on $H_{c2}-H_a$ near T_c, where K is constant. If Q* is the heat which must be supplied per unit volume to maintain isothermal conditions while increasing the applied field from H_a to H_{c2}, Q* is given by:

$$Q^* = -\frac{H_{c2}-H_a}{4\pi}\left\{1.16(2\kappa^2-1)\right\}^{-1} T\frac{dH_{c2}}{dT} - \frac{(H_{c2}-H_a)^2}{2\pi}\left\{1.16(2\kappa^2-1)^2\right\}^{-1} kT\frac{d\kappa}{dT} \qquad (75)$$

Equation (75) predicts that Q* will depend linearly on $H_{c2}-H_a$ very near H_{c2}, and that a correction depending on the square of $H_{c2}-H_a$ becomes important as $H_{c2}-H_a$ increases.

In the intermediate field range, A. L. Fetter has derived useful expressions for the free energy and induction of an extreme type II superconductor [8]. In the intermediate field range, the flux lines interact appreciably, and the interaction energy contributes to the free energy. Fetter evaluates the interaction energy by the use of lattice sums over the two-dimensional, periodic configuration assumed by the vortices. His expression for the Gibbs free energy of a triangular lattice is:

$$G(H_a)-G(H_{c1}) = -\frac{(H_a-H_{c1})^2}{8\pi} - \frac{(H_a-H_{c1})\phi_0}{32\pi^2\lambda^2}\left\{\ln\frac{\lambda^2(H_a-H_{c1})}{\phi_0} + 2.874\right\} \qquad (76)$$

The entropy difference is again obtained from equation (8), and considering λ and H_{c1} to be temperature dependent, the entropy difference is given by:

$$\Delta S = \frac{H_a-H_{c1}}{4\pi}\left(-\frac{dH_{c1}}{dT}\right) + \frac{\phi_0}{32\pi^2\lambda^2}\left\{\ln\frac{\lambda^2(H_a-H_{c1})}{\phi_0} + 3.874\right\}\left(-\frac{dH_{c1}}{dT}\right) \qquad (77)$$

$$+ \frac{(H_a-H_{c1})\phi_0}{16\pi^2\lambda^3}\left\{\ln\frac{\lambda^2(H_a-H_{c1})}{\phi_0} + 1.874\right\}\left(-\frac{d\lambda}{dT}\right)$$

A close examination of the second and third terms on the right

indicates that they are dimensionally compatible, and that the third term will be several orders of magnitude larger than the second. The energy, Q, which must be supplied per unit volume to increase the field isothermally from H_{c1} to H_a is given by:

$$Q = \frac{H_a - H_{c1}}{4\pi}\left(-T\frac{dH_{c1}}{dT}\right) + \frac{(H_a - H_{c1})\phi_o}{32\pi^2\lambda^3}\left\{\ln\frac{\lambda^2(H_a - H_{c1})}{\phi_o} + 1.874\right\}\left(-T\frac{d\lambda}{dT}\right) \qquad (78)$$

Equation (78) predicts that in the intermediate field range Q depends linearly on H_a-H_{c1}, with a correction term of the form ax ln bx. Verification of (78) amounts to being able to fit $Q(H_a-H_{c1})$ with an expression of the form x + ax ln bx reasonably well in the intermediate field range.

The theoretical situation near H_{c1} is far less clear. When H_{c1} is exceeded, a large number of vortices nucleate at the surface and begin to penetrate the interior of a body. The exact dependence of $B(H_a)$ on H_a depends on the lattice chosen (29). The interactions between flux lines near H_{c1} are weaker than their interactions with structural defects, so the observed form of $B(H_a)$ is very sensitive to the presence of crystalline imperfections. Moreover, the exact nature of the transition to the mixed state is uncertain. Goodman has suggested that the specific heat discontinuity at H_{c1} is of the λ type for a bulk type II material, but has a finite value in the presence of demagnetizing effects [30]. DeSorbo and Healy have demonstrated that the transition to the mixed state

is not abrupt in bodies having finite demagnetizing factors, but rather that a well defined phase boundary exists, and that a structure not unlike the intermediate state is established in the external applied field range (1-N) $H_{c1} < H_e < H_{c1}$ [31]. A question immediately arises as to how such a structure can exist if the surface free energy is negative. Such a structure could result if the flux lines were pinned to any extent in the bulk material.

Regardless of the exact form of $B(H_a)$, a prediction for the behavior of Q/L as a function of B/H_a can be made assuming that the flux lines interact negligibly. The ratio of B to H_a must always depend linearly on B in the limit of small B. That is, B/H_a depends linearly on the number density of flux lines near H_{e1}. If the flux lines are non-interacting, each flux line contributes the same "negative surface energy per unit length", and the total negative surface energy is proportional to the density of flux lines. The ideal Q is given by B/H_a times L, and the measured Q is equal to the ideal Q minus the surface energy and any irreversible work done on the sample. Neglecting any irreversible work done magnetizing the sample, the ratio of the measured Q to L is therefore linearly dependent on the density of flux lines. The conclusion is that for small values of B, Q/L should depend linearly on B/H_a.

The predictions of this section are strictly valid only for extreme type II materials, while the alloy studied had a K on the order of unity. The G-L equations can not be solved, even when linearized, for low-K materials. Apparently, efforts to obtain numerical solutions of the G-L equations for small values of K have also met with failure. A single exception was found in the literature. J. L. Harden and V. Arp applied numerical techniques to obtain the ratios H_{c1}/H_c and H_{c2}/H_c as functions of K [32]. There appears to be a consensus among workers in the field that the nature of type II superconductivity is not essentially different over the entire domain $K > 1/\sqrt{2}$. It is certainly worthwhile to interpret results obtained on low-K alloys in the light of predictions based on the solution of the linearized G-L equations for large values of K. There is certainly no shortage of precedents for such a procedure.

II EXPERIMENTAL METHOD

A. INTRODUCTION

The experiment consisted basically of simultaneously monitoring the magnetization and electrical energy supplied to an adiabatically mounted sample during an isothermal transition. The experiment was performed using two different techniques. In one method a magnetization curve was first obtained by the thermal pulse technique. Then a constant heating power was supplied electrically to the sample, and isothermal conditions were maintained by manually increasing the applied field so that diamagnetic cooling balanced the applied heating. The magnetization was determined as a function of time from a recording of the solenoid current and the magnetization curve. The heat required to isothermally magnetize the sample, Q, was determined from the applied heating rate, the heat leak, and time elapsed. The latent heat, L, was taken to be the value of Q when the applied field reached H_{c2}.

In the other method the applied field was increased at a constant rate, and the heating power was manually adjusted to maintain isothermal conditions. The voltage induced in a pickup coil surrounding the sample and the current supplied to a heater wound on the sample were recorded simultaneously. Magnetization was determined as a function of applied field

by the flux integration technique, and Q was obtained by integrating the heater power. Data taken by these methods were then reduced for comparison with theoretical predictions, and a check was made to determine whether results obtained by the different methods agreed.

The apparatus consisted of a cryostat, magnetization calorimeter, and associated equipment. The apparatus is shown schematically in figure (7) with alternate arrangements indicated. The cryostat consisted of a pair of nested nitrogen and helium dewars, a manostat, manometer, gauges, and a large vacuum pump. The magnetization calorimeter consisted of a brass can connected to an external vacuum system within which the samples were suspended, adiabatically mounted in a pick up coil. A homogeneous magnetic field was supplied by a corrected superconducting solenoid and current regulated power supply. The temperature was measured by a mercury manometer and a ½ watt carbon resistor attached to the sample. Magnetization was measured by a ballistic galvanometer connected to the pickup coil, or by recording the voltage induced in the pickup coil as flux penetrated the sample. The power supplied to the heater was monitored by measuring or recording the voltage drop across a standard resistor in series with the heater. Each aspect of the experiment will now be discussed in detail.

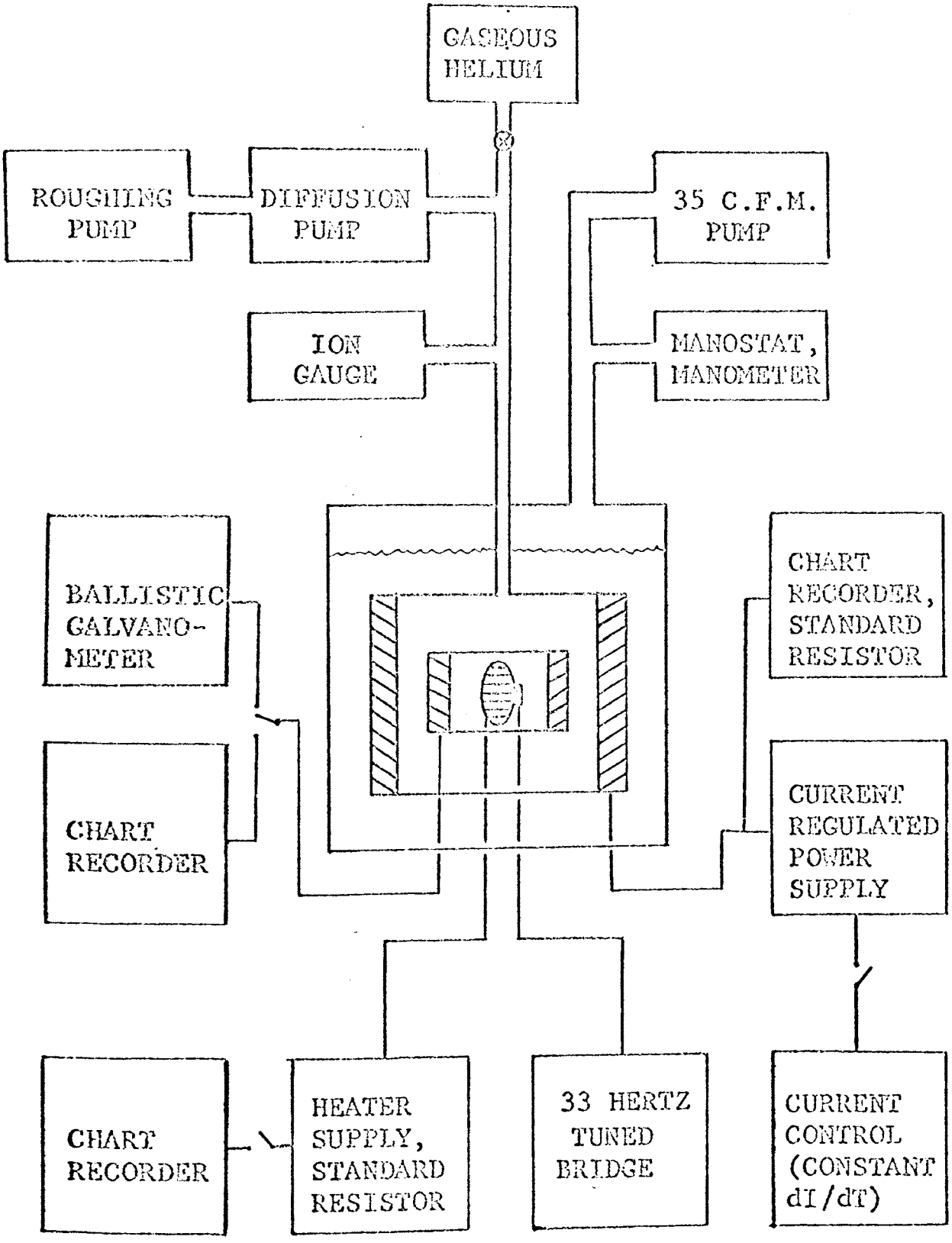

FIGURE 7. Schematic diagram of apparatus

B. TEMPERATURE MEASUREMENTS

The temperature of the sample was determined by measuring the resistance of a ½ watt Allen-Bradley carbon resistor with a 33 cycle A. C. Wheatstone bridge. The null detector was a narrow band amplifier designed by Blake, Chase, and Maxwell (33). The output of the null detector was displayed on an oscilloscope, and the sweep was triggered by the output of the oscillator that drove the bridge. The phase of the null detector output shifted by 180° when the bridge passed through balance, so it was possible to determine at a glance whether the sample was hotter or colder than the bridge setting. It was possible to detect resistance changes of a few tenths of an ohm near 4°K, where a typical resistance value was about 900 ohms, or a few ohms near 2°K, where a typical resistance value was about 6000 ohms. This degradation of precision was due to stray capacitance which obscured the null; however, the change in resistance with temperature increases very rapidly as the temperature is lowered, so that the ability to detect temperature changes was not degraded. The temperature dependence of a carbon resistor can be expressed by a two, three, or four parameter empirical relation. A simple two parameter empirical relation is given by:

$$\sqrt{\frac{\log R}{T}} = a + b \log R \qquad (79)$$

A carbon resistor must be calibrated each time it is immersed in liquid helium. The resistors used in this experiment were calibrated against the vapor pressure of the helium bath using the 1958 H_e^4 Scale of Temperature (34). The vapor pressure of the helium bath was measured to the nearest half millimeter of mercury with a mercury manometer. A correction was applied to account for the hydrostatic pressure at the sample depth. The temperature could be determined to within a few millidegrees near 4.2°K and to the nearest hundredth of a degree near 2°K.

The resistor and an Evanohm heater were securely attached to the sample with GE 7031 varnish thinned to a convenient consistency with toluene. This varnish not only provides a firm mechanical bond, but also insures good thermal contact. The plastic case was ground off all the resistors to reduce the time required to respond to temperature changes. A resistor responded immediately when current was passed through the heater. An order of magnitude calculation was made to estimate the maximum temperature differences within the sample and the time required to establish a steady state temperature distribution. The heat equation with a volume generation term to account for diamagnetic cooling was solved for an infinite cylinder having the diameter equal to the minor axis of the sample (35). The temperature at the surface was assumed

to remain constant, and typical published values for the thermal conductivity and heat capacity of lead and tin were used in the calculations. The results are summarized in table I.

TABLE I

Maximum Temperature Differences and Relaxation Times

Material	Temp.	Max. Temp. Diff.	Relaxation Time
Pb	4.0°K	3.5×10^{-7} °K	1.5×10^{-5} sec.
Pb	2.0°K	4.5×10^{-7} °K	3.2×10^{-5} sec.
S_n	3.5°K	8.8×10^{-10} °K	3.4×10^{-6} sec.
S_n	2.0°K	1.5×10^{-7} °K	1.6×10^{-5} sec.

On the basis of this calculation it appears that the samples quickly established steady state conditions and that temperature variations within the samples were not large. The limiting factor encountered in the effort to maintain isothermal conditions was the ability of the operator to respond to temperature changes. It is believed that isothermal conditions were maintained to within 0.001°K during the better runs.

C. TEMPERATURE REGULATION

The desired temperature was achieved by pumping on the helium bath with a 35 c.f.m. vacuum pump. The vapor pressure of the bath could be read on two gauges and a mercury manometer.

A CVC gauge covered the range from 0 to 700 torr, and a Wallace-Tierman gauge covered the range from 0 to 400 torr. The gauges were not consistent, and were calibrated against the manometer. It was found that the Wallace-Tierman gauge agreed with the manometer as closely as could be read. The vapor pressure was regulated by a manostat similar to that described by M. M. Kreitman [36]. The performance of this simple diaphragm regulator surpassed all expectations. On one occasion, the vapor pressure remained constant at 730 torr for a period of nine hours. When the pilot model was set at 2°K, Kreitman observed no pressure drift with an oil manometer having an observational limit of .01 torr [36]. It is believed that the bath temperature drifted no more than a few millidegrees per hour when the manostat was working properly.

D. MAGNETIZATION MEASUREMENTS

The construction details of the magnetization calorimeter are shown in figure (8). The samples were mounted with plastic spacers in a pickup coil consisting of about 10^4 turns of #33 copper wire wound on a brass form 2.5" in length by 0.75" outer diameter. In the thermal pulse method, a current of about 100 milliamperes was suddenly sent through the heater windings. Since the heater resistance was about 100 ohms, electrical energy was dissipated in the heater

KEY TO FIGURE 8.

A. Thin wall stainless steel tube (0.5" x 0.010")

B. Electrical leads

C. Copper thermal ground post

D. Cadmium-bismuth solder joint

E. Superconducting solenoid (Corrected to produce 1% field homogeneity over a region 3.8" in length)

F. Nylon supporting cord

G. Ellipsoidal superconducting sample

H. Evanohm heater (0.005" wire, 12 ohms per foot)

I. Pickup coil (10^4 turns #33 copper wire on brass form 2.5" x .75")

J. Allen-Bradley ½ watt carbon resistor (56 ohms @ 300°K)

K. Brass coil form and retaining ring

L. Plastic spacer

M. Solenoid retainer plate

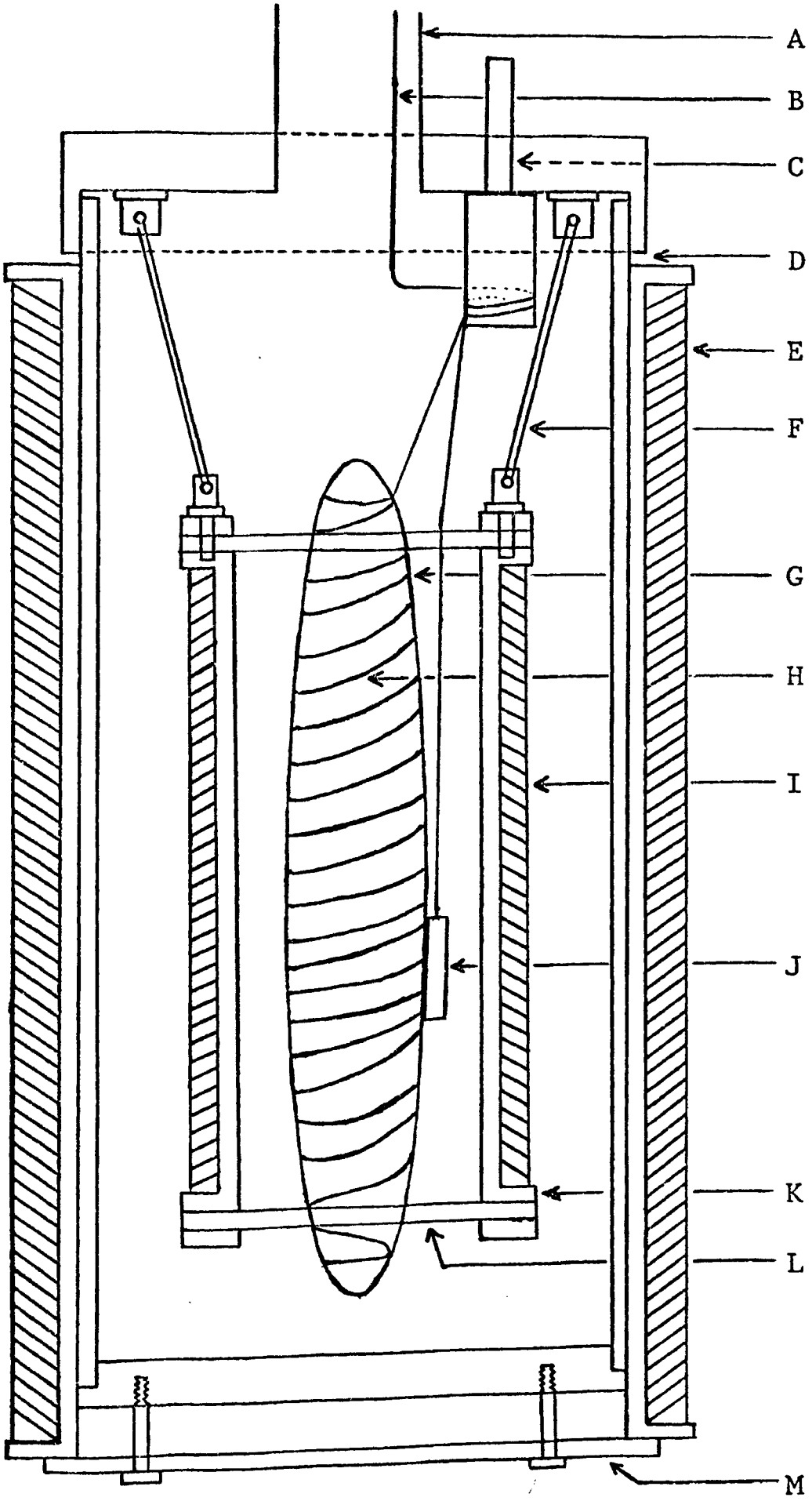

FIGURE 8. Magnetization calorimeter

at the rate of one joule per second. A calculation for lead based on heat capacity data reported by Clement and Quinnell shows that the sample should be driven normal in about three quarters of a second (37). The pickup coil was connected to a Leeds-Northrup model 2285 ballistic galvanometer. The deflection of the ballistic galvanometer when the sample is driven normal is proportional to the change in magnetization of the sample, provided the change occurs in a time short compared to the galvanometer period. The period of the galvanometer used in this work was about fifteen seconds, so the time criterion was satisfied. The galvanometer was calibrated by assuming a complete Meissner effect in applied fields less than $(1-N)\ H_{c1}$.

In the flux integration technique, the sample was driven through the transition by increasing the applied field at a constant rate under isothermal conditions. The voltage induced in the pickup coil was recorded on a Sargent model SRL chart recorder. The voltage induced in the coil, V, was due in part to the time rate of change of the applied field and in part to the time rate of change of the magnetization of the sample. The effect due to the sample alone was obtained by subtracting the voltage induced when the sample was normal, V_n, from V. The total change in magnetization during the transition is proportional to the area under the V-

V_n curve in the applied field range (1-N) H_{c1} to H_{c2}. The initial magnetization was calculated by assuming a complete Meissner effect for applied fields less than (1-N) H_{c1}. The magnetization for an applied field greater than (1-N) H_{c1} was then determined by measuring the area under $V-V_n$ from (1-N) H_{c1} to H_c with a planimeter. A magnetization curve was obtained for Pb-4at%Tl at 4.19°K using both methods, and the agreement was excellent.

F. MAGNETIC FIELD GENERATION

A superconducting solenoid corrected for end effects slipped over the calorimeter to provide a homogeneous magnetic field. The calorimeter with the solenoid in place is shown in plate (1). The solenoid consisted of ten layers of Supercon 0.010" copper clad niobium-zirconium wire wound on a brass form 7.0" in length by 1.6" outer diameter. Each layer consisted of approximately 470 turns, with half the turns left out of a section 2.7" long in the tenth layer to correct for end effects. The original intention had been to design a sixth order solenoid according to a procedure devised by Hopkins [38]. The length was to have been six inches, and the field was to have been homogeneous to within $\pm$ ½% over the volume of the sample. It proved impossible to attain these goals, so a longer solenoid corrected to fourth order was constructed. The axial field for this solenoid was

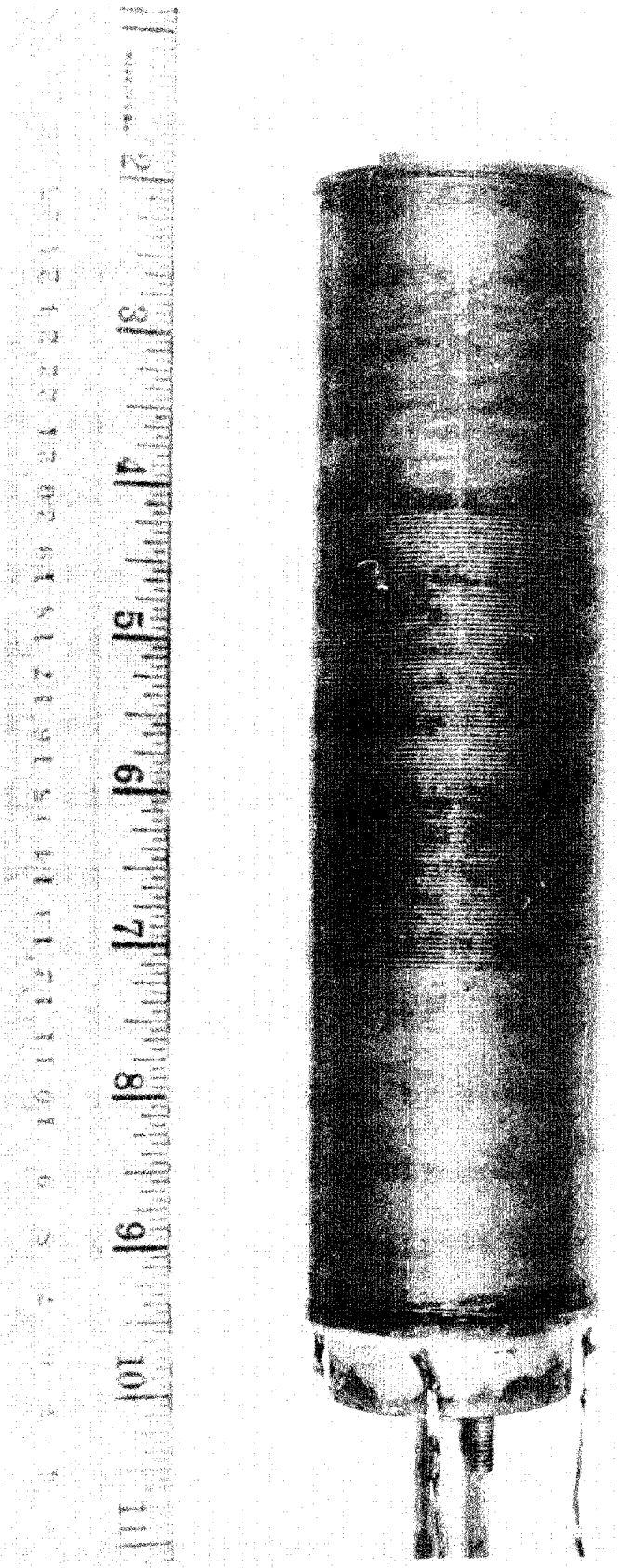

PLATE 1. Calorimeter with solenoid in place

computed using the tables of Mapother and Snyder for solenoids of finite thickness, and the field was uniform to ± ½% over a region 11.2 cm in length [51].

A shorted winding prevented immediate confirmation of this result, but did not prevent operation of the solenoid in the superconducting state. Repeated temperature cycling unshorted the windings, and the field homogeneity was measured at room temperature using a Bell "120" gaussmeter with a longitudinal Hall probe. The axial field was uniform to less than ± .1% over a region 8 cm in length and to less than ± ½% over a region slightly less than 11 cm in length. It was also ascertained that the samples (length 7.6cm) had been mounted entirely within the region of ± .1% homogeneity during the experiments.

The solenoid was calibrated against the critical field curves of lead and tin. The critical field curve of lead has been precisely determined by Decker, Mapother, and Shaw, who obtain a critical field polynomial [40]. The critical field curve of tin has been precisely determined by Shaw, Mapother, and Hopkins, who report raw data [41]. The critical fields were measured at several temperatures for the lead and tin samples, and the results were used to determine the solenoid constant from references (40) and (41). The average of 10 values gives 320.30 gauss/ampere for the solenoid constant with

a rms deviation of 1.95 gauss/ampere.

The solenoid current was supplied by a Harrison Laboratories model 6224A regulated power supply, which can be operated as a constant voltage or a constant current source. The maximum output current is about 3.7 amperes at an output voltage of up to 18 volts. The manufacturer claims 0.05% regulation in the constant current mode, but the actual regulation was about 0.01% when operated from a constant voltage transformer. There were provisions for remote operation, and since the panel controls were far too coarse to be used in calorimetric runs, the output current was remotely controlled by several 10 turn Helipot potentiometers. Output current changes of less than 100 microamperes were possible.

A constant rate of current increase was achieved by using a low speed induction motor to drive a 10 turn potentiometer which controlled the output current. A recording of the output current was very linear, but the instantaneous value of dI/dt fluctuated considerably. This problem was so serious that the flux integration technique was nearly abandoned. This difficulty was finally resolved by filtering techniques. The output current was fed through a 32 stage pi filter consisting of 4000 microfarad capacitors and twisted connecting leads. A 9000 microfarad capacitor was connected

across the 10 turn potentiometer to smooth the control voltage. A recording of voltage induced in the secondary of a mutual inductance connected to the power supply showed that dI/dt was constant with an acceptable noise level.

F. CALORIMETRIC MEASUREMENTS

The calorimetric measurements performed in this work consisted of monitoring the electric power dissipated in the heater windings. The heater consisted of about eight feet of Evanohm #32 wire (12.5 ohms/foot) wound bifilar on the sample as shown in plate (2) and attached to the surface with GE 7031 varnish to provide good thermal contact. The temperature dependence of Evanohm wire has been studied by Pandord, Lerner, and Daunt, who find that the resistivity varies less than 0.7% from room temperature to absolute zero [42]. The electrical leads going into the calorimeter were made of Evanohm #32 wire to reduce unwanted heat conduction.

The leads were wrapped around a copper post in contact with the bath and cemented down with GE 7031 varnish to provide a thermal ground. Niobium-zirconium wire was used for the three inch leads from the thermal ground to the heater during the tin runs, and Evanohm wire was used during the lead and lead-thallium runs. A correction was made for heat generated in the leads between the sample and the thermal ground. No correction was necessary when superconducting

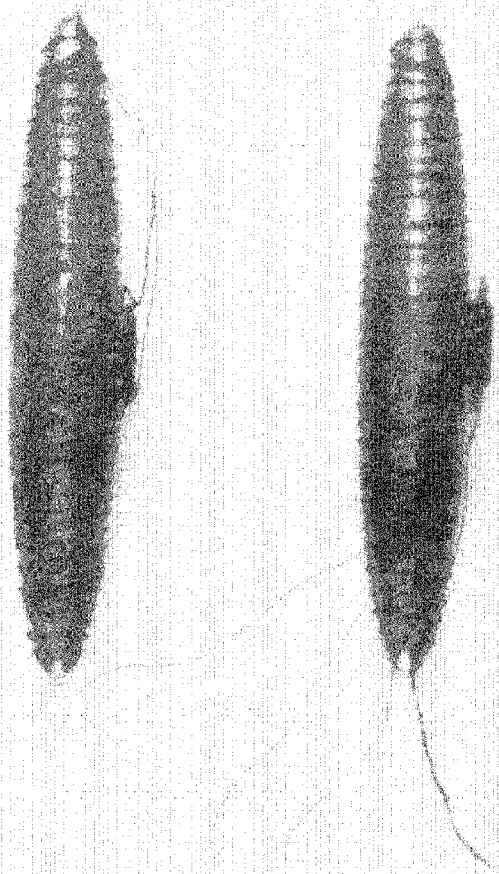

PLATE 2. Samples

leads were used.

Adiabatic conditions were established by pumping the exchange gas out of the calorimeter with an external vacuum system which could pump down to less than 5×10^{-6} torr when cold trapped. The pressure in the calorimeter was somewhat higher due to the pressure drop along the connecting line, but good thermal isolation never seemed to be a problem. In early experiments radiation coming down the vacuum line was a serious source of heat, so a blackened copper radiation baffle was attached to the copper grounding post to shield the sample from the opening of the vacuum line. The inner walls of the calorimeter were painted with India ink to absorb stray radiation. At first it was thought that vibratio might be a serious source of spurious heating, so the sample and pickup coil were suspended by bronze springs to damp external vibrations. However, vibration proved to be no problem, so the springs were then replaced by nylon threads. The heat leak due to operation of the resistance bridge was calculated to be about 0.2 ergs per second. When good thermal contact with the bath was desired, the vacuum system was closed off from the calorimeter and helium gas was admitted.

Calorimetric measurements were made in two different ways. After a magnetization curve was plotted using the thermal pulse method, the exchange gas was pumped out to

establish adiabatic conditions. The bath pressure was lowered until a slight heater current was required to maintain isothermal conditions. The current in the heater was determined by measuring the voltage across a 10 ohm standard resistor in series with the heater with a Leeds-Northrup K3 potentiometer. Heater current was supplied by a Heath EUW-17 transistorized power supply operated from a constant voltage transformer. The solenoid current was increased to just below the point of initial flux penetration and the heat leak determined. The heater current was then increased to a constant value somewhat larger, and the solenoid current was increased manually to maintain isothermal conditions. The voltage drop across a 0.1 ohm standard resistor in series with the solenoid was recorded on the Sargent SRL chart recorder. When the transition was completed, the heat leak was again determined. The heat leak at any time during the transition was obtained by assuming that the heat leak varied linearly with time from the initial value to the final value. The value of Q was determined from the integral of the heater power minus the heat leak. The latent heat was taken as the value of Q at the end of the transition. The ratio B/H_a was determined as a function of time from the magnetization curve and the recording of the solenoid current.

Calorimetric and magnetic data were obtained simul-

taneously in the flux integration method. The exchange gas was pumped out, and the bath pressure was lowered until heater current was required to maintain a constant temperature. The solenoid current was then brought up to a value near the point of initial flux penetration. A Bausch and Lomb chart recorder connected in series with the heater was switched on, and the heater current was recorded for several minutes to establish the heat leak. The voltage induced in the pickup coil was being recorded on the Sargent SRL chart recorder. The solenoid current was then increased at a constant rate, and the heater current was manually adjusted to maintain isothermal conditions. The magnetization data were obtained from the recording of the voltage induced in the pickup coil, and the value of Q was obtained from the recording of the heater current.

G. SAMPLE PREPARATION

Four samples were prepared during the course of this work. These included pure lead, pure tin, lead-4at% thallium, and tin-6at%indium. The materials used were of high purity, and care was taken to avoid contamination during the preparation of the ingots. The sources of supply and purities of the materials used are given in table II.

TABLE II

Suppliers and purities of materials used

Material	Supplier	Purity
Pb	Leytess Metal and Chemical Co.	99.999%
Sn	Leico Industries Incorporated	99.999%
Tl	American Smelting and Refining Co.	99.98%
In	Indium Corporation of America	99.999%

The materials used were supplied in the form of rods and bars. The surfaces were cleaned using procedures recommended by the manufacturers. The rods and bars were then cut into pieces of convenient size and weight. Lead, thallium, and indium are soft metals, and were easily cut with clean shears. Tin is somewhat harder, and a hacksaw with a clean blade was used to cut the tin bars. The pieces were etched and washed to remove surface contamination introduced in the cutting process.

The first sample prepared was lead-4at%thallium, (4.04 at %) which was chosen for several reasons. Lead alloys are easy to prepare, and lead-thallium alloys have long been recognized as type II superconductors [43]. Lead and thallium form a single phase solid solution over a wide range of compositions [44]. These solutions have the face-centered cubic crystal structure of lead, and possess sharp melting points. The phase diagrams of the lead-thallium and tin-

indium systems as obtained from reference (44) are shown in figure 9. A dilute alloy was chosen so that the critical field would fall within the capability of the available power supply. It was also hoped that a higher degree of structural perfection might be achieved with a dilute alloy.

Lead and thallium were weighed on a torsion balance in sufficient quantities to produce a cylindrical ingot 4" in length by 0.65" in diameter having 4% thallium by weight. The lead and thallium were melted in vacuum in a pyrex tube having an inner diameter of 0.65". The pressure over the melt was held at about 10^{-5} torr, but noticeable amounts of oxide were formed and floated on the surface. There were provisions in the vacuum furnace for a pyrex stirring rod to be lowered into the melt. The alloy was allowed to solidify and melt several times with periods of thorough stirring in the molten state. The melt was finally allowed to solidify over a period of an hour, and the ingot was cooled to room temperature over a period of several hours. The ingot was removed, etched, and the density determined. The ingot had a density of 11.43 grams/cm^3, and the grain size appeared to be about a millimeter.

The ingot was then given to a machinist, who produced an ellipsoid of revolution having a major axis of 3" and a minor axis of ½". The sample was etched and annealed for 24 hours

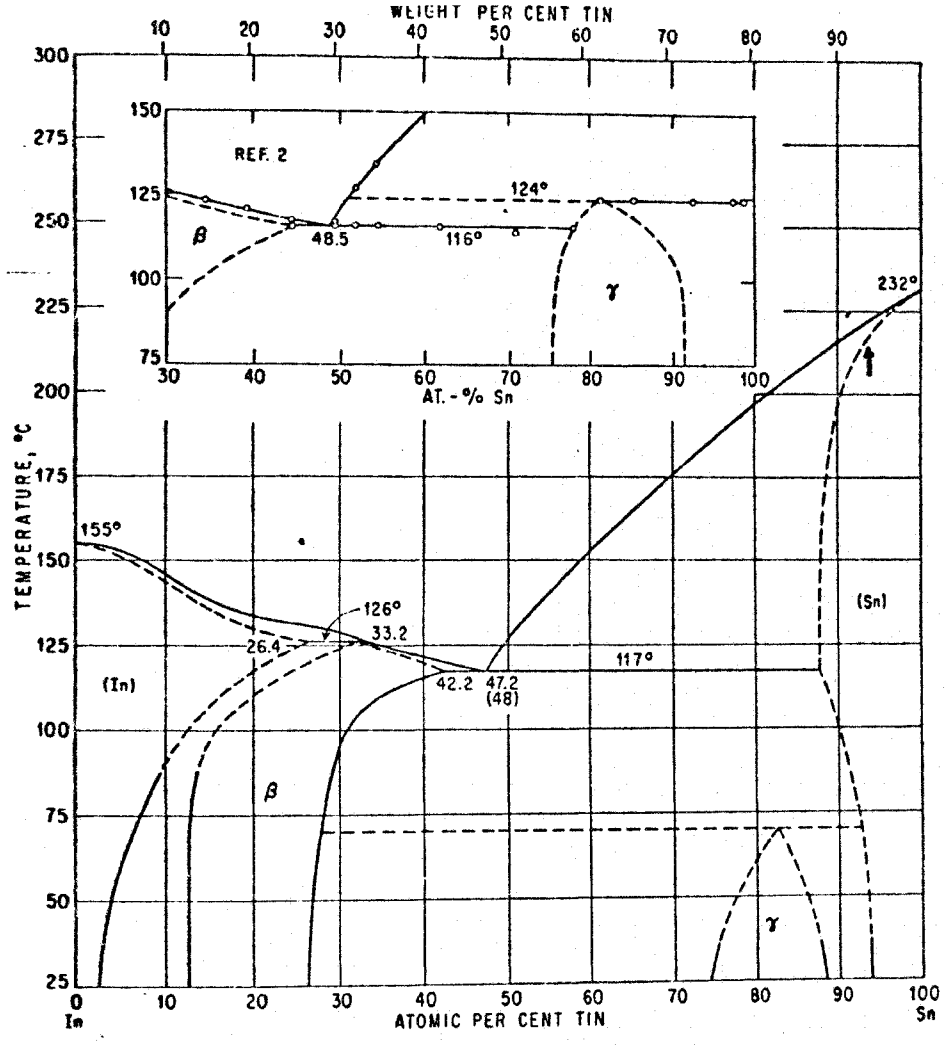

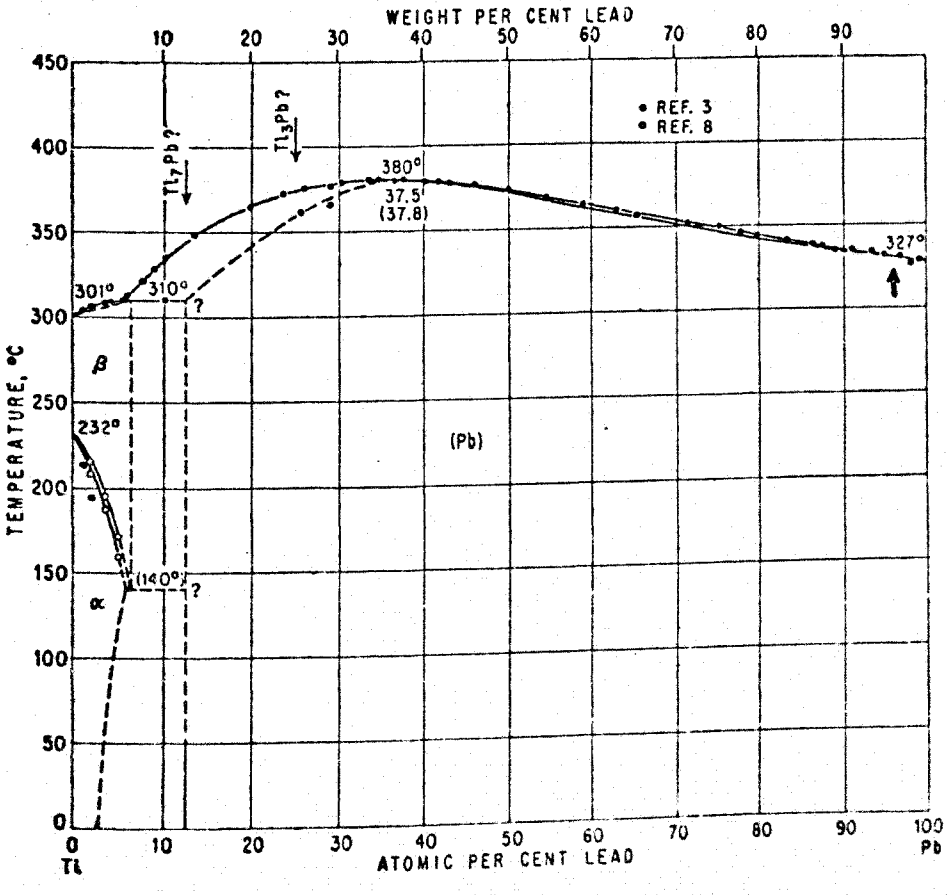

FIGURE 9. Phase diagrams of lead-thallium and tin-indium

at 300°C. The heater was wound on the surface and the carbon resistor attached with GE 7031 varnish. Care was taken to avoid straining the sample in the winding operation. After several months of measurements, it was decided to anneal this sample more carefully in the hope of improving its reverse transition. The heater and resistor were removed by soaking in acetone, and the sample was annealed in a pressure of 10^{-5} torr for 14 days at 315°C. The melting point is estimated from the phase diagram to be about 329°C. The surface was then polished using a chemical polish consisting of 70 parts glacial acetic acid and 30 parts 50% hydrogen peroxide as suggested by Livingston (45). A new resistor and heater were then attached to the sample using a fresh batch of GE 7031 varnish.

A pure lead sample of the same dimensions was prepared by melting pure lead in a pyrex tube having an inner diameter of 0.65" under vacuum. The melt was allowed to solidify over a period of several hours, and the ingot was slowly cooled to room temperature. The ingot was removed, etched, and given to the machinist, who produced an ellipsoid of revolution 3" by ½". The finished ellipsoid was etched to remove surface strains, and annealed for 24 hours at 300°C. The sample was then fitted with a heater and thermometer resistor. After several months the heater and resistor were removed, and the

sample was polished with the polishing agent mentioned previously. A new heater and resistor were then attached to the sample.

A pure tin sample was prepared by turning an ellipsoid from the bar stock furnished by Leico. This was not the original intention, however. A tin ingot was prepared using the same method as lead. The melt was allowed to freeze over a period of about 24 hours, and the ingot was slowly cooled to room temperature. A very deep etch was made with a solution of 95 parts ethanol and 5 parts fuming nitric acid (nital), and no grain boundaries were revealed. The density of the ingot was 7.29 grams/cm^3, which is exactly the value given by the CRC Handbook for single crystal tin. Unfortunately, the machinist attempted too deep a cut, and the tool dug into the ingot, bending it badly. Therefore a sample was prepared using the bar stock furnished by Leico. The finished ellipsoid was etched and annealed for 24 hours at 200°C. The grain size appeared to be a few millimeters in the original bar stock. A heater and resistor were attached to the surface with GE 7031 varnish. Superconducting leads made of niobium-zirconium wire were used to connect directly to the heater.

A tin-6wt%indium (6.19 at %) sample was prepared in the hope of obtaining a more reversible type II sample. Work

performed in single crystal samples showed type II behavior for several percent indium in tin with fairly reversible transitions [46]. An effort to produce a single crystal sample failed miserably since indium and tin segregate when a melt is slowly cooled. Homogeneity was achieved by quickly freezing the melt, and slowly cooling the ingot to room temperature. An etch revealed grain sizes ranging from a millimeter down. It appeared that the indium had been concentrated at the grain boundaries. An ellipsoid was made from the ingot. An attempt was made to electropolish the surface in a crude cell, but it proved impossible to establish uniform polishing conditions. The sample was then annealed several days in vacuum at 210°C. The surface was etched one final time, and the heater and resistor cemented in place. Two of the samples prepared in this work were shown in plate 1.

III RESULTS AND DISCUSSION

A. INTRODUCTION

The results obtained on type I materials will be discussed first to establish the validity of the experimental procedure. Calorimetric and magnetic data for lead and tin were generally quite plausible and seemed to verify the validity of the procedure. The positive surface energy expected from theoretical considerations was not directly detected, but calculations show that the effect would be small. The measured latent heats of transition agreed closely with values deduced from the critical field curves reported in references (40) and (41). It appeared that the transitions were sufficiently reversible to be analyzed thermodynamically without correction.

The results obtained with Pb-4%Tl were consistent with the negative surface energy models of the mixed state. The magnetization data taken were consistent with results reported by other authors on the Pb-Tl system. A peculiar feature was noted in magnetic data taken after a careful annealing, and a plausible explanation is offered. The magnetization data taken shows considerable irreversibility, but the curves obtained were quite similar to those reported by other authors. The calorimetric results are compared to the predictions of chapter I and the experimental results of

Otter. The results obtained with Sn-6% In are described, but the sample was too hysteretic to yield meaningful data.

B. LEAD

Magnetic and calorimetric data were taken for lead using both the thermal pulse method and the flux integration method. The magnetization curves obtained by both methods agree closely with equation (49). Figure (10) shows an expanded transition at 4.18°K taken by both methods. The agreement between the methods is excellent, although the data points are somewhat smoother with the flux integration method. The magnetic data taken this way are also considerably more reproducible. The inherent reproducibility of the ballistic galvanometer was about 1%, while the data obtained from the flux integration method were reproducible to within a few tenths of a percent. Magnetization curves at several temperatures are shown in figure (11). A complete reverse transition was obtained only for 4.18°K, but the remanent magnetization was measured for several temperatures. The remnant was about 3% of the maximum magnetization at 4.18°K, and appeared to remain constant with temperature.

The latent heat was measured at several temperatures in the course of calorimetric measurements. The latent heat was calculated from equation (20) and the critical field curve reported in reference (40). The measured values are compared

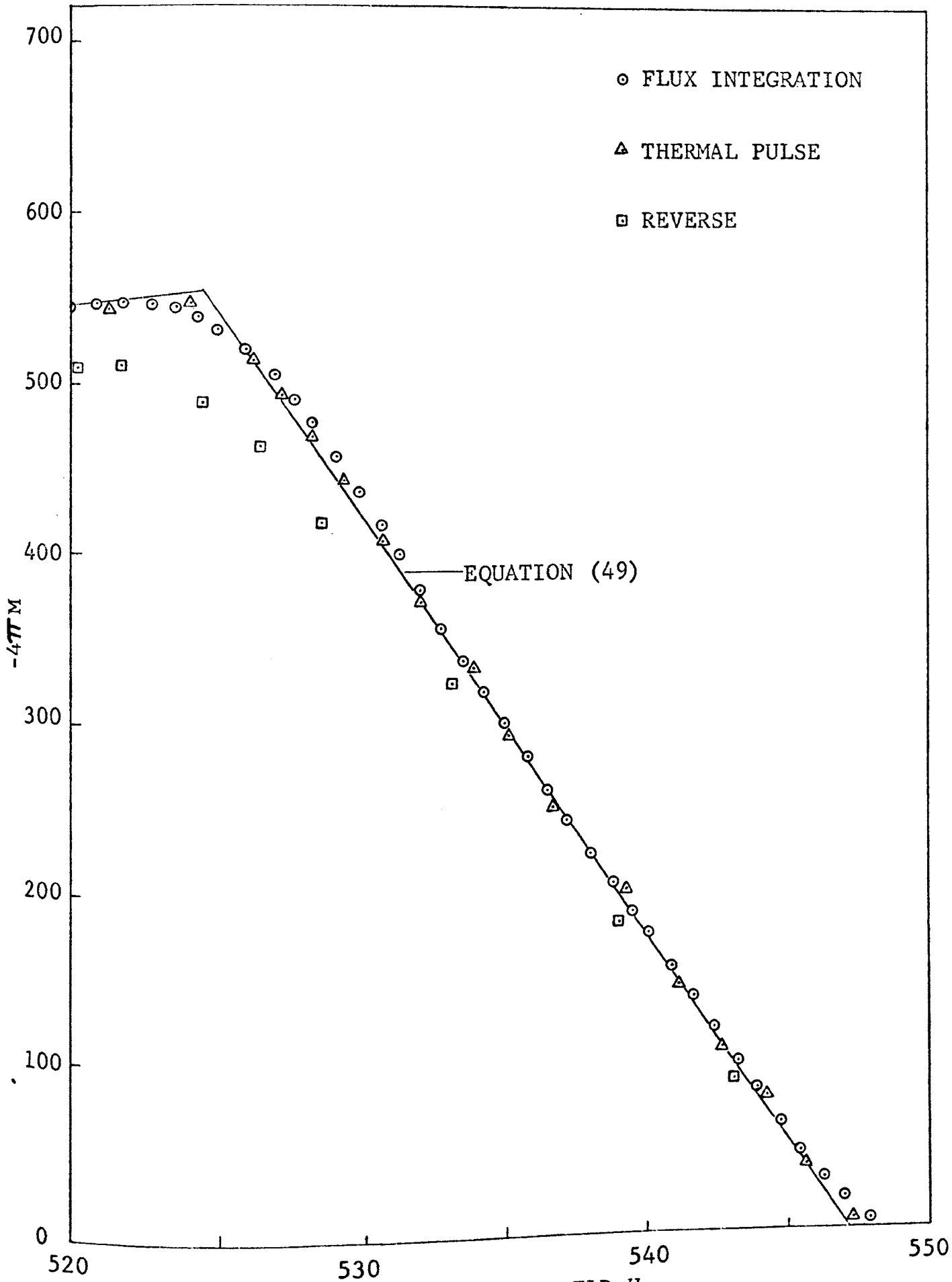

FIGURE 10. Magnetization curve of lead at 4.18°K

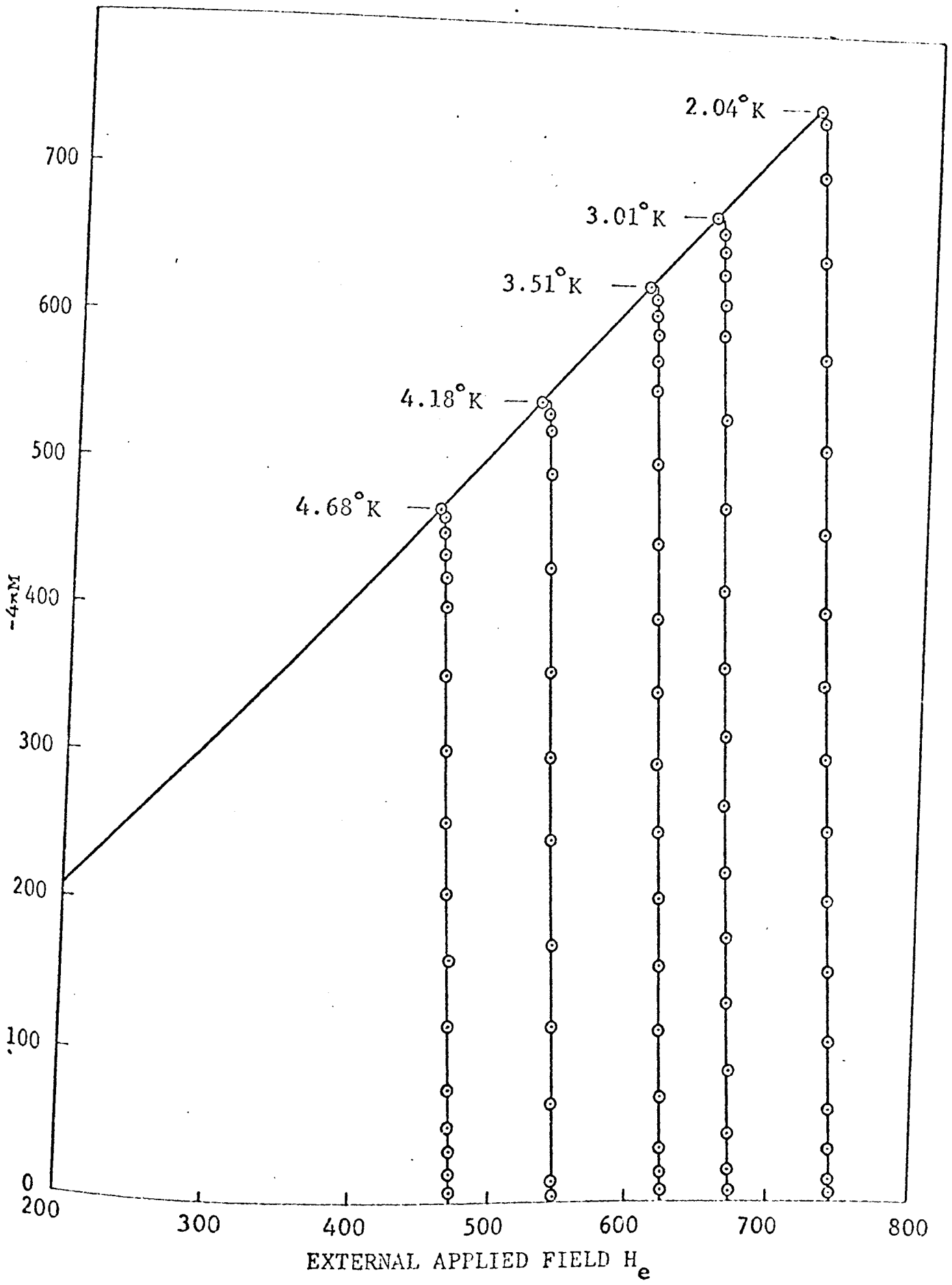

FIGURE 11. Magnetization curves for lead

with the calculated values in table III.

TABLE III

Latent Heat of Lead per Unit Volume

Temp.	L (meas.)	L (ref.40)	% Diff.
2.04°K	6,860 erg	6,939 erg	-1.11%
3.01°K	14,090 erg	14,280 erg	-1.33%
3.08°K	14,650 erg	14,770 erg	-0.81%
3.51°K	18,630 erg	18,450 erg	+0.98%
4.05°K	22,480 erg	22,730 erg	-1.10%
4.18°K	23,740 erg	23,680 erg	+0.25%
4.68°K	27,240 erg	26,840 erg	+2.11%

The agreement is fairly good over the entire temperature range. The large error at 4.68°K may be entirely due to a large temperature uncertainty. Two points on the resistance versus temperature curve below 4.2°K were used to evaluate a and b in equation (79), which was then used to find the temperature from the resistance. There may be an error of up to several hundredths of a degree in the temperature, which could account for the anomolously high latent heat at this temperature. A trend to negative differences with decreasing temperature is readily apparent. This may reflect the strong temperature dependence of magnetic hysteresis in lead which was observed by Shaw and Mapother [47]. The

latent heat of the lead transition was measured by Dolecek using a pulsed magnetic field [48]. His results agree well with the results reported in this work, although his data are considerably more scattered.

The calorimetric data taken fails to show a positive surface energy as was expected. Within the experimental error, there was no significant deviation from ideal behavior. Figure (12) shows Q/L versus B/H_a for lead at several temperatures. The possibility that irreversible magnetic work or eddy current heating in the normal portions of the sample were obscuring the surface energy was considered. This seems unlikely since the measured latent heats were in good agreement with the thermodynamically deduced values. Moreover, there were no systematic deviations above or below the ideal line at either end of the transition. The most reasonable explanation seems to be that the surface energy is too small to be detected by this method. Lock obtains a value of 2.5×10^{-6} cm for the surface energy parameter of lead at $4.24^{o}K$ from thin film studies [49]. R. B. Goldner established an upper limit to the surface energy parameter by studying the domain widths in a transverse lead cylinder in the intermediate state [62]. His value is 1.2×10^{-5} at $4.22^{o}K$ but this represents an upper limit and is therefore not inconsistent with Lock's result. The wall energy at $4.2^{o}K$

could not be larger than 0.139 erg/cm^2, and would be equal to 0.029 erg/cm^2 using Lock's value for the surface energy parameter. The latent heat of transition is on the order of 2 x 10^4 erg/cm^2 at this temperature, so even as much as 1000 cm^2 of boundary area per cm^3 would amount to only ½% of the latent heat. A realistic estimate of the total boundary area per unit volume based on the work of Kuper would be from 10 to 100 cm^2 (51). Since the scatter in the calorimetric data reported in figure (12) is a few percent, it seems reasonable to conclude that the surface energy in lead is simply too small to be detected directly by this method.

It seems that any calorimetric experiment designed to detect the surface energy in lead is doomed to failure unless precisions on the order of one part in 10^4 can be achieved. The values of Δ reported in references (49) and (50) were obtained indirectly from observation of the domain structure in the intermediate state (50) and magnetic field penetration studies (49). The reasonably small scatter of the calorimetric data and the good agreement between the measured and calculated latent heats confirm the validity of the experimental procedure. Since the temperature dependence of H_c for Pb-4%Tl is not known, the latent heat can not be calculated. The good agreement obtained with lead increases the confidence

level which can be assigned to the measured values of the latent heat of the alloy. Likewise, the fact that a material with a small positive surface energy was indistinguishable from an ideal material lends credibility to calorimetric results obtained with an alloy.

C. TIN

It was much more difficult to perform measurements on tin, and data were taken using the thermal pulse method only. The critical fields encountered were less than 200 gauss, so the transition occurred over a range of fields less than nine gauss. The latent heat of the tin transition is typically an order of magnitude less than for lead. The chief problems encountered in performing the tin measurements were reducing the heat leak to the sample and achieving sufficiently fine control of the solenoid current. A 10 turn 2.9 ohm infinite resolution potentiometer was finally used for current control. Since the power supply output current response was about five milliamperes per ohm change in the controlling resistance, the ultimate capabilities of the power supply were realized. Superconducting leads were used to connect to the heater so that no correction would be required for heat generated in the leads.

The magnetization curve of tin at 2.24^{o}K is shown in figure (13). The forward curve agrees fairly well with

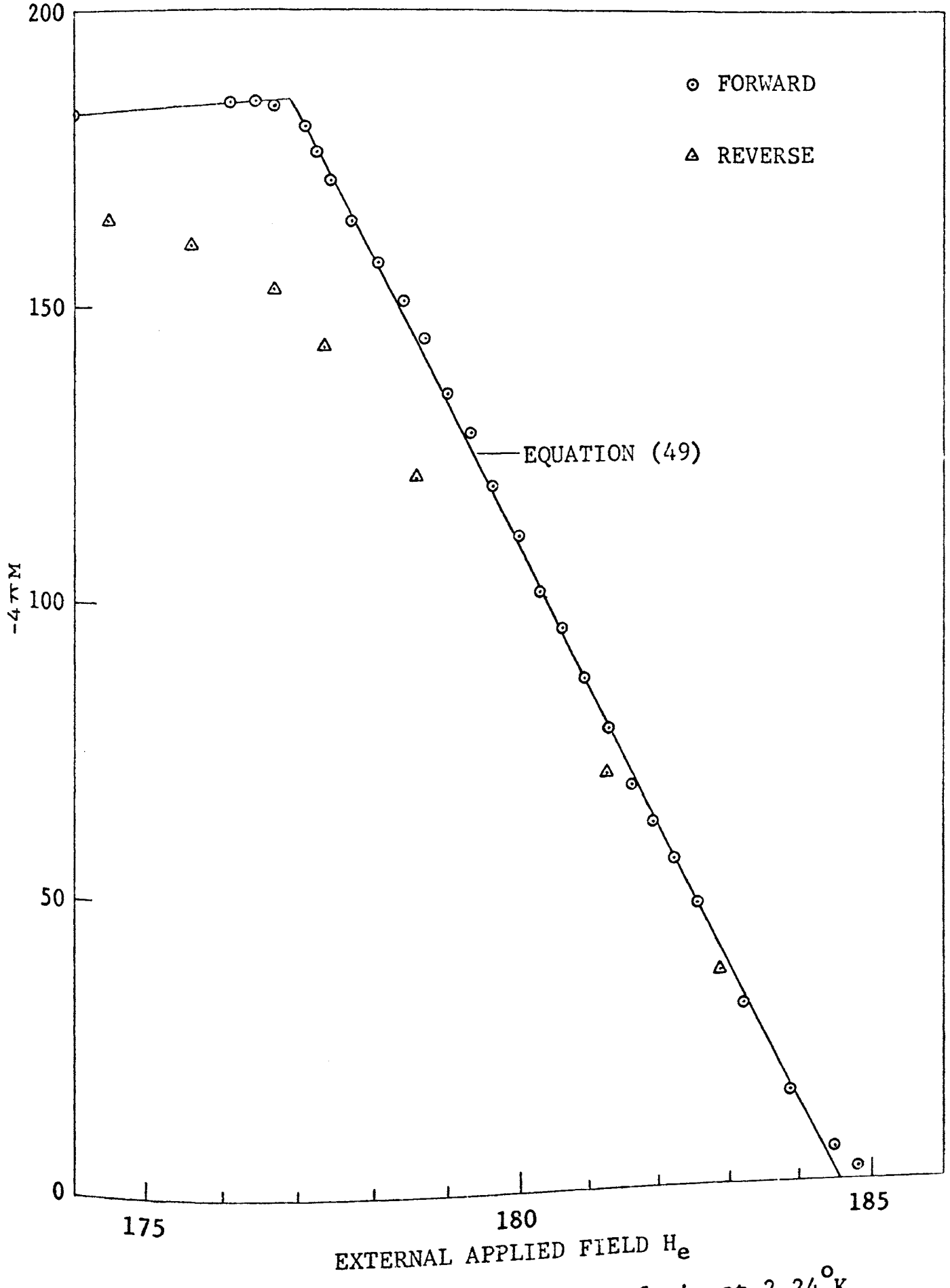

FIGURE 13. Magnetization curve of tin at 2.24°K

equation (49), although there are some significant deviations. Some supercooling was observed, but the reverse curve was fairly close to the forward curve for this temperature. A recent study of hysteresis in tin indicates that after the supercooled transition is completed, the magnetization changes nearly reversibly over the remaining part of the reverse transition [52]. Near (1-N) H_c, the individual measurements at a given applied field deviated from their mean by a few percent. However, the points were much more reproducible over the latter half of the transition. During the calorimetric runs it appeared that a slight amount of superheating occurred. No matter how slowly the applied field was increased at the beginning of the transition, a point was always reached at which flux abruptly penetrated with an accompanying burst of cooling which resulted in a momentary loss of temperature control. The precise point at which this occurred was not reproduced from run to run. Hence, the sample was probably not in an equilibrium state near the beginning of the transition, and conditions were not reproduced identically for each measurement.

The magnetization data for lead seem to verify that the magnetization near (1-N) H_c does depend to some extent on conditions. In figure (10) the flux integration data points are slightly higher than the thermal pulse data points near

(1-N) H_c. In the flux integration method, the field is constantly changing, so the sample can not be in an equilibrium state unless equilibrium is rapidly established. The two methods agree to within the experimental error over the latter two thirds of the transition, so apparently once the normal phase has been nucleated throughout the sample, equilibrium is rapidly established. Lynton and Serin observed that the magnetization of a composite tin wire sample attained its final value near (1-N) H_c in less than a minute [53]. The author feels that the scatter in the magnetization points at a given field near (1-N) H_c can best be explained by metastable states of relatively long duration.

The latent heat of transition for tin was measured at three temperatures during the course of this work. The latent heat was calculated using equation (20) and the tin critical field polynomial of Lock [54]. The latent heat was also obtained from the critical field curve reported in reference [41]. The results are presented in table IV below.

TABLE IV

Latent Heat of Tin Per Unit Volume

Temp.	L (meas.)	L (ref.54)	L (ref.41)	% Diff.
3.30°K	2072 erg	2144 erg	2160 erg	-3.72%
2.65°K	3325 erg	3465 erg	3415 erg	-3.35%
2.24°K	3301 erg	3402 erg	3380 erg	-2.68%

The measured latent heat values were consistently low by a few percent. The fact that the measured values were all low by about 3% might be due to an imperfect thermal ground which would permit heat generated in the leads to reach the sample. Such a spurious source of heat would produce an error in lead of only a few tenths of a percent. Given that a difference of a few percent exists between the calculated and measured latent heats, the possibility of eddy current heating in the sample can not be discounted.

The tin calorimetric results were much more erratic than the lead results, possible due to the uncertainties in the magnetization curve mentioned earlier. It seemed that the Q/L versus B/H curve deviated as much above the ideal line as below, with no clear trend evident. The better runs approximated the ideal curve, and the three most regular curves are shown in figure (14). The only safe conclusion which can be drawn is that the surface energy was not detected. The surface energy parameter is given by Davies as 2.3×10^{-5} cm at absolute zero with a temperature dependence of the form $(1-t^4)^{-\frac{1}{2}}$ (55). At 2.24°K the surface energy parameter would be 1.2×10^{-5} cm, and the wall energy would be .0163 erg/cm^2. Since the latent heat is about 3300 erg/cm^3 at this temperature, 1000 cm^2 of boundary area per unit volume would amount to only ½% of the latent heat. Moreover, a more

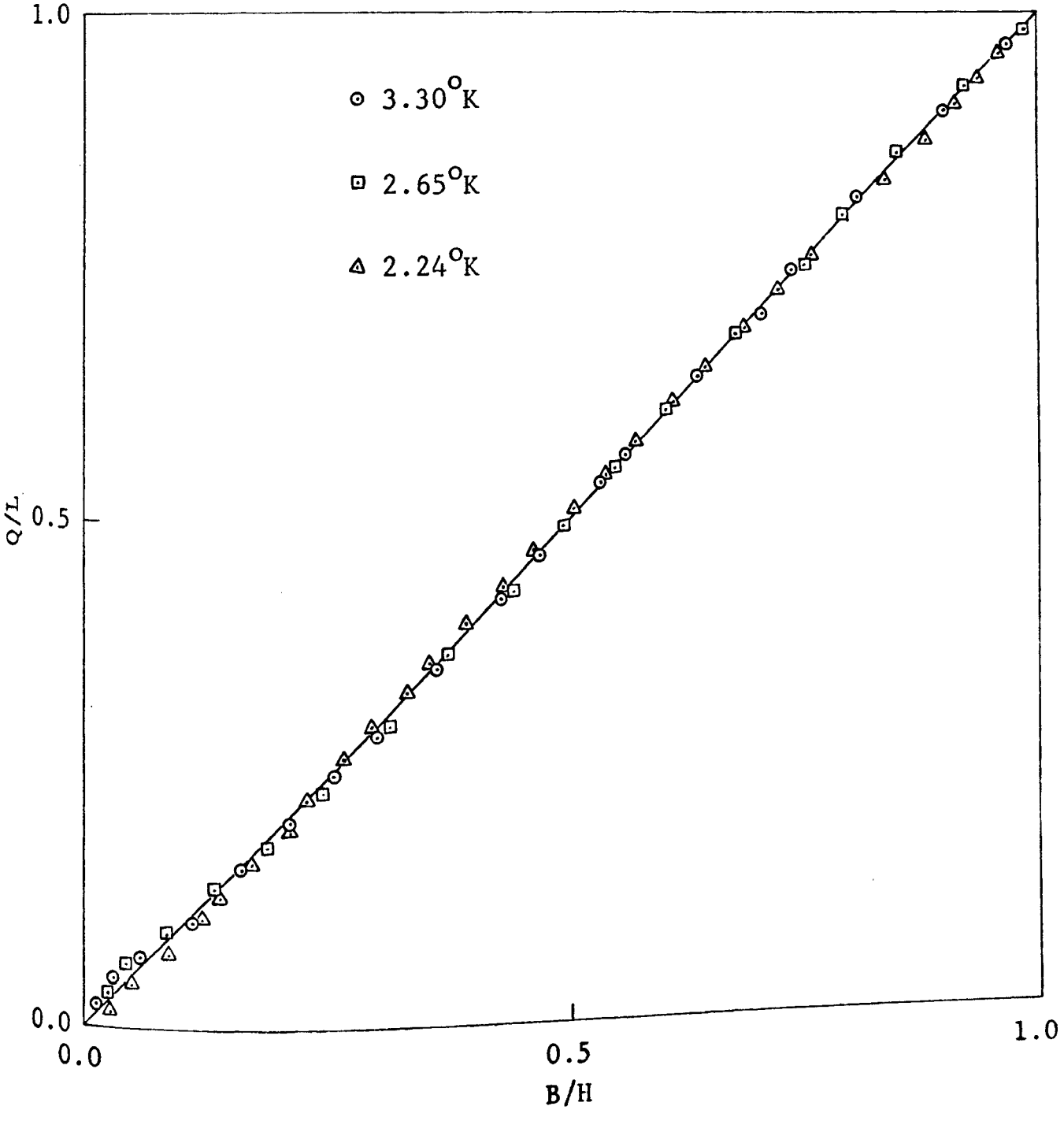

FIGURE 14. Q/L versus B/H for tin

realistic value for the boundary area per unit volume would be between 10 and 100 cm^2 per cm^3. Considering the erratic results obtained in the tin calorimetric runs, it does not seem very likely that the surface energy in tin can be detected calorimetrically. There have been no reports in the literature to the effect that the surface energy has been detected calorimetrically in either tin or lead.

D. LEAD-THALLIUM

1. MAGNETIC PROPERTIES

Lead-4at%thallium was studied at several temperatures using both the flux integration and thermal pulse methods. The initial measurements were made using only the thermal pulse method, and after all desired data were obtained by this technique, it was decided to try the flux integration method. Since flux integration worked very well, it was decided to repeat the earlier measurements on lead and lead-4 at%thallium. The lead-4at%thallium sample was first given a second careful annealing for 14 days at 315°C, and the surface was chemically polished. When the measurements were repeated, it was learned that the magnetic properties of the sample had undergone rather drastic changes as a result of this annealing and polishing. The calorimetric results obtained before annealing were quite consistent with predictions based on current negative surface energy theories.

The transition temperature of the sample could not conveniently be measured with any degree of accuracy since the calorimeter was not designed for operation above 2.4°K. The transition temperatures for lead-thallium alloys have been determined over a wide range of thallium concentrations by Claeson [56]. The transition temperature decreases linearly with increasing thallium concentration up to several percent thallium. The transition temperature for Pb-4at%Tl is 7.10± .02°K from Claeson's results. Since H_{c2} for the temperatures studied changed only slightly as a result of annealing, it is considered unlikely that T_c changed very much during the second annealing. The alloys studied by Otter, Pb-40at%Tl and Pb-60at%Tl, had critical temperatures of 6.35°K and 6.20°K, respectively.

After the first annealing, magnetization curves obtained by the thermal pulse method had the appearance of typical low-K type II magnetization curves. Three such curves at different temperatures are shown in figure (15). The transition was not very reversible after the first annealing, as can be seen from the reverse curve at 4.19°K. The remanent magnetization after the first annealing was about 128 gauss at 4.19°K, or about 26% of the maximum ascending magnetization. The two values of the Ginzburg-Landau parameter, K, as

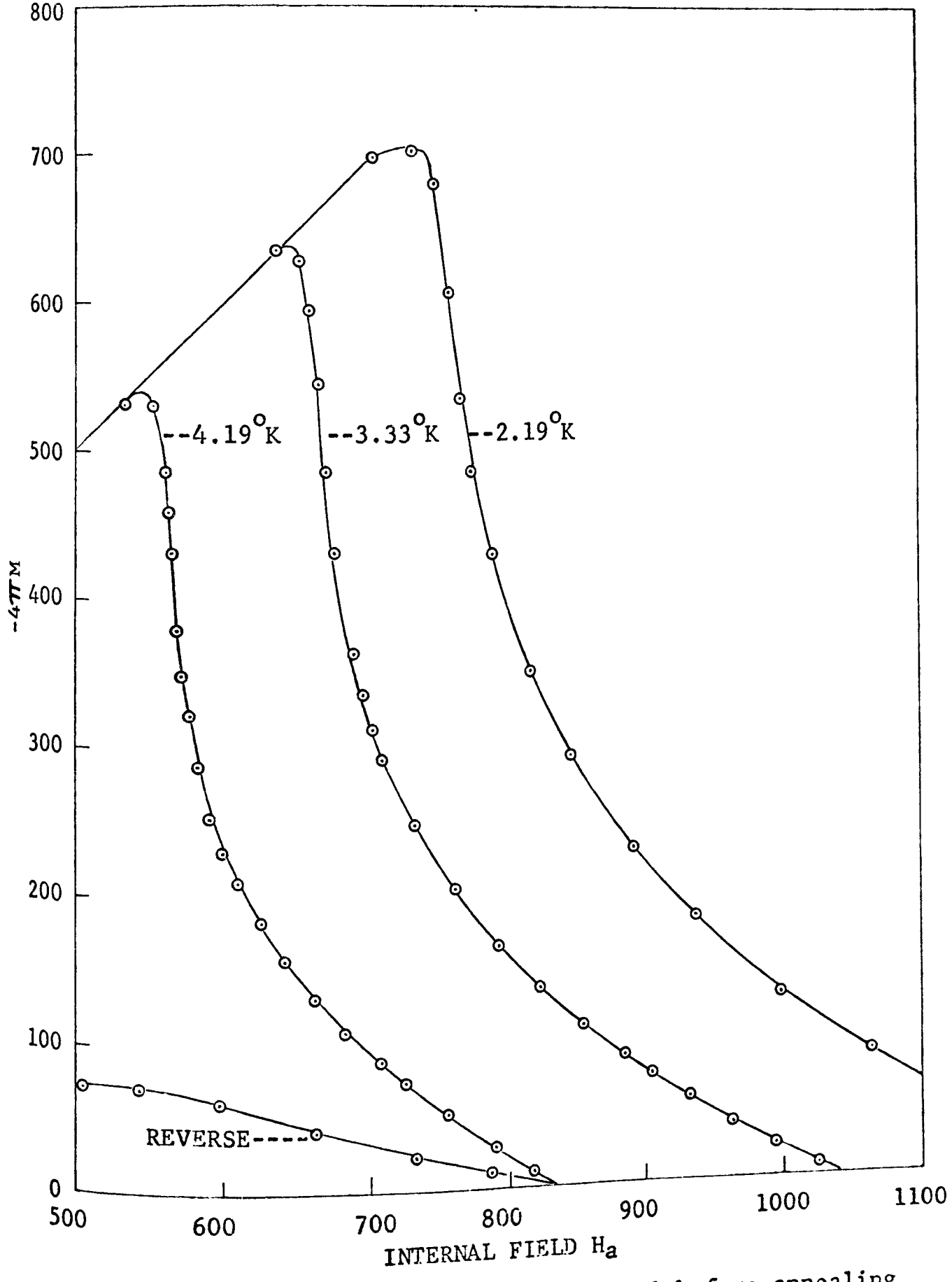

FIGURE 15. Magnetization of Pb-4at%Tl before annealing

determined from equations (68) and (70) differed from each other by several percent at each temperature. Hereafter, the value of K determined from equations (68) and (70) will be referred to as K_1, and K_2, respectively. For the three temperatures studied before the second annealing, both K_1 and K_2 increase with decreasing temperature with $K_2 > K_1$. Among other results, the values of K_1 and K_2 before and after the second annealing are presented in table V, page 89, for each temperature studied.

Such authors as Gor'kov, Shapoval, Bardeen, and Maki have discussed the extension of the G-L theory to temperatures below T_c and derived theoretical expressions for $K_1(t)$ and $K_2(t)$ (57)(58)(59)(60). In practice, the values of $K_1(t)$ and $K_2(t)$ are obtained from equations (68) and (70) using the appropriate temperature dependent values of H_{c2}, H_c, and $(dM/dH)_{H_{c2}}$. If K is the limit of $K_1(t)$ and $K_2(t)$ as T approaches T_c, the temperature dependence of $K_1(t)$ is given by:

$$K_1(t) = K a_1(t) \tag{80}$$

The two theoretical expressions for $a_1(t)$ which best fit most experimental data are due to Gor'kov and Maki, who obtain:

(81)

Gor'kov: $a_1(t) = 1.25 - 0.30t^2 + 0.05t^4$

Maki: $a_1(t) = \begin{cases} 1.20 - 1.27t^2 & t \ll 1 \\ 1.39 - 0.39t & t \approx 1 \end{cases}$

Maki also calculates the temperature dependence of $a_2(t)$ from fundamental microscopic quantities. He obtains asymptotic expressions of the form:

$$a_2(t) = \begin{cases} 0.69 + 7.23\,t^2 & t \ll 1 \\ 0.913 + 0.087\,t & t \approx 1 \end{cases} \qquad (82)$$

Maki therefore predicts that $K_1(t)$ and $K_2(t)$ respectively increase and decrease with decreasing temperature. The observed behavior of $K_2(t)$ contradicts this prediction in every reported instance. The authors own observations of Pb-4at%Tl indicate that $K_2(t)$ has very nearly the same temperature dependence as $K_1(t)$. Sekula and Kernohan report that $K_2(t)$ is greater than $K_1(t)$ for Pb-27at%Tl at all temperatures [61]. Bon Maridon and coworkers have studied the magnetic properties of the lead-thallium system and report that the temperature dependence of $K_2(t)$ is essentially the same at all thallium concentrations [62]. Kinsel and coworkers have studied the magnetic properties of dilute indium-bismuth alloys and report also that both $K_2(t)$ and $K_1(t)$ increase with decreasing temperature [63].

It would seem safe to conclude that Maki has predicted behavior which is not observed. Maki concludes further that under certain conditions a third type of reversible magnetic behavior should occur. An alloy having $K \approx 1/\sqrt{2}$ would have $K_2 < 1/\sqrt{2} < K_1$ at and below some temperature, were Maki's

prediction regarding the temperature dependence of $K_2(t)$ correct. According to Maki, below this temperature the transition to the normal state at H_{c2} is of the first order, and the magnetization curve of a type III superconductor should show an abrupt drop to zero at H_{c2}. Such behavior is vaguely reminiscent of the magnetization curves predicted by Goodman's laminar theory [9]. No one has reported observing type III behavior, and the evidence cited previously militates strongly against the existence of such a phenomenon.

After the second annealing, the magnetic properties of the Pb-4at%Tl sample resembled those predicted for a type III superconductor. The most striking change which occurred as a result of annealing and polishing was the appearance of a small, but quite significant drop in the magnetization curve near H_{c2}. This is precisely the magnetic behavior which would be expected in the presence of structural flaws for a material having a first order transition to the normal state at H_{c2}. Figure (16) shows the magnetization curves obtained by the flux integration technique after the sample had been annealed for 14 days at 315°C. Figure (17) shows the transition at 4.19°K before annealing and at 4.15°K after annealing. The drop in magnetization is more pronounced at the higher temperatures, but the effect is present at all temperatures studied. The chart recordings of the voltage

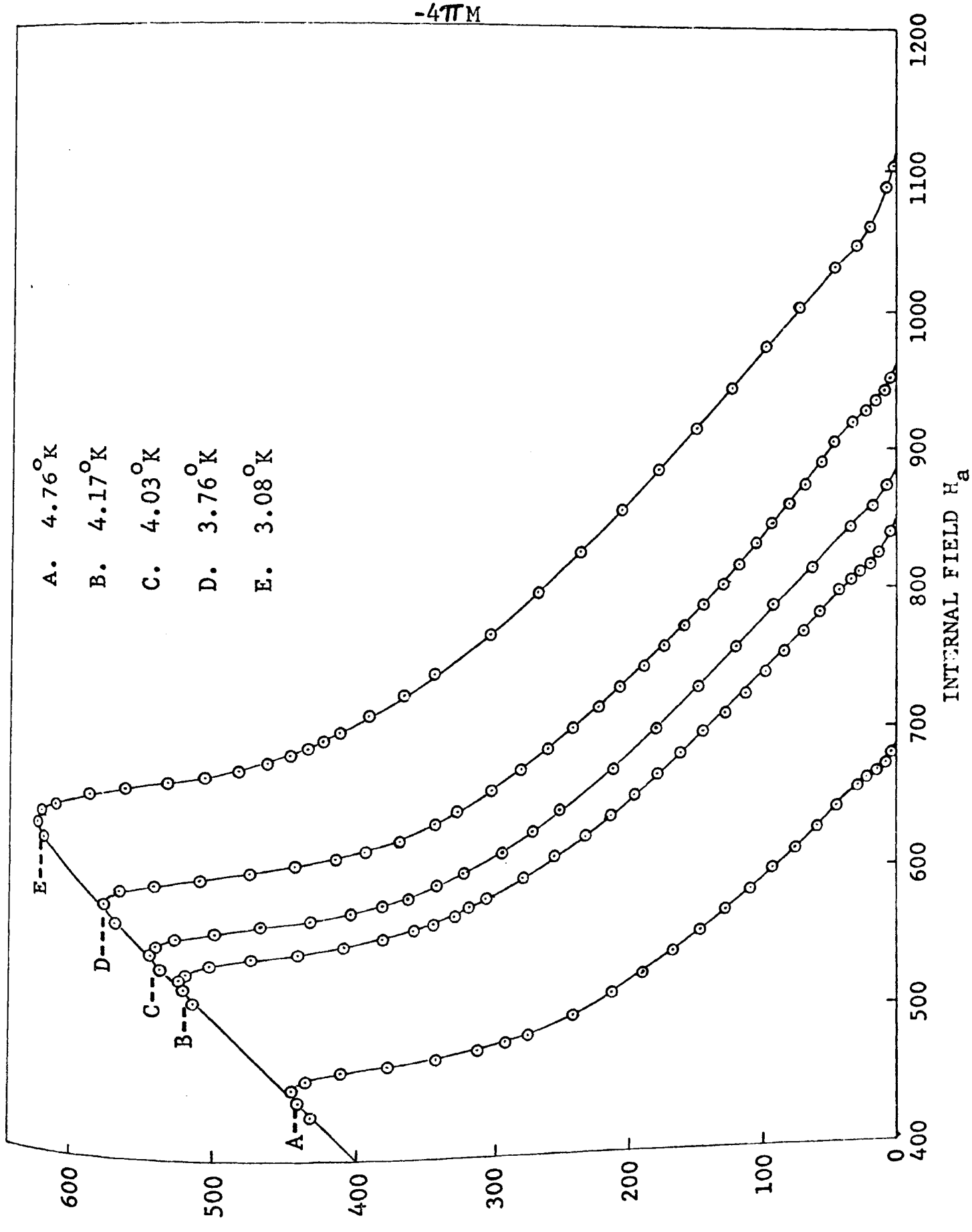

FIGURE 16. Magnetization curves of Pb-4at%Tl after annealing

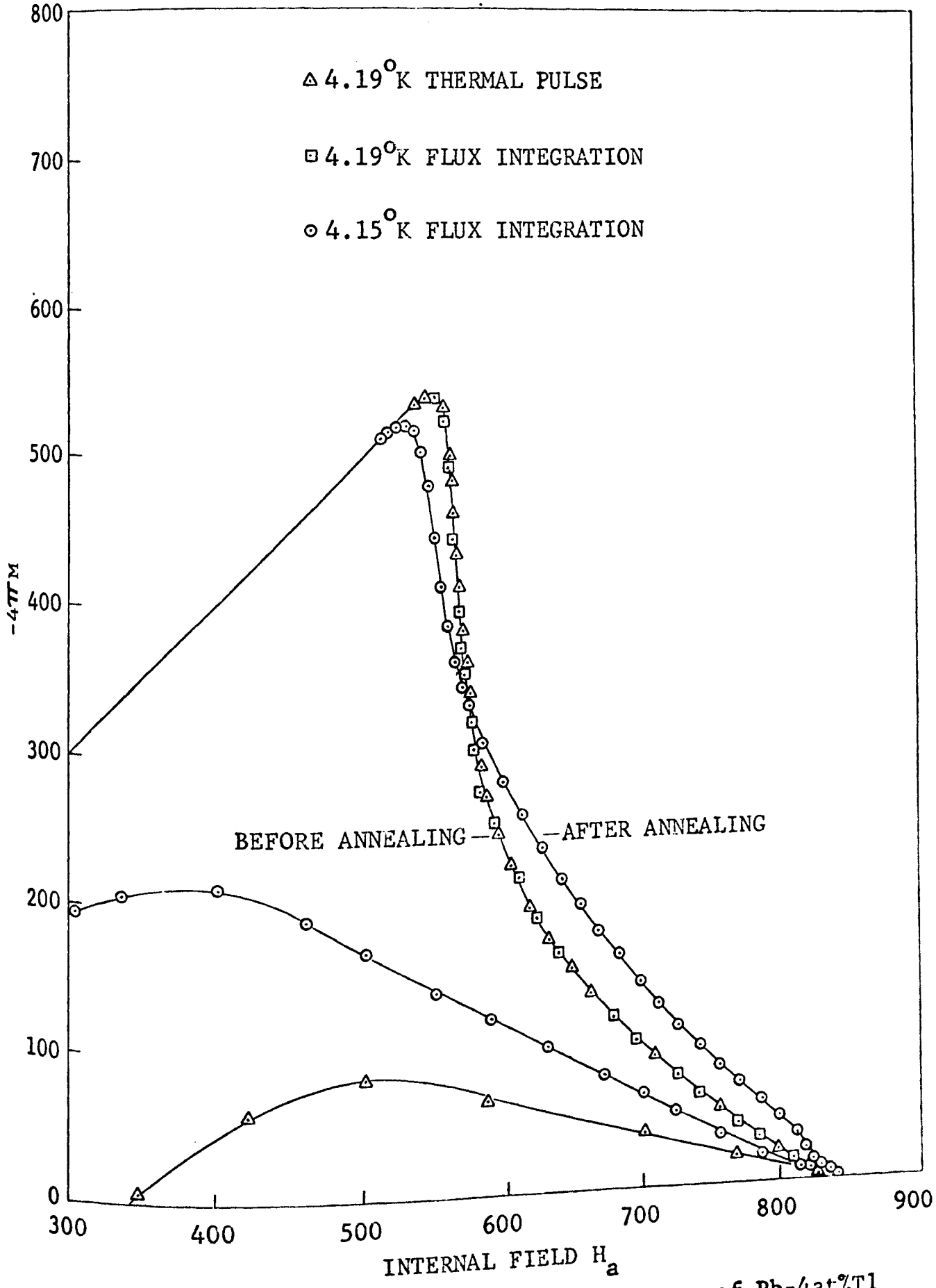

FIGURE 17. Expanded magnetization curves of Pb-4at%Tl

induced in the pickup coil as the applied magnetic field is isothermally swept at a constant rate show a small, sharp peak at the end of the transition. The relative position of this peak does not change with temperature, and similar chart recordings made before the second annealing show no trace of this peak. The calorimetric data show clear signs of a small latent heat associated with the transition to the normal state. The magnetic data were taken at a sweep rate of 30 gauss per minute, which may have been too fast to permit sharp definition of the transition.

The values of K_1 and K_2 were in much closer agreement at all temperatures after the second annealing. At each temperature studied, K_2 was less than 2% greater than K_1. The value of K_1 dropped a few percent after annealing, but K_2 dropped between 5% and 10% as a result of annealing. The magnetization curve was somewhat higher over the latter half of the transition, and the slope was greater. The curve did not drop quite so sharply at H_{c1}, and the peak was a bit more rounded after annealing. The measured critical field, H_c, increased slightly after annealing as a result of the changes mentioned. This was unexpected, since annealing usually improves the reversibility of a sample and lowers the apparent H_c. However, by all commonly accepted criteria of reversibility, the sample was significantly improved by

annealing. The remanent was reduced by about 50% to 64 gauss at 4.17°K, which is about 12.5% of the maximum ascending magnetization. The reverse curve was much closer to the ascending curve after annealing and polishing. It is therefore quite puzzling that H_c increased after annealing.

There have been several studies of irreversibility in alloys conducted in the past several years. While the magnetic transition in a type II material is reversible in principle, it is never completely reversible in practice. There are three mechanisms which are widely regarded as responsible for magnetic hysteresis. They are flux pinning at dislocations, flux trapping by inhomogeneities, and surface barrier effects. Dislocation pinning is responsible for most of the hysteresis which can be removed by careful annealing [45]. Inhomogeneities and precipitates are largely responsible for flux trapping in well annealed specimens [64]. Surface effects are thought to be responsible for most of the low field hysteresis observed in homogeneous, well annealed specimens [64].

The condition of the surface of a well annealed specimen can certainly influence its magnetic properties [62]. Livingston observed that the magnetization curve of a well annealed Pb-8%Tl specimen was unchanged after half the volume had been etched away [64]. Such size independent hysteresis

is strong evidence that there are no appreciable flux gradients in a well annealed specimen, and that the observed low field hysteresis is largely due to surface effects. Livingston and Bean have discussed flux thread motion near a specimen surface and conclude that local field variations at surface irregularities will aid the penetration of flux threads into the superconductor (65). The same irregularities serve to block the expulsion of flux, and a barrier to flux expulsion exists down to zero field. It is commonly supposed that the ascending virgin magnetization curve is very close to the thermodynamic equilibrium curve for well annealed specimens that trap very little flux. The nearly reversible magnetization curves for niobium reported by Finnemore were obtained by jarring the sample until no further changes occurred (16). The jarring may have locally compressed or stretched the lattice near the surface thereby affecting the magnitude of the surface barrier. The lead-4at%thallium sample studied by the author was about as reversible after the second annealing as the better samples studied by Bon Maridon and coworkers (66).

If the magnetization curve is not reversible and an appreciable remnant is trapped, the value of H_c obtained from the area under the magnetization curve represents an

upper limit to the thermodynamic critical field. However, the critical field can be obtained if the critical field is assumed to obey the parabolic law, or if sufficient data are taken to apply a numerical procedure based on the first law of thermodynamics. Assuming the critical field obeys a parabolic law, the corrected critical field is given by:

$$\frac{H_c^2}{8\pi} = \frac{1-t^2}{1+3t^2}\left\{-\int_0^{H_{c2}} M(H_a)\,dH_a + L(meas.)\right\} \qquad (83)$$

Given enough data, H_c can be determined by a numerical integration. One obtains:

$$\frac{H_c^2}{8\pi} = T\int_T^{T_c}\left\{L(meas.) - \int_0^{H_{c2}} M(H_a)\,dH_a\right\} \qquad (84)$$

The detailed derivations of equations (83) and (84) are given in Appendix I. The corrected values of H_c are from 15% to 20% less than the values of H_c computed from equation (18), as can be seen in table V. Figure (18) shows H_c as a function of t^2 before and after annealing both corrected and uncorrected for hysteresis using equation (83). It proved impractical to use equation (84) for lack of sufficient data points. The corrected curve shows some departures from a parabolic law, apparently in the strong coupling direction. The extrapolated value of H_o was 792 gauss, as compared to 803 gauss for pure lead and 757 gauss for lead-27at%thallium [61]. The extrapolated value of H_o for the uncorrected values of H_c before annealing is 935 gauss and 970 gauss after annealing. It is gratifying that the

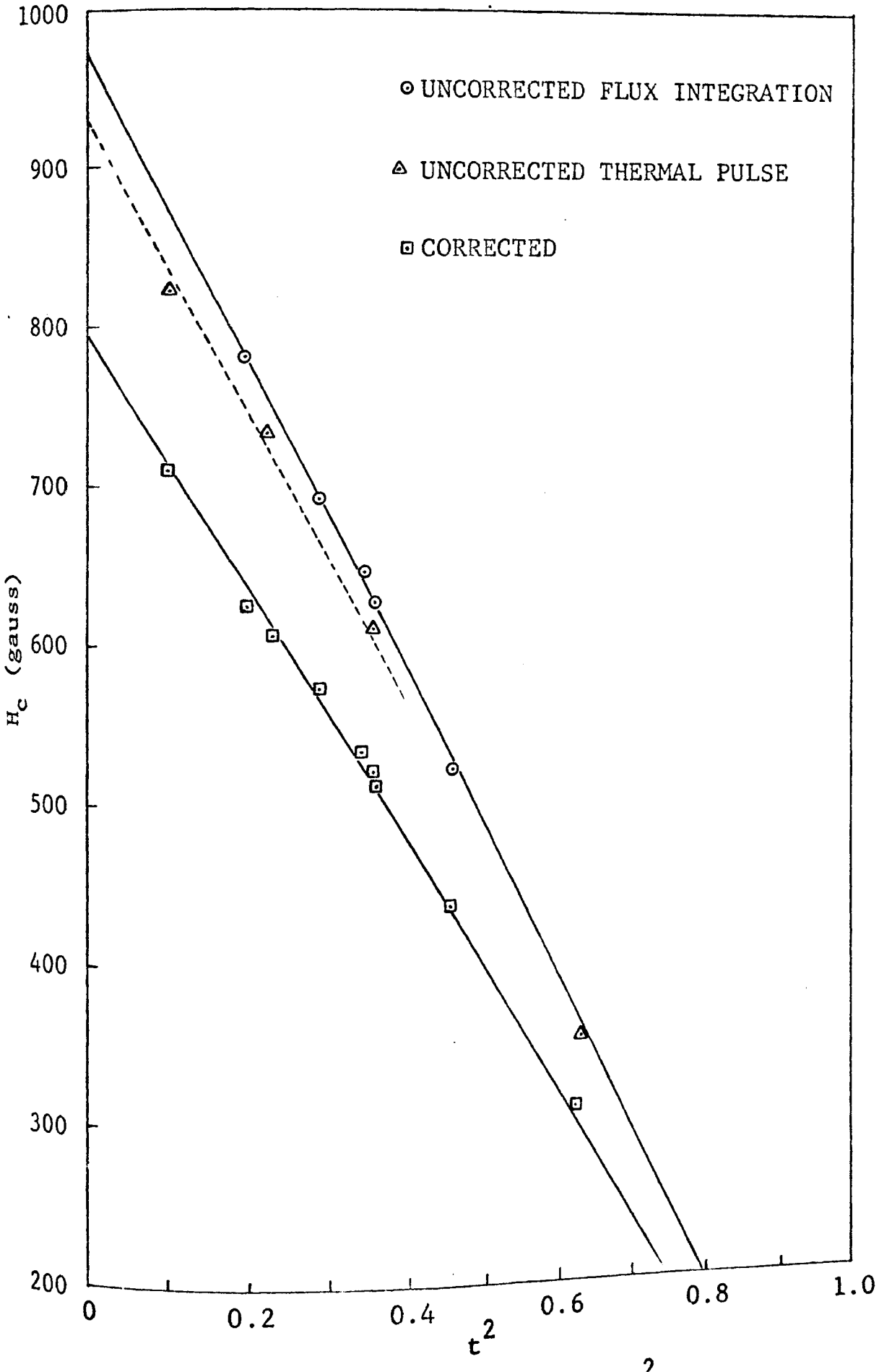

FIGURE 18. H_c versus t^2

value of H_o obtained by extrapolating the corrected H_c data falls between the values of H_o for pure lead and Pb-27at%Tl.

The measured magnetic properties of Pb-4at%Tl alloy are tabulated in Table V. The temperatures were determined from the vapor pressure of the helium bath corrected for hydrostatic pressure. H_{c1} was determined by extrapolating the linear portion of the magnetization curve near the beginning of the transition to the extrapolated diamagnetic curve. H_{c2} was determined by extrapolating the best linear fit for the latter part of the magnetization curve to the point where it crosses the axis. The slope of this line was taken to be $-4\pi (dM/dH_a)_{H_{c2}}$ for the determination of K_2 using equation (70). L was determined from the calorimetric measurements, and used in equation (83) to obtain the value of the critical field corrected for hysteresis, H_c'. K_1 was determined from equation (68) using the measured values of H_c and H_{c2}. K_3 was determined from the numerical calculations of Harden and Arp with the ratio of H_{c1} to H_c [32].

2. CALORIMETRIC RESULTS

The calorimetric data were taken by the two methods described in chapter II. Due to difficulty in data reduction, data taken with a constant heater power are more reliable than those taken by increasing the field at a constant rate. The effects of magnetic hysteresis are difficult to assess,

TABLE V

Tabulated Magnetic Properties of Pb-4at%Tl Alloy

Temp. (^{o}K)	H_{c1} (gauss)	H_{c2} (gauss)	H_c (gauss)	L (erg/cm^3)	H_c' (gauss)	K_1 --	K_2 --	K_3 --
*5.65	349	479	370.0	19,465	308.0	.915	1.001	.80
4.76	458	680	524.9	21,500	437.4	.916	.931	.88
*4.19	556	830	614.3	18,250	516.2	.955	1.028	.85
*4.19	553	830	614.4	18,250	516.2	.955	1.028	.85
4.17	535	835	629.4	18,200	524.1	.938	.953	.90
4.15	536	842	630.1	--	--	.943	.960	.90
4.03	555	877	652.4	16,244	536.2	.945	.964	.90
3.76	587	950	695.6	14,700	577.4	.961	.988	.90
*3.33	654	1033	735.7	10,096	611.2	.993	1.042	.88
3.08	644	1077	783.0	5,840	627.9	.972	.989	.92
*2.19	736	1207	847.9	0	711.4	1.006	1.095	.91

*Before Second Annealing

'Corrected For Hysteresis

although errors can be estimated if assumptions are made about the magnetic properties of the alloy. The calorimetric results were generally consistent with current negative surface energy theories. There were several predictions made in chapter I regarding Q as a function of H_a. Among the predictions to be tested were:

1. Q* should depend linearly on $H_{c2}-H_a$ near H_{c2} (p.32).
2. Q/L versus B/H_a should be linear near H_{c1} (p.27, p.34).
3. $Q(H_a-H_{c1})$ should be represented by $a(H_a-H_{c1}) + b(H_a-H_{c1}) \ln c (H_a-H_{c1})$ in the field range $H_{c1} < H_a < H_{c2}$ (p.33).
4. The data of F. A. Otter was to be compared with the results of this work. Each prediction was tested in the course of this work, and agreement was good with the exception of $Q^*(H_{c2}-H_a)$ after the second annealing.

The magnetization is a linear function of $H_{c2}-H_a$ near H_{c2} in the GLAG (Ginzburg-Landau-Abrikosov-Gor'kov) theory, and hence the free energy difference between the superconductor in field H_a and the normal state varies quadratically with $H_{c2}-H_a$. The entropy difference and Q* should therefore depend linearly on $H_{c2}-H_a$ near H_{c2}. Figure (19) shows Q* as a function of $H_{c2}-H_a$ at 4.19°K before annealing and at 4.17°K after annealing. The data can be fit very well with a straight line before annealing. The slope of the line is 41.6

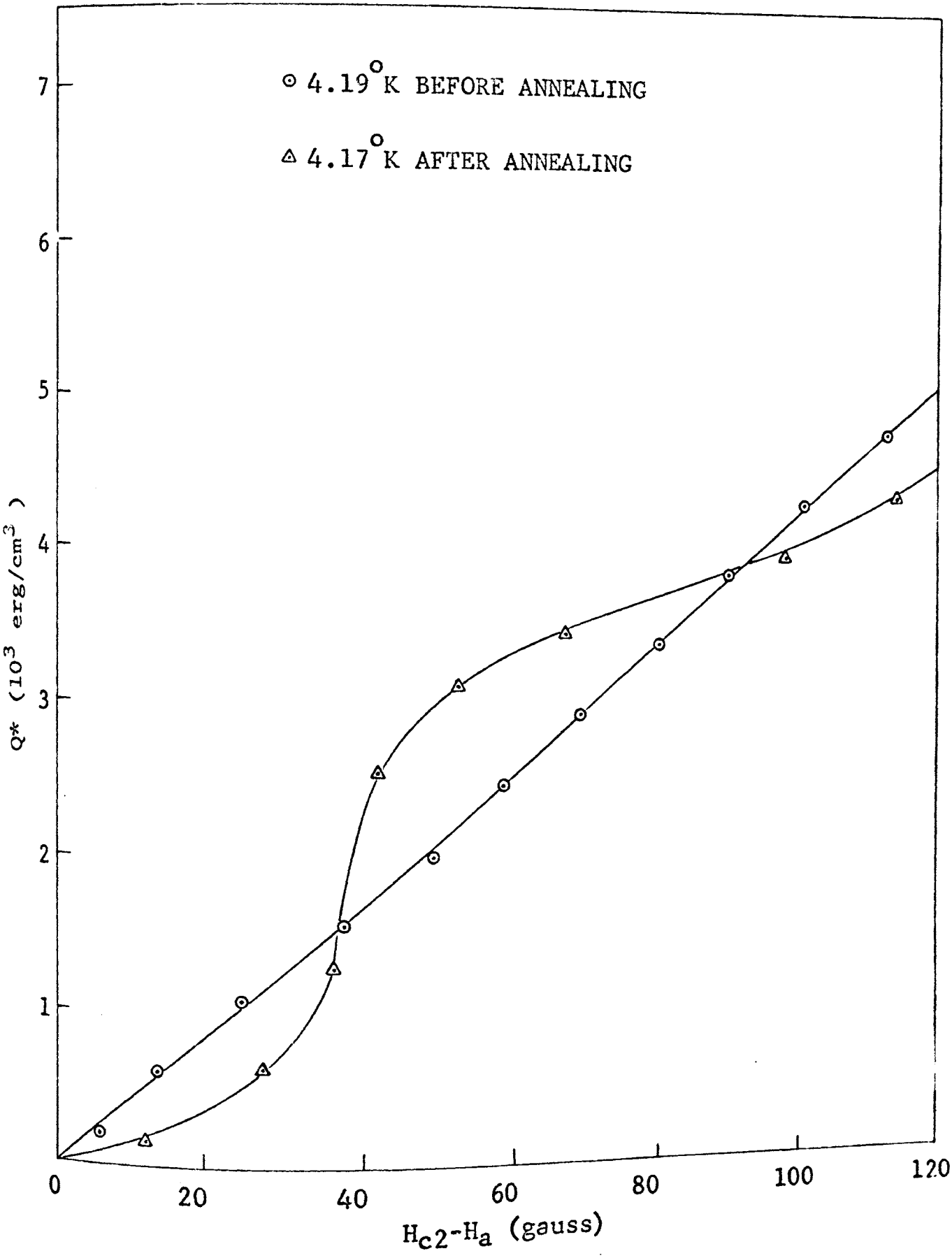

FIGURE 19. Q* versus $H_{c2}-H_a$ near H_{c2}

erg/cm^3-gauss, from which dH_{c2}/dT is found to be -165.5 gauss/^oK using equation (75). Using a parabolic law to approximate $H_{c2}(T)$, the value of dH_{c2}/dT is found to be -212$\pm$ 10 gauss/^oK. The agreement is not very good, the relative error amounting to -22%.

The major source of error is probably an irreversible entropy increase which occurs when flux lines are forced to move and overcome pinning forces. One expects that the measured latent heat must be lower than the reversible latent heat by an amount comparable to -22%. If the alloy has the strong coupling characteristics of pure lead, the critical field curve will be similar, and the latent heat can be calculated from the lead critical field curve with appropriate scaling of H_o and T_c. The critical field data reported in this work and the critical field data of Sekula and Kernohan tend to confirm the strong coupling characteristics of dilute Pb-Tl alloys, although the data are too sketchy to assert that the critical field curves differ only be scaling factors [61]. The calculated latent heat at 4.19^oK according to this procedure is 22,800 erg/cm^3, compared to a measured value of 18,250. The relative error is -20%, which is fairly close to the value of -22% obtained from comparing calculated and inferred values of dH_{c2}/dT at 4.19^oK.

The behavior of $Q^*(H_{c2}-H_a)$ near H_{c2} was drastically

altered as a result of annealing and polishing. The data are not even approximately linear, but rather has a pronounced wiggle shaped like an "S". For values of $H_{c2}-H_a$ larger than 120 gauss, the curve again becomes quite linear and approximately parallel to the curve before annealing. The curve becomes nearly vertical at $H_{c2}-H_a \approx 35$ gauss, which strongly suggests a first order transition to the normal state. The latent heat associated with the transition appears to be on the order of a few thousand ergs/cm^3. A thermodynamic analysis can be made to determine the latent heat due to a given discontinuity in M at H_{c2}. One obtains an expression for ΔQ given by [21]:

$$\Delta Q = -T \Delta M \, (dH_{c2}/dT) \tag{83}$$

The change in magnetization at H_{c2} appears to be about 1.5 gauss on the magnetization curve, although this value is only certain to within $\pm$ .5 gauss. Using -212 gauss/^{o}K for dH_{c2}/dT and 4.19^{o}K for T, ΔQ is equal to 1335 erg/cm^3. This value is quite reasonable, but could easily be in error by 50%. There seems to be considerable evidence that the transition to the normal state is first order with a latent heat on the order of 10^3 erg/cm^3.

The second prediction was that Q/L versus B/H_a should be linear near H_{c1}. This prediction was made on the basis of Goodman's laminar model of the mixed state and a plausibility

arguement based on the entropy of an isolated vortex line. Using Goodman's model, the initial slope of Q/L versus B/H_a was equal to q, the surface energy parameter (p.27). The properties of q are quite similar to the properties of $.7071/K_1$ That is, the material becomes type I for q=1, and exhibits progressively more extreme type II behavior as q decreases. It would not be correct to equate q and $.7071/K_1$, since q is defined by equation (58). However, if q is known, K_1 can be calculated from equations (58) and (68).

A serious question arises as to whether q can be determined from calorimetric data in the presence of magnetic hysteresis. If the irreversible entropy increase per unit change of B/H_a is constant throughout the transition, the shape of Q/L versus B/H_a will not be affected by hysteresis. The measured latent heat will be low by an amount equal to $T\Delta S_{irr}$. There is good reason to believe that the irreversible entropy increase in Pb-4at%Tl is uniformly distributed throughout the transition above about 4^oK, but is generated preferentially near the beginning of the transition below 4^oK.

Figure (20) shows Q/L as a function of B/H_a for several temperatures after the second annealing. All curves show an initial linear portion with a smooth curve completing the transition. The curves for 4.03^oK, 4.17^oK, and 4.76^oK are very nearly identical with an initial slope between 0.60 and

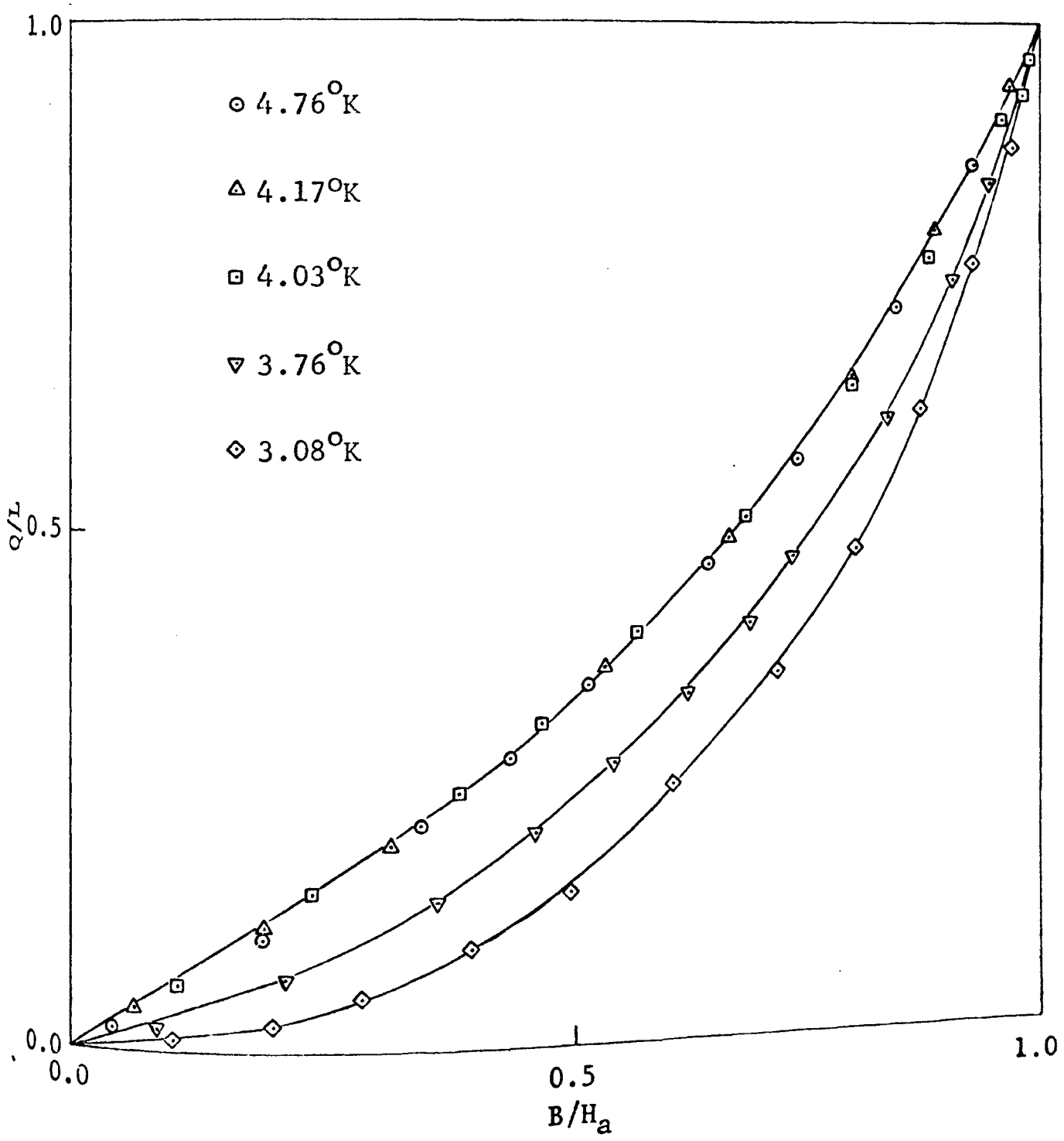

FIGURE 20. Q/L versus B/Ha after annealing

0.65. Using equations (58) and (68), K_1 is found to be between 0.867 and 0.916, while values obtained directly from the magnetization curves range between 0.916 and 0.945. Above 4°K, the close agreement between the values of K_1 obtained directly from magnetization data and the values deduced from calorimetric data is strong evidence that the shape of Q/L versus B/H_a has not been altered by magnetic hysteresis. The value of $K_1(t)$ changes only 3.1% between 4.03 °K and 4.76°K, so the initial slope of Q/L versus B/H should change by a few percent over this temperature range. The data is too scattered to discern such small changes, but the fact that the curves appear to be identical above 4°K is a further indication that hysteresis has not affected the shape of the curve.

It was pointed out earlier that dH_{c2}/dT at 4.19°K as determined from $(dQ/dH_a)_{H_{c2}}$ was about 22% less than the value determined from magnetic data. The latent heat at that temperature was about 20% lower than the value determined from the critical field curve of lead scaled with respect to T_c and H_o. The fact that $(dQ/dH_a)_{H_{c2}}$ was about 22% lower than expected, while L was only 20% low, leads to the conclusion that more irreversible work was being done near the end of the transition than near the beginning. This conclusion is further supported by the observation that the deduced and

observed values of K_1 could be made to agree exactly, were the initial slope of Q/L versus B/H_a reduced a few percent. But the initial slope would be too low, were more irreversible work being done near the beginning of the transition than near the end. At any rate the irreversible entropy increase does not appear to vary more than a few percent over the transition, so it can be concluded that the curves obtained above 4°K accurately represent the situation in a perfectly reversible specimen.

This was hardly the case below 4°K. The curves obtained after the second annealing for 3.76°K and 3.08°K deviated significantly from the curves obtained above 4°K. The initial slope progressively diminishes with decreasing temperature. Such behavior is not expected, since K_1 and hence q is no more strongly temperature dependent below 4°K than it is at higher temperatures. Below 4°K, more irreversible work is apparently done near the beginning of the transition than near the end. At 2.19°K, there was so much irreversible work done near the beginning of the transition that the sample warmed initially when flux began to penetrate. Otter observed similar behavior at lower temperatures (10). Mapother noted that the transition in dilute lead-calcium alloy was reversible above a certain temperature, but that hysteresis and flux trapping rapidly increased below this

temperature [47]. It appears that all calorimetric data taken below 4°K were essentially worthless, except possible to indicate the temperature dependence of hysteresis effects. The surface energy parameter certainly can not be inferred from calorimetric data in the presence of non-uniform irreversibility. Q/L versus B/H_a curves can be regarded as plausible only if their temperature dependence is quite weak.

Figure (21) shows Q/L versus B/H_a for Pb-4at%Tl at several temperatures before and after annealing. Also shown is Q/L versus B/H_a for Pb-40at%Tl at 3.96°K as given by Otter [10]. The curves at 4.19°K were taken by the two different methods described in chapter II. The agreement is excellent, and it can be asserted that data obtained by the two different methods are entirely equivalent.

The results obtained at 4.17°K after annealing are shown to indicate the effects of annealing. There is really not a great deal of difference between curves taken before and after annealing. The curves are nearly identical up to B/H_a = 0.4, at which point the annealed curve rises slightly above the earlier results. Near the end of the transition, the annealed curve bends across the earlier curve and approaches the end of the transition a bit more steeply. This change is associated with the anomolous magnetic and calorimetric behavior near H_{c2} which was described previously. As there

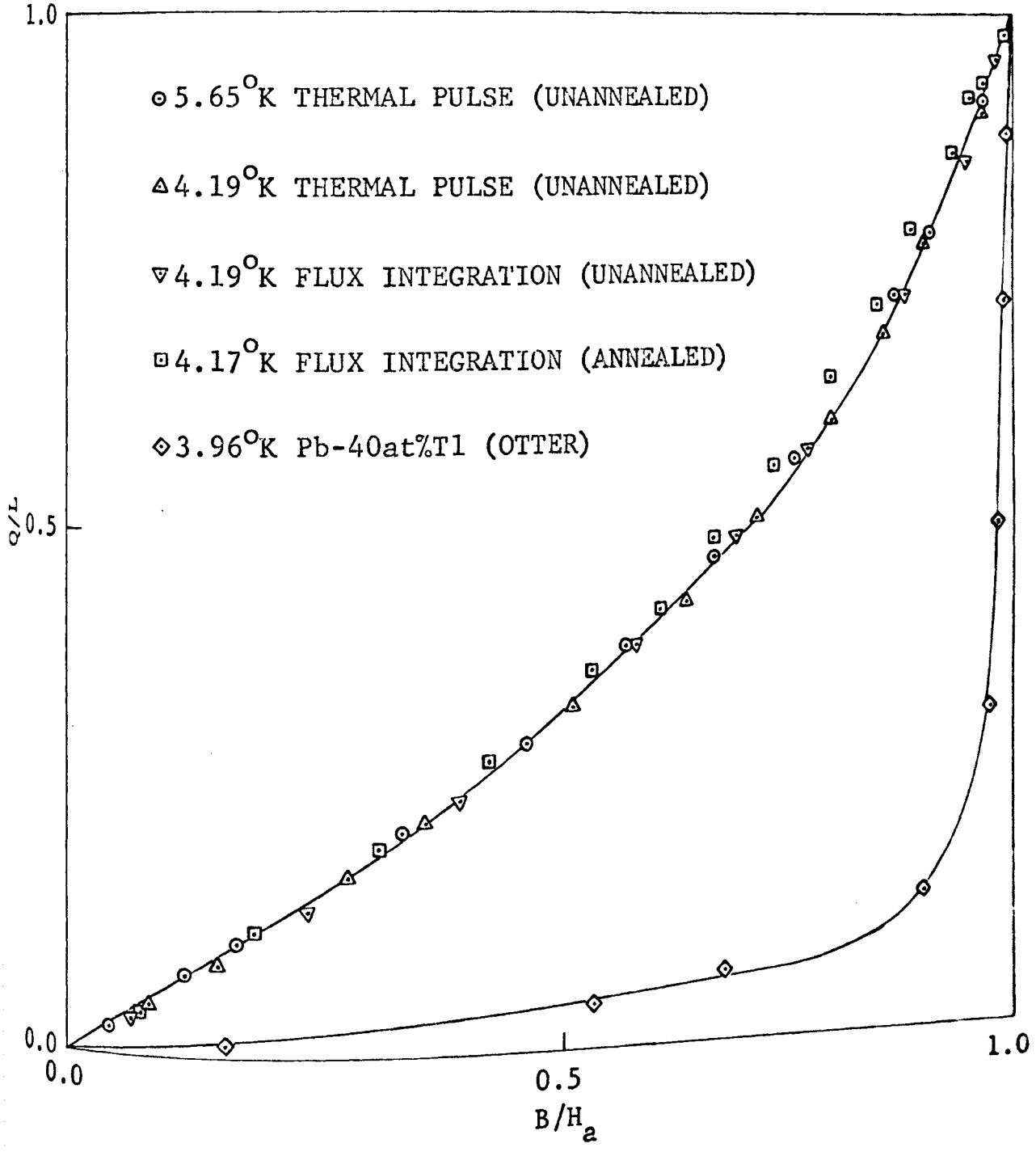

FIGURE 21. Q/L versus B/H_a for Pb-4at%Tl

was only a few percent change in K_1 after annealing, the initial slope of Q/L versus B/H_a was not expected to change more than a few percent after annealing. Considering the amount of scatter present, it can only be said that the initial slope did not change a great deal as a result of annealing.

Otter's results on Pb-40at%Tl are consistent with the results reported in this work. The curve obtained by Otter for Pb-40%Tl at 3.96°K shows the same features observed in this work for Pb-4%Tl, modified in precisely the way that would be expected for a more extreme type II alloy. There is an initial linear portion having a measured slope of 0.094. Using this value for q leads to a deduced value of K_1 equal to 7.10. The measured value of K_1 determined from the reported magnetization curve is equal to 6.39. The agreement is fairly close, but it was difficult to determine K_1 and q from the reported data.

The third prediction was that $Q(H_a-H_{c1})$ should be given by $a(H_a-H_{c1})+b(H_a-H_{c1})\ln c(H_a-H_{c1})$ in the field range $H_{c1} < H_a < H_{c2}$. This expression was obtained by differentiating the expressions for the free energy of a lattice of flux lines with respect to temperature. Figure (22) shows $Q(H_a-H_{c1})$ for Pb-4at%Tl at 4.76°K after annealing. The solid curve represents the best fit with an equation of the form $ax+bx\ln cx$.

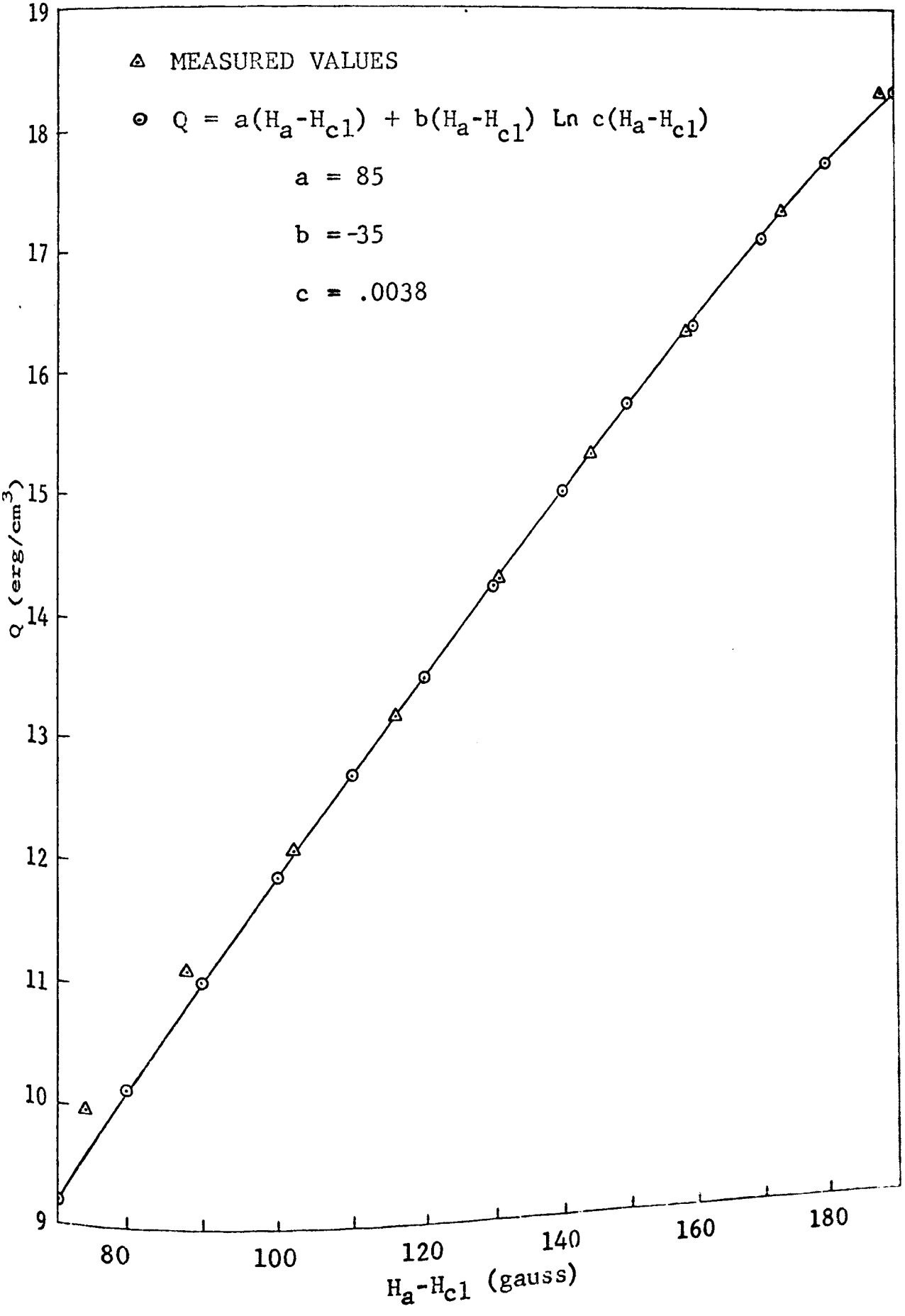

FIGURE 22. $Q(H_a-H_{c1})$ for $H_{c1} \ll H_a \ll H_{c2}$

The value of the parameters a, b, and c were found to be 85, -35, and 0.0038, respectively. Comparison with equation (78) shows that $c = \lambda^2 / \phi_o$. Using the measured value of c, λ is found to be about 28×10^{-6} cm, as compared to 5×10^{-6} cm for pure lead at the same temperature. The penetration depth is expected to be greater for the alloy, but probably no more than twice as great. The fit is fairly sensitive to the value of c, so there is little error in the value of c. The deduced value of λ is probably within a factor of three of the actual value. The assumption made in the derivation of equation (78) was that $\lambda >> \xi$, so perhaps it should not be surprising that a more plausible result is not obtained. It is not feasible to obtain $d\lambda/dT$ and dH_{c1}/dT from equation (78), since it requires having an accurate value of λ . However, the excellent agreement between the measured values and the fitted curve indicates that the model predicts a reasonable variation of Q with H_a in the range $H_{c1} < H_a < H_{c2}$.

It was possible to determine the average heat input per unit length of flux line from the data taken. The ratio of Q to B is multiplied by the flux quantum, ϕ_o , to get the average heat input per unit length of vortex. From this viewpoint, flux lines are nucleated at the surface of the specimen and then propagate into the interior carrying entropy along with them. The heat input per unit length of flux line can

be calculated as a function of B. In the limit of weakly interacting flux lines, the average heat input per unit length of vortex is given by:

$$Q/n = -T\frac{\partial \mathcal{J}}{\partial T} + \left(\frac{\phi_o}{4\pi c} + \mathcal{J}\right)\frac{T}{B}\frac{\partial B}{\partial T} \qquad (85)$$

where $\mathcal{J}$ is the Helmholtz free energy per unit length of vortex.

c is the slope of the linear portion of B/H_a versus B.

n is the number of flux lines per cm^2.

It appears from this simple calculation that the average heat input per unit length of vortex will be a function of B. The exact variation depends on the form of $\frac{1}{B}\frac{\partial B}{\partial T}$ as a function of B and its limit as B goes to zero. It is not exactly clear what this limit should be, although as B goes to H_e, $\frac{1}{B}\frac{\partial B}{\partial T}$ will vanish. Otter observed that $(dQ/dB)\,\phi_o$ as a function of B underwent a minimum then rose to nearly a constant value near the end of the transition [10]. This means that Q/n also underwent a minimum as a function of B and then rose to a nearly constant value near the end of the transition. This constant value is equal to $-T\frac{\partial \mathcal{J}}{\partial T}$ according to equation (85).

Figure (23) shows Q/n as a function of B for 4.17°K and 4.76°K after annealing and 4.19°K before annealing. The solid line at the bottom of the figure is Pb-40at%Tl at 3.9°K according to F. A. Otter [10]. The data reported by Otter exhibit minima at a few hundred gauss for both Pb-40

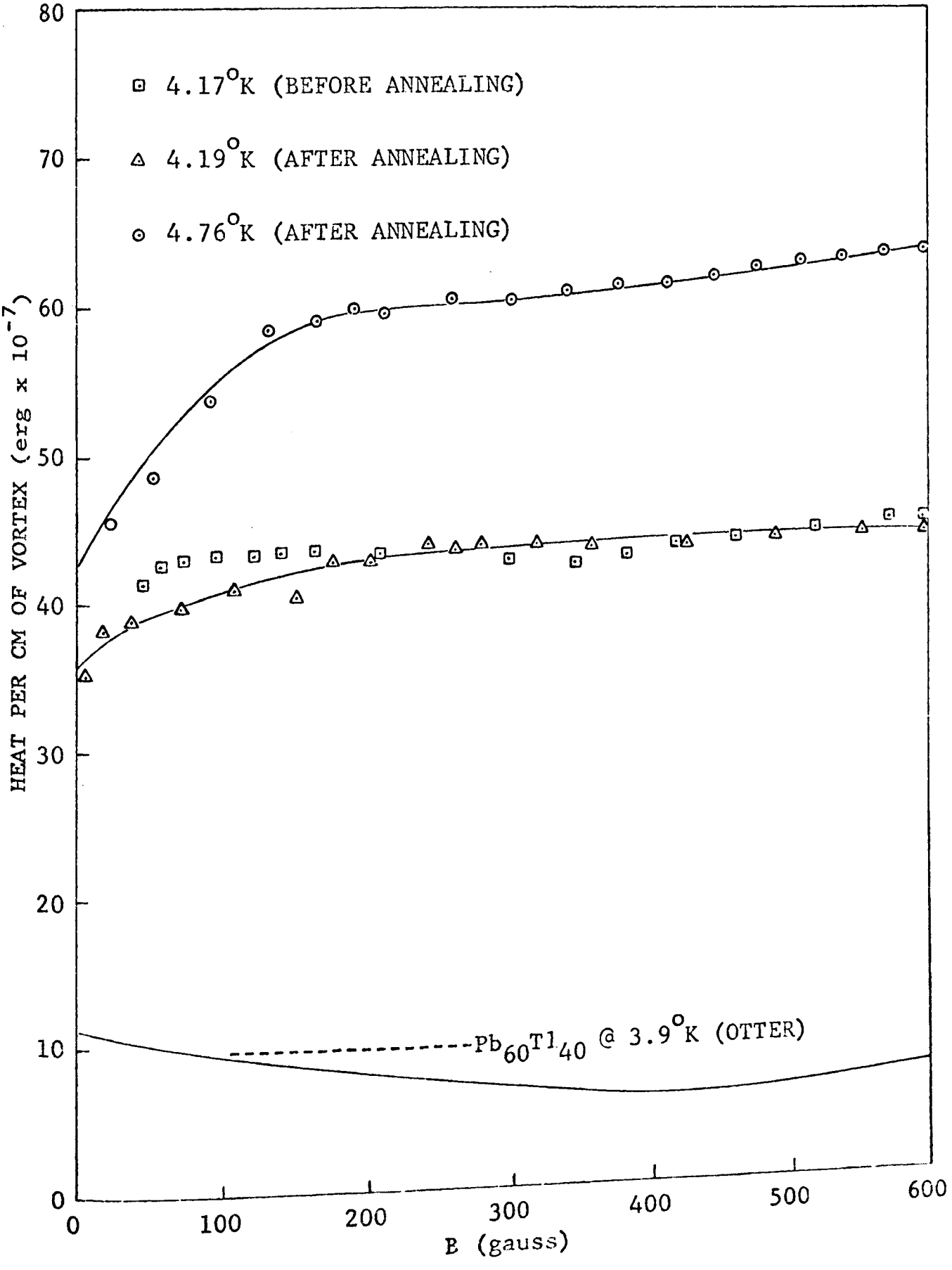

FIGURE 23. Average heat input per cm of vortex

at %Tl and Pb-60 at all temperatures. The data obtained in this work show no minima in Q/n at any temperature. The data for small values of B are somewhat unreliable, but the minima in Q/n reported by Otter do not seem to be present in Pb-4at%Tl. It should be pointed out that the minimum in Q/n reported by Otter at 3.9°K for Pb-40at%Tl is not nearly so sharp as the corresponding minimum for Pb-60at%Tl at 3.96°K. Perhaps this minimum in the average heat input per unit length of vortex line is a property of extreme type II materials. At any rate, the values of Q/n obtained in this work rose initially to a value that remained nearly constant after a few hundred gauss. Presumably this value is equal to $-T\frac{\partial \mathcal{J}}{\partial T}$, and $\frac{\partial \mathcal{J}}{\partial T}$ would be respectively equal to 1.03×10^{-6} and 1.34×10^{-6} erg/cm-°K at 4.17°K and 4.76°K. If the calorimetric data near H_{c1} are reliable, $\frac{1}{B}\frac{\partial B}{\partial T}$ must be a monotonically decreasing function of B for Pb-4at%Tl.

E. TIN-INDIUM

The results obtained with tin-6at%indium were rather disappointing, and very little data were taken. A magnetization curve was obtained at 2.04°K, and two calorimetric runs were attempted. The magnetization curve was very rounded, and had a long tail. In the reverse direction, the curve started down at once, and trapped a remanent somewhat larger than the maximum ascending magnetization. It appeared

that the indium had concentrated at the grain boundaries. The specimen had magnetic properties similar to those predicted for Mendelssohn's filamentary model [67]. In the filamentary model, a type II superconductor is treated as a multiply connected matrix of filaments possessing high critical fields. The interstitial material, which comprises the bulk of the superconductor, is considered to be type I material with a low bulk critical field. Such materials have been fabricated, and extremely inhomogeneous, polycrystalline superconductors such as Nb_3Sn behave similarly [68].

The calorimetric properties of a filamentary superconductor should be quite different from a homogeneous, well-annealed type II specimen. Since the type I material comprises the bulk of the superconductor, the total entropy change for the transition will have been nearly completed when all the interstitial material has become normal. The long tail will account for little of the latent heat. The Q/L versus B/H curve should look very nearly ideal (since type I material is being driven normal) up to nearly the end of the transition. The curve should then drop below the ideal line as the type II material at the grain boundaries is driven normal.

This is precisely the calorimetric behavior observed with Sn-6at%In during the two calorimetric runs made. It

appeared that the latent heat was drastically reduced in the faster transition. One transition was completed in six minutes, and the other was completed in fifteen minutes. The latent heat was nearly an order of magnitude lower for the faster transition. Since the purpose of preparing a Sn-In sample was to obtain a very reversible transition, the work on Sn-6at%In was pursued no further. It would seem that calorimetric techniques can easily distinguish between the filamentary and negative surface energy models, and indicate which model best describes the magnetic properties of a given specimen. Figure (24) shows Q/L versus B/H_a for Sn-6at%In at 2.04°K, and the inset magnetization curve indicates the magnetic properties of the specimen.

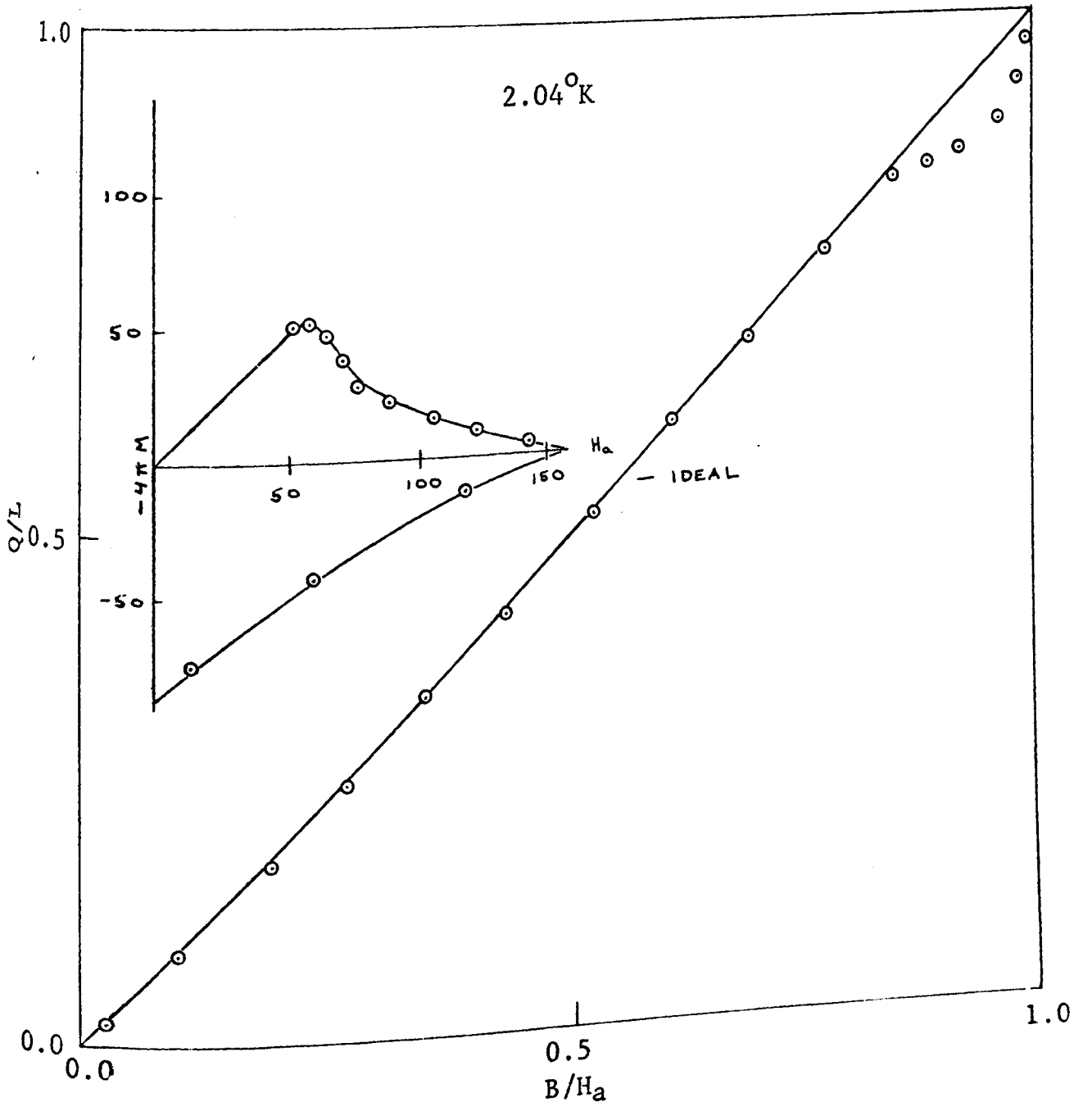

FIGURE 24. Q/L versus B/H_a for tin-6at%indium

IV CONCLUSIONS

The lead and tin samples did not deviate significantly from ideal behavior, and it was concluded that the interphase boundary energy was not detected in either material. The values for the surface energy parameter reported by other authors for lead and tin are quite small. In view of this fact, it is further concluded that the experimental procedure failed to detect the surface energy because the effect is much smaller than the experimental undertainty. The facts that lead and tin behaved ideally within the experimental error and that the measured latent heats agreed closely with the values deduced from reported critical field curves are considered proof that the experimental procedures are valid.

The magnetic properties of Pb-4at%Tl were quite typical of low K alloys before annealing, but were quite different after annealing. On the basis of magnetization and calorimetric evidence, it is concluded that the transition to the normal state at H_{c2} may very well have been first order after annealing. It seems unlikely that Maki's calculations can adequately explain the anomolous magnetic behavior observed, since they fail to predict the correct temperature dependence of K_2. It is certain that the anomolous magnetic behavior observed is not instrumental in origin, and all the explanations which might be offered to explain the observed

magnetic behavior fail at some point. There is no second phase which could be precipitated and account for the sudden drop in magnetization at the end of the transition. The enhanced reversibility after annealing also militates against a second phase origin of the anomaly and seems to rule out strain as an explanation. There seems to be no really satisfactory explanation of the magnetic behavior near H_{c2} after annealing.

The calorimetric results for the Pb-4at%Tl specimen studied in this work were consistent with current negative surface energy models of the mixed state. Q/L as a function of B/H_a looked very much like curves predicted by Goodman's model. It was possible to obtain values of K_1 from the initial slope of Q/L versus B/H_a that agreed with values of K_1 obtained from the magnetization curves to within 5%. Such close agreement was surprising in view of the simplicity of Goodman's model. The behavior of Q as a function of H_a closely followed the form predicted from Fetter's model for fields such that $H_{c1} < H_a < H_{c2}$, although a somewhat large value of λ was obtained. Near H_{c2}, the variation of Q* with $H_{c2}-H_a$ was very linear before annealing, as predicted by the GLAG (Ginzburg-Landau-Abrikosov-Gor'kov) theory. After annealing there was calorimetric evidence of a first order transition to the normal state at H_{c2}.

It is concluded that the interphase surface energy in Pb-4at%Tl is indeed negative. The effects of hysteresis do not appear to alter the shape of Q/L as a function of B/H_a above about 4^oK. The reduced transitions above 4^oK reported in this work represent the situation in a perfectly reversible transition to within a few percent. It is concluded that both Goodman's model and the vortex model can be used to interpret the experimental data for different ranges of H_a. It does not appear that this experiment can distinguish between a vortex and laminar structure. Goodman's model is valid only for fields near H_{c1}, while the vortex model is valid for fields much greater than H_{c1} and near H_{c2}. It was also demonstrated that Otter's calorimetric results for Pb-40at%Tl at 3.9^oK were in essential agreement with those reported in this work for Pb-4at%Tl.

The Sn-6at%In specimen seemed to behave like a filamentary superconductor. There were insufficient data to draw any firm conclusions, but a filamentary superconductor probably has calorimetric properties quite different from those of a homogeneous, well annealed type II specimen. Possibly this difference could be useful to differentiate between the two types of behavior.

BIBLIOGRAPHY

1. H. London, Proc. Roy. Soc. A152, 650 (1935).

2. L. D. Landau, Phys. Z. Sowjet. 11, 129 (1937).

3. A. P. Pippard, Proc. Roy. Soc. A203, 210 (1950).

4. V. L. Ginzburg and L. D. Landau, J.E.T.P. USSR 20, 1064 (1950).

5. A. A. Abrikosov, J. Phys. Chem. Solids 2, 199 (1957).

6. V. K. Tkachenko, J.E.T.P. USSR 23, 1049 (1966).

7. A. L. Fetter, P. C. Hohenberg and P. Pincus, Phys. Rev. 147, 140 (1966).

8. A. L. Fetter, Phys. Rev. 147, 153 (1966).

9. B. B. Goodman, Phys. Rev. Letters 6 597 (1961).

10. F. A. Otter, Proc. of the 1966 Low Temp. Calorimetry Conf., Ann. Acad. Sci. Fennicae AVI, No. 210 (1966).

11. C. Kittel, Introduction to Solid State Physics (John Wiley & Sons, New York, 1966), pp. 335-341.

12. E. A. Lynton, Superconductivity (John Wiley & Sons, New York, 1961), p. 6.

13. C. J. Gorter and H. B. G. Casimir, Physics I, 306 (1934).

14. For a discussion of magnetostatics see: J. D. Jackson, Classical Electrodynamics (John Wiley & Sons, New York, 1962).

15. Dr. Robert Meyerhoff, Linde Co., Speedway Laboratories, Private communication.

16. For a discussion of reversible niobium see: D. K. Finnemore, T. F. Stromberg and C. A. Swenson, Phys. Rev. 149, 231 (1966).

17. M. W. Zemansky, Heat and Thermodynamics (John Wiley & Sons, New York, 1957), p. 244

18. F. London and H. London, Proc. Roy. Soc. A149, 71 (1935).

19. A. B. Pippard, Proc. Roy. Soc. A216, 547 (1953).

20. L. P. Gor'kov, Soviet Phys. J.E.T.P. 10, 998 (1960).

21. P.G. DeGennes, Superconductivity of Metals and Alloys (W. A. Benjamin, Inc., New York, 1966), p. 176.

22. J. A. Cape and J. M. Zimmerman, Phys. Rev. 153, 416 (1967).

23. E. C. Stoner, Phil. Mag. 36, 803 (1945).

24. For example, see: T. E. Faber, Proc. Roy. Soc. A248, 464 (1958).

25. Fr. Haenssler and L. Rinderer, Helv, Phys. Acta 38, 448 (1965).

26. see also: D. Shoenberg, Superconductivity (Cambridge University Press, London, 1960), pp. 105-110.

27. D. C. Hopkins, Calorimetric Measurement of Negative Surface Energy in Superconductors of the Second Kind, Univ. of Mo. Rolla Research Proposal (1964).

28. D. Criber, B. Jacrot, L. Rao and B. Farnoux, Phys. Letters 9, 106 (1964).

29. J. Matricon, Phys. Letters 9, 289 (1964).

30. B. B. Goodman, Phys. Letters 12, 6 (1964).

31. W. DeSorbo and W. Healy, Cryogenics 4, 257 (1964).

32. J. L. Harden and V. Arp, Cryogenics 2, 105 (1963).

33. Blake, Chase, and Maxwell, Rev. Sci. Instr. 29, 715 (1958).

34. F. Brickwedde, H. VanDijk, M. Durieux, J. R. Clement, and J. Logan, J. Res. Natl. Bur. Standards 64A, 1 (1960).

35. For a discussion of the inhomogeneous heat equation see: K. S. Miller, Partial Differential Equations in Engineering Problems (Prentice-Hall, Englewood Cliffs, N.J., 1963), pp. 124-127.

36. M. M. Kreitman, Rev. Sci. Instr. 35, 749 (1964)

37. J. R. Clement and E. H. Quinnell, Phys. Rev. 85, 502 (1952).

38. D. C. Hopkins, private communication.

39. D. E. Mapother and J. H. Snyder, "The Axial Variation of the Magnetic Field in Solenoids of Finite Thickness," University of Illinois Engineering Experiment Station Circular No. 66 (1955).

40. D. L. Decker, D. E. Mapother, and R. W. Shaw, Phys. Rev. 112, 1888 (1958).

41. R. W. Shaw, D. E. Mapother, and D. C. Hopkins, Phy. Rev. 120, 88 (1960).

42. R. C. Pandorf, E. Lerner, and J. G. Daunt, Rev. Sci. Instr. 35, 1070 (1964).

43. Shubnikov, Khotkevich, Shepelev, and Riabinin, Zh. Exsperim. i Teor. Fiz. 7, 221 (1937).

44. R. P. Elliot, Constitution of Binary Alloys (McGraw Hill, New York, 1965).

45. J. D. Livingston, Phys. Rev. 129, 1943 (1963).

46. P. R. Doidge, Phil. Trans. Roy. Soc. A248, 553 (1956)

47. R. W. Shaw and D. E. Mapother, Phys. Rev. 118, 1474 (1960).

48. R. L. Dolecek, Phys. Rev. 94, 540 (1954).

49. J. M. Lock, Proc. Roy. Soc. A208, 391 (1951).

50. R. B. Goldner, J. Appl. Phys. 33, 338 (1962).

51. C. C. Kuper, Phil. Mag. 42, 961 (1951).

52. J. R. Birchak, J. Phys. Chem. Solids 28, 917 (1967).

53. E. A. Lynton and B. Serin, Phys. Rev. 112, 70 (1959)

54. J. M. Lock, A. B. Pippard, and D. Shoenberg, Proc. Camb. Phil. Soc. 47, 811 (1951).

55. E. A. Davies, Proc. Roy. Soc. A255, 407 (1960).

56. T. Claeson, Phys. Rev. 147, 340 (1966).

57. L. P. Gor'kov, Soviet Phys. J.E.T.P. 10, 593 (1960).

58. E. A. Shapoval, Soviet Phys. J.E.T.P. 14, 628 (1962).

59. J. Bardeen, Phys. Rev. 95, 554 (1954).

60. K. Maki, Physics 1, 21 (1964).

61. S. T. Sekula and R. H. Kernohan, J. Appl. Phys. 36, 2895 (1965).

62. G. Bon Maridon, B. B. Goodman, and A. Lacaze, J. Phys. Chem. Solids 26, 1143 (1965).

63. T. Kinsel, E. A. Lynton, and B. Serin, Rev. Mod. Phys. 36, 107 (1964).

64. J. D. Livingston, Rev. Mod. Phys. 36, 54 (1964).

65. C. P. Bean and J. D. Livingston, Phys. Rev. Letters 12, 14 (1964).

66. G. Bon Maridon, B. B. Goodman, and A. Lacaze, Phys. Letters 17, 210 (1962).

67. K. Mendelssohn, Proc. Roy. Soc. (London) A152, 34 (1935).

68. C. P. Bean, M. V. Doyle, and A. G. Pincus, Phys. Rev. Letters 9, 93 (1962).

69. L. M. Kells, Elementary Differential Equations (McGraw-Hill, New York, 1954), pp. 41-42.

APPENDIX I

The thermodynamic critical field for a type II superconductor is determined from the integral of the equilibrium magnetization curve according to equation (18). When the ascending magnetization curve is not the equilibrium curve, the critical field computed using equation (18) represents an upper limit to the actual H_c. A value for the critical field can be obtained in the presence of magnetic irreversibility by applying the first law of thermodynamics. A superconductor in the superconducting state at zero field is in a well defined thermodynamic state, and a superconductor in the normal state at applied field H_{c2} is also in a well defined state. Since the internal energy, U, is a state function, the difference in internal energy, ΔU, does not depend on the intermediate states of the body. Equating the change in free energy to the heat added to the sample minus the work done by the sample leads to:

$$-\int_0^{H_{c2}} M\,dH_a + L = \Delta U = -\int_0^{H_{c2}} M_{eq}\,dH_a + L_{rev} \qquad \text{(A-I-I)}$$

Assuming that the critical field of the alloy obeys the parabolic law, one gets:

$$L_{rev} = \frac{4t^2}{1-t^2}\,\frac{H_c^2}{8\pi} \quad , \quad -\int_0^{H_{c2}} M_{eq}\,dH_a = \frac{H_c^2}{8\pi} \qquad \text{(A-I-2)}$$

The right side of (A-I-1) is therefore equal to:

$$L_{rev} - \int_0^{H_{c2}} M_{eq}\,dH_a = \frac{1+3t^2}{1-t^2}\,\frac{H_c^2}{8\pi} \qquad \text{(A-I-3)}$$

Substituting (A-I-3) into (A-I-1) leads to equation (83).

It is also possible to obtain the critical field in the presence of magnetic hysteresis without assuming that the alloy obeys the parabolic law. Equation (A-I-1) can be written using equation (18) and (20) as:

$$\frac{H_c^2}{8\pi} - T\frac{d}{dT}\left(\frac{H_c^2}{8\pi}\right) = -\int_0^{H_{ca}} M\,dH_a + L \qquad \text{(A-I-4)}$$

This equation can be written in slightly different form as:

$$\frac{d}{dT}\left(\frac{TH_c^2}{8\pi}\right) - \frac{2}{T}\left(\frac{TH_c^2}{8\pi}\right) = \int_0^{H_{ca}} M\,dH_a - L \qquad \text{(A-I-5)}$$

This equation is a linear differential equation for which the solution can be written immediately [69]. The solution is:

$$\frac{H_c^2}{8\pi T} = \int_T^{T_c} \frac{1}{T^2}\left\{\int_0^{H_{ca}} M\,dH_a - L\right\} dT \qquad \text{(A-I-6)}$$

Equation (84) is obtained from this result.

VITA

The author was born in Indianapolis, Indiana, on January 31, 1940. He was graduated from high school in Indianapolis in 1958 and entered Indiana Central College, Indianapolis, where he graduated in 1962, receiving a B.A. in Chemistry and Mathematics. He entered the Missouri School of Mines in September 1962, where he held a graduate assistantship and a National Science Foundation Cooperative Fellowship. Upon receiving the M.S. in Engineering Physics in June 1964, he joined McDonnell Aircraft Corporation as an engineer. He enrolled in the University of Missouri at Rolla in September 1965, and since that time has held a research fellowship sponsored by the U.S. Army Research Office, Durham, North Carolina.

He is married to the former Mary Ganote of Indianapolis, Indiana, and they have a son, Robert Lynn.